1-1-2009

Fatigue damage and life assessment of welded joints based on energy methods

Faertom Pakandam
Ryerson University

FATIGUE DAMAGE AND LIFE ASSESSMENT
OF WELDED JOINTS BASED ON ENERGY
METHODS

by

Faertom Pakandam

B.Sc. in Mechanical Engineering

Tehran Azad University Central Branch, Tehran, Iran, 1997

A thesis

presented to Ryerson University

in partial fulfillment of the

requirements for the degree of

Master of Applied Science

in the program of

Mechanical Engineering

Toronto, Ontario, Canada, 2009

© Faertom Pakandam

Author's Declaration

I hereby declare that I am the sole author of this thesis.

I authorize Ryerson University to lend this thesis to other institutions or individuals for the purpose of scholarly research.

I further authorize Ryerson University to reproduce this thesis by photocopying or by other means, in total or in part, at the request of other institutions or individuals for the purpose of scholarly research.

Ryerson University requires the signatures of all persons using or photocopying this thesis.
Please sign below and give address and date.

iii

Acknowledgments

I would like to express my greatest thanks to my supervisor Professor Ahmad Varvani-Farahani for his encouragement, advice, and support. He has provided me with guidance, inspiration, and motivation, helping me greatly throughout my work on this thesis. He has definitely contributed to the success of this work very much.

I would like to express my sincerest appreciation for my lovely mother for her patience, inspiration, unconditional support, and love. I undoubtedly owe her greatly for being able to complete my studies and perform this work.

I would also like to thank my friends who morally supported me over the period of this study, particularly Mr. Kian Marzban and my thanks to Mr. Hassan Abbasi, Mr. Ali Haji-Abedin, Mr. Alireza Sayyidmousavi, and Mr. Mahdi Takaffoli for assisting with the ANSYS finite element analysis.

Moreover, thanks to Mighty God for all the blessings he has given me.

Abstract

'Fatigue Damage and Life Assessment of Welded Joints Based on Energy Methods',
Faertom Pakandam, Master of Applied Science Thesis in Mechanical Engineering,
Ryerson University, Toronto, Canada, 2009.

The present study intends to evaluate fatigue damage of different welded joints under loading conditions and their response on fatigue lifetime. The main variables influencing the fatigue life of a welded joint are: applied stress amplitude, material properties, geometrical stress concentration effects, and size and location of welding defects. In order to carry out the study, calculations have been performed using the parameters in three energy-based models. Calculations have been carried out separately for each model from the original experimental data obtained from available literature related to each welded joint. The data variables used as a basis for the calculations of the energy-based models for different welded joints include: cyclic stress-strain properties related to the base metal material type of the welded joints, dimensional and geometrical information on the welded joints, and stress versus endurance cycle tables obtained from the tests performed on the welded joints. All the mentioned variables are parameters influencing the fatigue life of a welded joint.

Fatigue damage assessments were performed and discussed based on earlier developed energy damage approaches consisting of: (i) the hysteresis loop based parameter of Masing type material, (ii) the notch stress-intensity based parameter and (iii) the critical plane/energy based parameter. In evaluating fatigue damage of welded joints, these approaches were discussed based on the comparison of energy-lifetime diagrams obtained from each energy model and how readily coefficients/constants are determined and employed in the parameters. In addition, a finite element analysis was performed on selected welded joints to obtain local peak stress values and their location. Numerically obtained stress concentration factor and fatigue notch factor values were also compared with their analytical values.

To assess fatigue damage of welded joints based on various energy models, different sets of experimentally obtained fatigue data performed by different laboratories under uniaxial loading conditions available in literature were chosen. The welded joints used in this study

were butt joint, cruciform joint, butt-ground joint, and butt-strap fillet joint. The welded joint base metals included low carbon structural steel, aluminium alloys, and carbon steel.

The energy models were compared for their energy-fatigue life curve slopes and their ability to converge the related nominal stress-life scatter. The energy values calculated based on their models included the effect of variables of cyclic stresses. Important results were concluded for welded joints from the study including: the relation between fatigue notch factor and fatigue strength, the stress-life diagram slope and fatigue resistance, the ability of the energy models to reflect the fatigue notch factor, and merits and disadvantages of each energy model.

Objective and Scope of the Thesis

Welding technology has progressed quickly recently due to the rapid growth of industries and the high demand of practical, economical and reliable joining methods. Today welding is without any doubt the main joining method used in different industries, and if not for this technique, many structures or even whole sectors may not be existent. Considering the fact that in many cases welded joints are exposed to repeated loading, the prevention of structural damage highlights the importance of the study of fatigue in welded joints, which is the cause for numerous failures happening in working conditions. In this regard and in order to reach an optimum reliable welded joint, it is important that appropriate fatigue damage-assessment and life prediction methods are developed for welded joints and utilized by design engineers, to protect welded structures from unwanted fatigue failures.

Although fatigue design of welded joints has usually been based on *S-N* diagrams, obtained from experimental data from fatigue tests mentioned in the form of nominal stress, there are significant restrictions to this approach, resulting in the development and usage of local approaches. The nominal stress approach cannot reveal the local effect near weld toes on the fatigue strength. Energy based methods which are considered local approaches, consider the local stress and strain for modeling the fatigue process through reflecting on the influence of all important parameters affecting fatigue of welded joints.

The objective of this study is to find a suitable energy based method for assessing the fatigue damage of welded joints. Three energy approaches are applied to different welded joints in terms of material and joint type, in a comparison style, analytical format of study. The comparison is performed for two different joint types of the same material, one joint type (with different weld cap heights), and two different joint types with similar alloys. The advantages and disadvantages of the energy approaches, considering the important evaluation criteria for fatigue damage-assessment, are taken into account for finding the most appropriate energy approach. The evaluation criteria for the energy parameters are convergence ability, curve slope, and how readily coefficients/constants are determined and employed in the parameters.

A finite element analysis is also performed on selected welded joints to verify peak stress locations and to obtain local peak stresses resulting in numerically obtained stress concentration factors and fatigue notch factors for the verification of their analytically obtained values.

Table of Contents

List of Figures

List of Tables

Nomenclature

$\Delta\sigma$: Stress range defined as; $\Delta\sigma = \sigma_{maximum} - \sigma_{minimum}$

σ_a: Stress amplitude defined as; $\sigma_a = \Delta\sigma/2$

$\Delta\sigma_{loc}$: Local stress range

$\sigma_{loc\ (FE)}$: Local stress obtained from finite element analysis

$\Delta\sigma_{nom}$: Nominal stress range

σ_m: Mean stress defined as; $\sigma_m = (\sigma_{maximum} + \sigma_{minimum})\ /\ 2$

σ_{nt}: Nominal tensile stress (normal stress)

σ_u: Ultimate tensile strength

σ_E: Stress endurance limit

$\tau_{n(per)}$: Nominal perpendicular shear stress

$\tau_{n(par)}$: Nominal parallel shear stress

$\Delta\varepsilon$: Strain range defined as; $\Delta\varepsilon = \Delta\varepsilon_e + \Delta\varepsilon_p$

$\Delta\varepsilon_e$: Elastic strain range

$\Delta\varepsilon_p$: Plastic strain range

ε_E: Strain endurance limit

e: Nominal strain defined as; $e=S/E$

a_0: Initial crack length

a_c: Critical crack length

$D_{per(max)}$: Maximum permissible damage parameter in Miner's rule

K_{IC}: Critical stress intensity factor or plain strain fracture toughness; $K_{IC} = Y\sigma(\pi a)^{1/2}$

ΔK: Stress intensity factor range defined as; $\Delta K = K_{maximum} - K_{minimum}$

$K_{t(FE)}$: Stress concentration factor obtained from finite element analysis

$K_{f(num)}$: Fatigue notch factor obtained numerically

N: Fatigue lifetime of component

N_E: Endurable limit

$N_{exp.}$: Experimental lifetime obtained from applying nominal stress

R: Regression value

Stress ratio: Defined as; $\sigma_{minimum} / \sigma_{maximum}$

S: Strength or stress of component also used for nominal stress

ΔS_{nom}: Nominal stress range

$S_{nom(max)}$: Maximum nominal stress

ΔW_p: Plastic strain energy

W_{HL}: Hysteresis loop energy

W_{NS}: Notch stress intensity energy

W_{CP}: Critical plane energy

Definitions & Abbreviations

BS: British Standard.

Cyclic hardening: For a soft material, initially the dislocation density is low. As the cyclic load is applied, the dislocation pile-up increases and the material shows greater strength.

Cyclic softening: For a hard material, as the cyclic load is applied, a rearrangement of dislocations takes place and the material deforms with less resistance.

Design stress: Characteristic stress value issued by a safety factor, limiting the applied stress.

Deviatoric strain: The deviatoric strain tensor can be obtained by subtracting the volumetric strain tensor from the strain tensor. Deviatoric components are responsible for plastic deformation.

Electroslag welding: Is a highly productive, single pass welding process for thick (greater than 25mm up to 300mm) materials in a vertical or close to vertical position. An electric arc is initially struck by wire that is fed into the desired weld location and then flux is added.

Fatigue life: Number of stress cycles of a specific magnitude needed to cause fatigue failure in a component, also known as *service life*.

Fatigue strength: Magnitude of stress range leading to a particular fatigue life.

Fracture mechanics: A branch of mechanics dealing with the behavior and strength of components containing cracks.

Hot spot stress: The value of structural stress on the surface at a hot spot, also known as *geometric stress*.

Hysteresis loop: An S-shaped stress-strain diagram for loading-unloading of a specimen that obeys the Hooke's law, in which the increase in length starts from the start point of the closed

loop, with loading on one path, and the decrease in length starts from the end point of loading and ends at the start point of the loop, on another path. The area in the centre of the hysteresis loop is the energy dissipated as heat.

IIW: International Institute of Welding.

Ideal weldment: Is a weldment that has blended weld toes and no considerable weld discontinuity or defect resulting from high-quality welding process.

J-integral: Represents a way to calculate the energy per unit-fracture surface area, in a material. An energetic contour path integral called J around the crack is independent of the path around the crack.

Load carrying (lc) cruciform joint: A cruciform welded joint in which the weld carries shear load.

Local stress: Is the stress near a local notch such as a welded joint. A local notch generates a nonlinear stress peak.

Macro geometry: Is the global or geometrical configuration of a structure.

Manual metal arc welding (MMAW): Is a manual arc welding process in which a consumable flux coated electrode is used to form an electric arc between the electrode and the base metals to be joined. An alternating current or direct current from a welding power supply, is used to form an electric arc. The flux on the electrode results in a shielding gas that protects the process from the surrounding. This procedure is also known as *stick welding* or *shielded metal arc welding*.

Metal inert gas welding (MIG): Is a semi-automatic or automatic arc welding process in which a continuous and consumable wire electrode and a shielding gas are fed through a welding gun. A constant voltage, direct current power source is most commonly used with this process. This procedure is also known as *gas metal arc welding*.

Miner's rule: Fatigue failure is expected when the sum of Miner's equation reaches unity.

Mode I crack: Caused by mode I stress, also known as 'opening mode' crack.

Mode II crack: Caused by mode II stress, also known as 'sliding mode' crack.

Mode III crack: Caused by mode III stress, also known as 'tearing mode' crack.

Nominal stress: Also known as far-field stress is the applied stress, disregarding the stress raising effects of the welded joint, usually resolved using general theories such as beam theory.

Non-load carrying (nlc) cruciform joint: A cruciform welded joint in which the weld does not carry shear load.

Paris' law: An empirical relation between crack growth rate and stress-intensity factor range.

Parent metal: Main plate, also called *base plate*, where the welding takes place on.

Pearlitic steel: Is steel with a two phase structure composed of alternating layers of 88 weight percentage ferrite (iron) and 12 weight percentage iron carbide.

Quench and tempering: Is a process in which carbon steel is heated to normalizing temperatures and then rapidly cooled (quenched) in water or oil to the critical temperature. Tempering involves reheating quenched steel to a temperature below the melting point.

Residual stress: Is a stress that remains in a cross section of a component, even without the external cause. Welding heat can cause localized expansion, taken up by the molten metal, but when the weldment cools, some areas contract more than others leaving residual stresses.

Ripple: A slight transverse wave or shadow mark appearing at intervals along a weld seam.

Stage-I crack growth: Micro crack joining and micro-crack propagation stage.

Stage-II crack growth: Micro cracks turning into macro-cracks and macro-crack propagation stage.

Stress intensity factor: The main parameter in fracture mechanics, including the combined effect of stress and crack size at the crack tip region.

Submerged arc welding (SAW): Is a common welding process using electric arc between electrode and base metal to melt the metals at the welding point. The molten weld and the arc zone are protected from atmospheric contamination by being submerged under a blanket of granular fusible flux.

Variable amplitude loading: A type of loading causing irregular stress fluctuation with stress amplitudes of variable magnitude.

Weld toe angle: Is the obtuse angle between the line tangent to the weld at the point of intersection of the weld toe and the base metal with the base metal, also known as *weld angle*. Sometimes the supplementary angle (acute angle) of the weld toe angel is considered.

Preface

The following provides a brief description of materials covered in the chapters that follow.

Chapter 1 reviews the present state of the art of fatigue strength assessment of welded joints and major features in the fatigue assessment process of welded joints.

Chapter 2 reviews the fundamentals of global and local approaches of fatigue damage assessment and reviews all the available approaches used for fatigue damage assessment and life prediction of welded joints. The reviewed fatigue models are the nominal stress approach, the structural stress approach, the notch stress approach, the notch strain approach, the crack propagation approach, and the notch stress-intensity approach.

Chapter 3 introduces the energy method concept and the main features and reasons for the application of energy based approaches, followed by the different energy methods used in this study including the hysteresis-loop energy method, the fracture-mechanics energy-method, and the critical plane/energy method.

Chapter 4 studies the cyclic stress – fatigue life data assortment and calculations based on energy models for welded joints. Five sets of data extracted from the literature including Chapetti et al. data for low carbon structural steel joint, Livieri and Lazzarin data for low carbon structural steel joint, Livieri and Lazzarin data for aluminium alloy joint, Reemsnyder data for carbon steel joint, and Webber data for aluminium alloy joint are presented. Energy-based fatigue damage analyses of welded joints are also conducted following the systematic procedure of the hysteresis loop energy method, the fracture mechanics energy method, and the critical plane/energy method. In addition, a numerical analysis for the notch stress-concentration factor, K_t, has been carried out using finite element analysis.

Chapter 5 presents the calculated energy values based on the three models introduced in the previous chapter. The nominal stress versus fatigue life (S-N) diagrams for the tested welded joints extracted from the literature are presented followed by the energy-life (W-N) diagrams for the same tested welded joints. The results of the performed finite element analysis of chapter 4 are also presented.

Chapter 6 evaluates the energy models by means of various fatigue data and compares the energy-life curves with each other. This chapter further examines the energy models for both butt joint and fillet joint for the same welded component material, butt joints with different materials, and aluminium alloys with different joint types.

Chapter 7 summarizes the conclusions obtained from this study and presents future recommendations.

Appendix A tabulates the nominal stress versus fatigue life for the tested welded joints of various types extracted from the literature.

Appendix B lists the monotonic and cyclic properties for metallic materials of the tested welded joint base metals extracted from the literature.

Appendix C presents the specimen dimensions and geometry of the tested welded joints.

Appendix D depicts diagrams to estimate stress concentration factors of welded joints under axial loads.

Appendix E tabulates the parameters required for obtaining notch stress-concentration factor.

Appendix F tabulates the results of predicted energy values.

CHAPTER ONE

Introduction

1.1 Fatigue strength assessment of welded joints; present state of the art

Today welding is without any doubt the main joining method used in different industries. Welded joints are prone to damage (cracking and deterioration) particularly under external forces. Fatigue of welded components is critically important and many catastrophic failures are reported to occur in welded joints subjected to repeated loads. The prevention of progressive structural damage under cyclic loading in welded joints requires an extensive examination of failure mode of welded joints in service loading conditions.

An important fact is that the existence of a welded joint in a structure or member can significantly reduce its fatigue strength, and it is usually found that design stresses in repeatedly loaded structures or components are restricted by the fatigue strength of the welded detail. Although today fatigue failure of welded joints remains the most widespread type of failure, unfortunately the detection of this problem at the design stage is not complete yet, and some of the factors affecting it are still vague due to the complicated nature of material fatigue. Figure 1.1 compares the fatigue strengths of a plane, a notched, and a welded plate in an empirically obtained stress-life diagram.
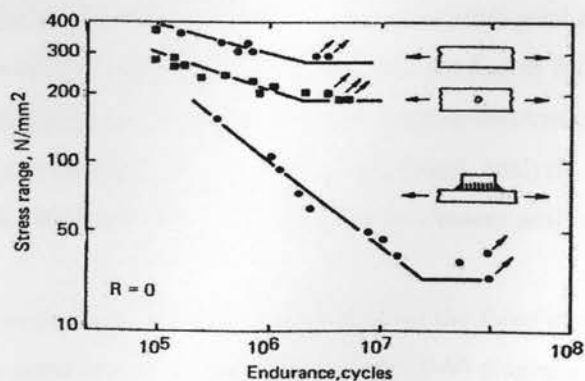
Figure 1.1 Comparison between fatigue strengths of: plain steel plate, notched plate, and plate with fillet weld attachment (steel to BS 4360, grade 50B) [1].

The fatigue damage process is presented by fracture mechanics in three main stages: 1. Crack initiation, 2. Stage I and stage II crack growth[1], 3. Ultimate fracture. Generally, fatigue in welded joints is caused because of stress concentrations. Vast fluctuations in fatigue strengths in welded joints for different metallic materials are a result of variations in stress concentration intensity due to different weld type design and different loading directions. In addition, a weld includes imperfections such as cracks, pores, cavities and undercuts that initiate fatigue cracks.

Fatigue failures in welded joints happen mostly close to the welds rather than in the base metal far from the weld. Fatigue in welded joints is even more complicated due to the great influence of the procedure on the material because of heating and cooling as well as addition of filler weld metal in the fusion procedure to connect the base metals resulting in different inhomogeneous materials and different zones. Finally, residual stresses and deformations resulting from the procedure, affect the fatigue behavior [2]. There are several developed approaches for fatigue analysis of welded joints in the literature. Capability of a fatigue approach is highly dependant upon its affecting parameters in fatigue analysis of welded joints under axial loads.

Fatigue failure in welded joints is a localized procedure and is affected or influenced by loading condition. All local approaches are incomplete and cannot be completely standardized due to many procedures and numerous fatigue cases [3]. The effect of loading type in fatigue design of welded joints is highly pronounced. Weld codes have been developed based on the nominal stress approach, and welded joints subjected to variable amplitude loading conditions are yet to be addressed.

Welded joints are graded according to their shape, weld type, loading type and manufacture quality. Then they are allocated to detail classes representing the design S-N curves based on the results of related fatigue tests. The English designation 'detail class' or 'fatigue class' (FAT) is more customary. The endurable or permissible nominal stress amplitudes are reduced greatly by high tensile residual stresses caused by welding. Stress relieved welded joints allow higher permissible stress amplitudes depending on the stress ratio [3].

---

[1] The stable crack propagation stage is consisted of stage I and II crack growth.

2

1.1.1 The S-N diagram and fatigue strength

The cyclic stress-fatigue life data are obtained as welded components are tested under several cyclic stress levels until failure occurs. The applied stress, plotted versus the number of cycles to failure, is known as the *S-N* curve. Figure 1.2 schematically shows the graphical presentation of an *S-N* curve.
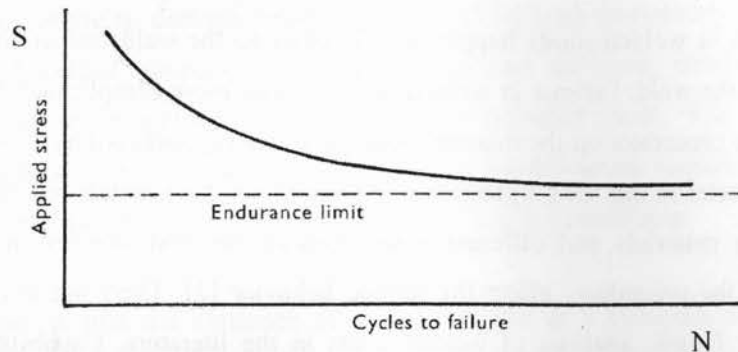
Figure 1.2 Typical *S-N* curve [4].

In typical *S-N* curves, with the increase in number of cycles, the applied stress decreases and the curve flattens out horizontally, and a small decrease in stress results in a large number of cycles that the specimen can resist. For plain ferrous specimens, after about 2-5 million cycles, the curve moves to a parallel position with the horizontal *N* axis, showing that at a slightly smaller stress, the specimen would have infinite life. This stress is called the endurance limit of the tested material specimen. In welded joints, *S-N* curves are determined for an endurance range from 10^5 to 2×10^6 cycles [4].

1.2 Major features in the fatigue assessment process of welded joints

Considering the high quantity of welding performed in the manufacturing sector, it is very important for designers to be able to protect their welded structural designs from unwanted fatigue failures. It is not adequate to design to some random safety factor based on the yield strength of the material and assume that it will prevent fatigue failure. This may be appropriate for other connection types except welded joints; welded design can introduce

much more severe stress concentrations; therefore, fatigue failures in such structures are customary. In addition, if a large safety factor is introduced in a welded design, it will result in an over designed and out of proportion structure. The only practical approach to the design of a structure containing welded joints subjected to fatigue loading is to relate the working stresses to fatigue strength data for the specific joint required. In this regard, precise working stresses may not be available or the number of loading repetitions may be unknown [5].

A welded joint is a stress raiser and different types of stress raisers in welded joints result in different local stresses at the joints. The choice of stress depends on the fatigue assessment process used. The stress raiser types and their corresponding effects are presented in table 1.1.

Table 1.1 Stress raisers and notch effects [6].

Type	Stress raisers	Stress determined	Assessment process
A	General stress analysis using general theories		
B	A + Macrogeometrical effects due to the design of the component (also effects of concentrated loads)	Nominal stress range	Nominal stress approach
C	A + B + Structural discontinuities due to the structural detail of the welded joint	Range of structural geometric stress (hot spot stress)	Geometric stress (hot spot stress) approach
D	A + B + C + Notch stress concentration due to the weld bead, e.g. at the weld toe or weld root a) actual notch stress b) effective notch stress	Range of elastic notch stress (total stress)	a) crack propagation approach b) effective notch stress approach

4

Fatigue of welded joints is very much dependant on local stress/strain components acting at the joint as stress raisers. Fatigue assessment of welded joints should address material microstructure, elastic-plastic response of the material under cyclic deformation, and modes of failure at the joints. There are also other influencing variables resulting in crack initiation where the local stresses and strains are highly concentrated [3].

Table 1.2 introduces all critical parameters affecting fatigue crack initiation in reference to the local approach in fatigue assessment of welded joints.

Table 1.2 Factors affecting fatigue crack initiation [7].

Structural member	Surface	Material
Shape	Roughness	Type
Size	Hardness	Alloy
Dimensions	Residual stress	Microstructure
Loading type	**Loading spectrum**	**Environment**
Stress amplitude	Amplitude spectrum	Temperature
Mean stress including residual stress	Amplitude sequence	Corrosion
Multiaxiality including phase angle	Rest periods	

1.3 Parameters affecting fatigue cracking in welded joints

Weld toes in welded joints are more likely places for crack initiation when subjected to cyclic stresses. The variables influencing the fatigue life of a welded joint consist of [8]:

- *Applied stress amplitude*: The magnitudes of the axial or bending stresses at the weld toe (ΔS_{axial} or $\Delta S_{bending}$) greatly affect the fatigue strength of a welded joint.

- *Material properties*: Strain-controlled fatigue properties (σ'_f, ε'_f, b, c) determine the resistance to crack nucleation and early crack propagation. The residual stresses in the weldment are limited by the metal's yield strength (S_y); therefore, yield strength of the welded joint base metal is of great significance, specially in non-stress relieved weldments.

- *Geometrical stress concentration effects*: The concentration of stress and strain at a notch/weld toe, increases the effects of the applied stress; therefore, notches reduce the fatigue life, specifically the crack nucleation life (N_i) and the early crack growth life (N_{P1}). The effects of the notch are taken into consideration by the fatigue notch factor (K_f), which influences N_i and N_{P1}.

- *Size and location of welding defects*: Weld defects, also known as welding discontinuities, both at the notch root and elsewhere, magnify the stress-concentrating effects of the critical notch, and can greatly reduce crack initiation life, N_i, short crack growth life, N_{P1}, and long crack growth life, N_{P2}.

In addition to the above mentioned variables, mean and residual stresses also influence fatigue life of a weld.

CHAPTER TWO

Global and local approaches of fatigue damage assessment

Diverse approaches are used for the fatigue analysis of welded joints, differentiated from one another by the factors used for the description of fatigue strength S or fatigue life N. Strength assessments are named 'global approaches' if they result from external forces or nominal stresses in the critical cross section under constant stress distribution assumption, also named 'nominal stress approach'. Strength assessments are named 'local approaches' if they result from local stress or strain parameters. The local damage that is the stress raiser appears as crack initiation, crack propagation and final fracture. Crack initiation is defined by 'notch stress approach' or 'notch strain approach' based on stresses or strains at the notch root. Crack propagation and final fracture are explained by the 'crack propagation approach' that results from an existing crack already present in the welded joint. Thus, a complete local stress assessment consists of notch stress or strain and the crack propagation approach. An approach that relates the global and local concepts is the 'structural stress approach'. It must be noted that the stress concentration resulting from the weld macro-geometry reflects the considered notch effect of the weld, lowering the S-N curve as an outcome. Generally, fatigue damage approaches are categorized as [2]:

- Nominal stress approach; utilizes the nominal stress range, $\Delta\sigma_{nom}$, established by internal or external loads and the related cross section characteristics.
- Structural or hot spot stress approach; utilizes the structural stress range, $\Delta\sigma_s$, near to the welded region, considering the structural discontinuity effect.
- Notch stress approach; utilizes the elastic notch-stress range, $\Delta\sigma_k$, considering the notch effect of the weld toe (or weld root).
- Notch strain approach; utilizes the local elastic-plastic strain range, $\Delta\varepsilon_k$, explaining the related material damage procedure.
- Crack propagation approach; utilizes the J-integral or stress-intensity range, ΔK, explaining the crack propagation rate, da/dN.
- Notch intensity approach; utilizes the weld notch-stress intensity considering the notch effect of the weld toe.

Figure 2.1 shows the different parameters together with characteristic diagrams, subdividing the approaches into different classes.

| Cross section | Structural discontin. | El. notch effect | El.-pl. notch effect | Short crack | Long crack |

| Cyclic load | Cyclic nominal stress | Cyclic structural stress | Cyclic notch stress | Cyclic notch strain | Cyclic J-integral | Cyclic stress intensity |
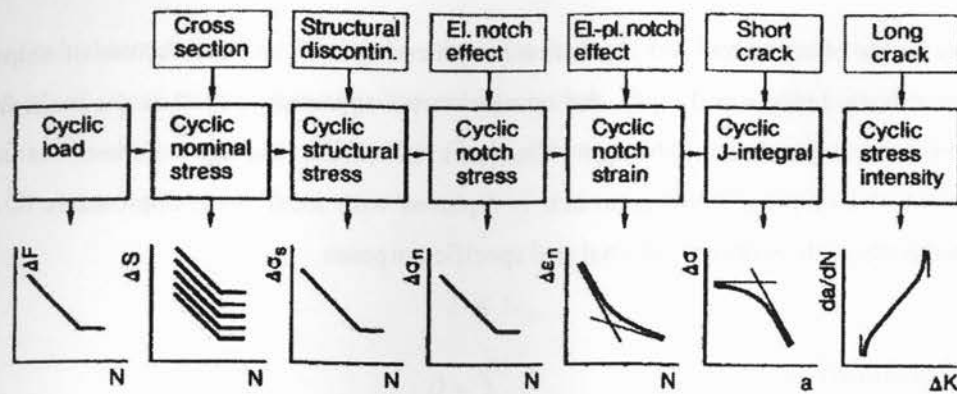
Figure 2.1 Global and local approaches subdivided into separate classes for describing the fatigue strength and life of weldments [9].

The local approaches evaluate the fatigue strength of welded joints by means of improving components, joint geometry and design based on local stress/strain factors. Fatigue damage based on local stress/strain parameters includes both crack initiation and propagation stages. These local approaches replace the older nominal stress approach, resulting in enhancement in fatigue and lifetime assessment of welded joints.

The present chapter reviews various stress based and strain based approaches and the fracture mechanics approach, employed for fusion-welded joints in the literature. Approaches are discussed for their formulation, parameters involved and applicability to fatigue assessment.

2.1 Nominal stress approach

2.1.1 Principals

The nominal stress approach is a basic method to evaluate fatigue strength and life assessment, based on the applied nominal stress in the critical cross section of the welded joints. The nominal stress-fatigue life (*S-N*) curve is classified dependant on material, notch, joint attachment specifications and weld quality classes. The nominal stress is defined in the

cross section of the base plate. The nominal stress approach is essential to design codes and guidelines [3].

In many fields of structural and mechanical engineering such as manufacture of ships, rail vehicles, cranes, bridges and pipes, the nominal stress approach is used as the main fatigue assessment method. For lightweight structures in which damage tolerance is a key assessment, the nominal stress approach is replaced with local stress approaches in code-regulated parts such as unconventional and specific purposes.

2.1.2 Formulation

The nominal stress (σ_{na}) is related to the number of fatigue cycles, N, through a power law equation [3]:

$$\sigma_{na} = \sigma_{na(E)} (\frac{N_E}{N})^{1/k} \quad (N \leq N_E) \tag{2.1}$$

where $\sigma_{na(E)}$ is the constant amplitude endurance limit, which is related to N_E ($N_E = 10^7$ cycles for axial loading or $N_E = 10^8$ cycles for shear stresses and $k = 3.0$ for normal stresses or $k = 5.0$ for shear stresses according to IIW recommendations) [6].

The actual nominal stress amplitude, σ_{na}, should not pass the permissible nominal stress amplitude, $\sigma_{na(per)}$. The permissible stress amplitudes are derived using the endurance amplitude, by introducing the safety factor j_σ:

$$\sigma_{na} \leq \sigma_{na(per)} \tag{2.2}$$

$$\sigma_{na(per)} = \frac{\sigma_{na}}{j_\sigma} \tag{2.3}$$

The permissible cycles, N_{per}, and the number of cycles at endurance limit, N_E, are related by the safety factor j_N ($j_N = (j_\sigma)^k$):

$$N \leq N_{per} \tag{2.4}$$

$$N_{per} = \frac{N_E}{j_N} \qquad (2.5)$$

The nominal stress approach due to its simplicity is used with Miner's rule to assess fatigue damage of welded structures under stress cycles. Based on Miner's damage rule, accumulation of damage over life cycles, D, should not exceed the permissible total damage, D_{per} ($D_{per(max)} = 1.0$):

$$D \le D_{per} \qquad (2.6)$$

$$D = \sum_{i=1}^{m} \frac{n_i}{N_f} \qquad (2.7)$$

where n_i is the progressing cycle and N_f is the number of cycles to failure (i=1,2,…,m).

Fatigue life is estimated from accumulated damage as:

$$N = \frac{1}{\sum_{i=1}^{m} \frac{n_i}{N_{fi}}} \qquad (2.8)$$

2.2 Structural stress or strain approach

The structural stress approach is employed for fatigue strength and life assessment of welded joints at which geometry of the joint results in an increase of stress at the notch root. The structural stress approach evaluates the stress distribution at certain distances away from the weld to minimize the effect of stress concentration in the welded joint. Figure 2.2 schematically shows that the stress distribution decreases as the distance from the weld toe increases.
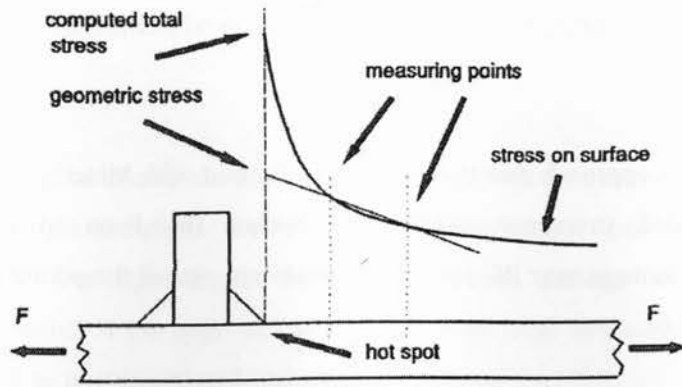
Figure 2.2 Stress distribution ahead of a welded joint subjected to axial load [6].

The structural stress approach minimizes the stress concentrations due to the welded joint profile itself. The local stresses, however, are normally greater than nominal stresses due to structural discontinuities. In fatigue assessment, the geometric stress is determined at the critical point of a welded joint (referred to as the 'hot spot'). The fatigue crack initiation most likely takes place at this point due to the presence of a notch. This approach is used for complicated geometric shapes where there is no clearly defined nominal stress and where the structural discontinuity cannot be compared to any of the classified structural details as shown in figure 2.3 [6].
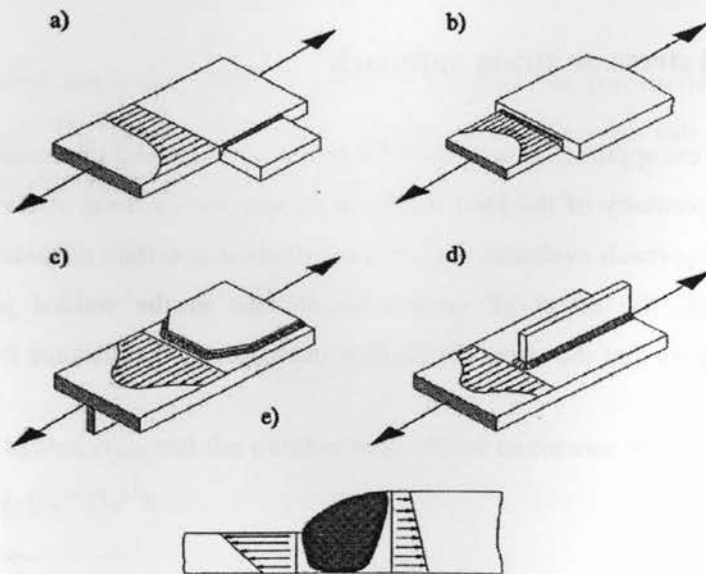
Figure 2.3 Stress in welded joints with complicated geometric shapes [6].

2.3 Notch stress approach

2.3.1 Principals

The fatigue strength of a structural component depends greatly on stress concentration in the presence of notches. The method is most applicable for welded joints subjected to constant amplitude loading conditions. This approach assumes no considerable plastic deformation induced at the notch root, and that deformation at the notch root is dominantly elastic. The endurable limit of the structural component is slightly reduced according to the elastic stress concentration. The elastic stress concentration factor is determined by geometry and loading of the structural component. It is dependent on the dimensional ratios but not on dimensions or elastic modulus. The fatigue notch factor depends on the notch radius in addition to the parameters controlling the stress concentration factor.

The notch-stress approach theories that are widely employed for fatigue strength assessment of welded joints are:
- the stress averaging approach originally proposed by Neuber [10]
- the critical distance approach proposed by Peterson [11]
- the highly stressed volume approach originally proposed by Kuguel [12]

Only small differences were found in the calculated fatigue strength values when comparing these theories [3].

2.3.2 Formulation

Due to the dominancy of the elastic deformation at the notch root, both the elastic notch approach and the nominal stress approach show similar response in fatigue assessment of welded joints. The relationship between the fatigue-effective notch stress amplitude, $\sigma_{k(eff)a}$, and the related nominal stress amplitude, σ_{na}, is given as:

$$\sigma_{k(eff)a} = K_f \times \sigma_{na} \qquad (2.9)$$

where K_f is the fatigue notch factor and the following relations stand:

$$\sigma_{k(eff)a} \leq \sigma_{keffa(per)} \tag{2.10}$$

$$\sigma_{keffa(per)} = \frac{\sigma_{k(eff)A}}{j_\sigma} \tag{2.11}$$

where terms $\sigma_{keffa(per)}$ and j_σ in the equations, respectively correspond to the permissible fatigue-effective notch stress amplitude and the safety factor.

The present fatigue-effective notch stress amplitude depends on the fatigue notch factor and the nominal equivalent stress amplitude. The equivalent endurable fatigue-effective notch stress amplitude depends on failure probability, the considered number of cycles until failure, the mean stress and the material condition [3].

2.3.3 Notch stress concentration factor and fatigue notch factor

The elastic notch stress concentration factor, K_t, is defined as the ratio of the maximum notch stress, σ_k, also known as the local stress (σ_{loc}), to the nominal stress, σ_n (σ_{nom}), determined under linear elastic deformation:

$$K_t = \frac{\sigma_k}{\sigma_n} \tag{2.12}$$

The elastic notch stress concentration factor can be either calculated through formulae or obtained from diagrams for standard welded joints (see Appendix D). This factor is required to find the elastic fatigue notch factor, K_f. The elastic fatigue notch factor, K_f, is similarly defined as the ratio of the fatigue effective notch stress and the nominal stress amplitude (see Equation 2.9). This factor is also obtained from the endurance limit (at $N_E = 10^6$ to 10^7 cycles) of the polished specimen without a notch (the stress amplitude σ_{aE}) to the endurance limit of the notched specimen (the nominal stress amplitude $\sigma_{na(E)}$) in the absence of mean stress ($\sigma_m = 0$) [3]:

$$K_f = \frac{\sigma_{aE}(K_t = 1)}{\sigma_{na(E)}(K_t > 1)} \tag{2.13}$$

The 'fatigue notch' and the 'stress concentration' factors for welded joints are related by a material-dependant notch sensitivity factor q:

$$q = \frac{K_f - 1}{K_t - 1} \qquad (2.14)$$

Diagrams in figure 2.4 present the variation of K_t and K_f as the q factor changes. This figure shows that, as notch radius, ρ, increases, the change in K_t is more pronounced than that of the K_f factor [3].
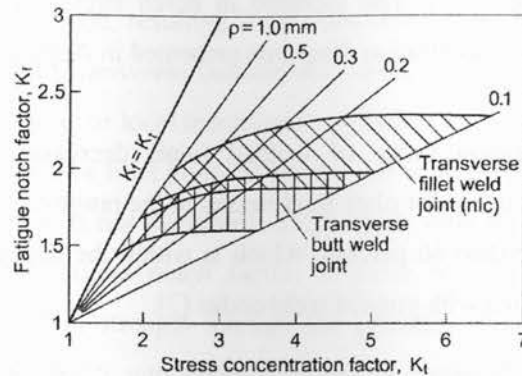
Figure 2.4 Fatigue notch factor of welded joints (nlc: non-load carrying) as function of the stress concentration factor under constant notch sensitivity factor conditions and various notch radius ranges.

It must be noted that if the fatigue notch factor, K_f, can be calculated and if material conditions at the crack site are the same as the parent metal, K_f is preferred to notch stress-intensity factor, K_t, according to Topper's suggestion in 1969 [13]. Because fatigue cracks in welded joints initiate at the weld toe (base metal) and propagate through the base metal, encompassing the characteristics of the parent metal, the fatigue notch factor replaces the notch stress-intensity factor, K_t.

14

2.3.4 Effect of geometrical weld parameters on fatigue strength of welded joints

The fatigue strength of welded joints depends directly on the elastic notch stress-concentration factor, K_t, and the elastic fatigue notch factor, K_f. The existence of a welded joint as a stress raiser results in the increase of the notch stress-concentration factor, K_t, and the fatigue notch factor, K_f. Any increase in K_t and K_f is a basis for the decrease in fatigue strength in welded joints. The notch effect is also pronounced with plate thickness, weld toe radius, weld toe undercut depth, weld reinforcement height, weld toe angle or weld angle, notch opening angle and weld reinforcement width. Only the first three parameters have major influence, whereas the reinforcement height has less influence and notch angle and weld width can be neglected [3]. The increase in notch stress-concentration factor K_t is evident in the notch stress-concentration diagrams presented in Appendix D.

The notch stress-concentration factor of welded joints decreases with increasing plate thickness. It has been shown that for plate thicknesses in the range of 2-150 mm, the decrease in fatigue strength is more than 60 percent, which is within the acceptable range of welded joint design curves associated with present weld codes [7].

The fatigue notch factor of welded joints is also influenced by weld toe angle or weld angle. Its effect has already been studied for the double-V butt-welds and the cruciform joint with flat fillet welds in tensile and bending loading conditions. The stress concentration factors, for the two main weld joints mentioned, increase as weld angle increases below 60° stating that the weld angle should be reduced as far as possible. In addition, it has been found for fillet and cruciform joints that the increase in weld root face length to base metal thickness ratio results in the increase in the stress concentration factor, concluding that the weld root face length should be reduced by decreasing the base metal thickness in the weld root [3].

Weld toe undercut is a defect that happens at the weld toe with the occurrence of the welding process, shown in figure 2.5. It reduces the fatigue strength of welded joints. The IIW guidance defines this reduction as being dependant on undercut depth, a, and radius, ρ, and plate thickness, t. The typical undercut depth and notch radius are: $0.05 < a < 1.1$ mm, $0.005 < \rho < 1$ mm, respectively [3].
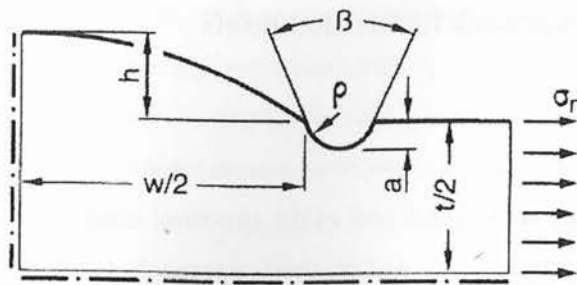
Figure 2.5 Cross sectional schematic model of welded joint with undercut defect [3].

A weld grinding procedure is used for removing the undercut and defects at the weld toe and to decrease the weld toe angle, resulting in an even changeover between the weld metal and base metal. In the case of transverse butt-welded joints, the excess weld metal or weld cap can be removed completely, or local treatment by grinding the weld toes can be performed on the weld edges. In the case of fillet joints, if grinding is to be performed, it must be made sure that weld throat thickness is not decreased, resulting in weld throat failure or as previously mentioned, increase in fatigue notch factor. It must be noted that in order to obtain appropriate improvement in strength through toe grinding, the process must penetrate the base metal surface about 0.5 mm under any visible undercut, also resulting in a slight decrease in the local plate thickness, which leads to a fatigue notch factor decrease [4,14].

Weld defects such as small, sharp, slag intrusions, are unavoidably present at the weld toe, like undercuts, and act as crack initiation sites, and thus are a significant variable in weld fatigue. Examinations have shown that the average depth of these defects is 0.15 mm and the maximum depth is 0.4 mm. It has also been suggested that high quality welds contain defects up to 0.1 mm. With respect to the relation between present welding defects and their effect on fatigue life, there are two main views: one suggesting that the fatigue life is dominated by the crack propagation process, and the other different view suggesting that the fatigue strength of welded joints is made up of crack initiation and propagation [15].

2.4 Notch strain approach for welded joints

2.4.1 Principals

The stresses and strains at the notch root of the structural component are calculated resulting from the cyclic stress-strain curve and Neuber's approach. In addition, the effect of micro-structure has to be considered due to sharp notches. The notch root strain can also be measured using a strain gauge [3].

Although the combination of the notch strain approach for crack initiation and the crack propagation approach have been applied to welded joints frequently, the extent of agreement with empirical results has not always been satisfactory. The reason for this is that the notch-strain approach was originally designed for medium-cycle fatigue in mild notches in homogeneous material, whereas welded joints are inhomogeneous material with sharp notches with high-cycle fatigue range application.

Application of the variants of the notch strain approach is only likely if the micro-structural notch support effect is considered. Notch stresses and strains can either be introduced without accounting for this effect, using the notch stress concentration factor, K_t, or by considering its effect, using the fatigue notch factor, K_f. The result of combining the notch strain and crack propagation approaches is shown in the schematic S-N curve in figure 2.6. Prevailing elastic conditions are considered in the high-cycle fatigue range.
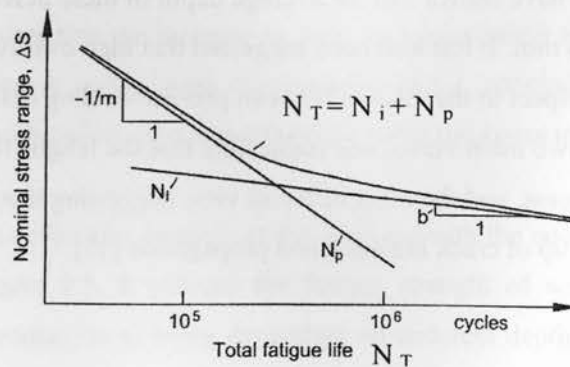
Figure 2.6 Schematic S-N diagram of a welded joint resulting from combining notch strain and crack propagation approaches related to crack initiation life N_i and crack propagation life N_p respectively, with exponents m and b respectively in the Paris and Basquin equations [3].

Different types of welded joints with crack initiation sites have been shown in figure 2.7. The scatter in fatigue strength is inversely associated with K_f. In addition, welded joints with greater fatigue resistance show more scatter in their S-N diagrams (for the ripple and toe class welds) and the slopes in their S-N diagrams are more nearly horizontal [8].
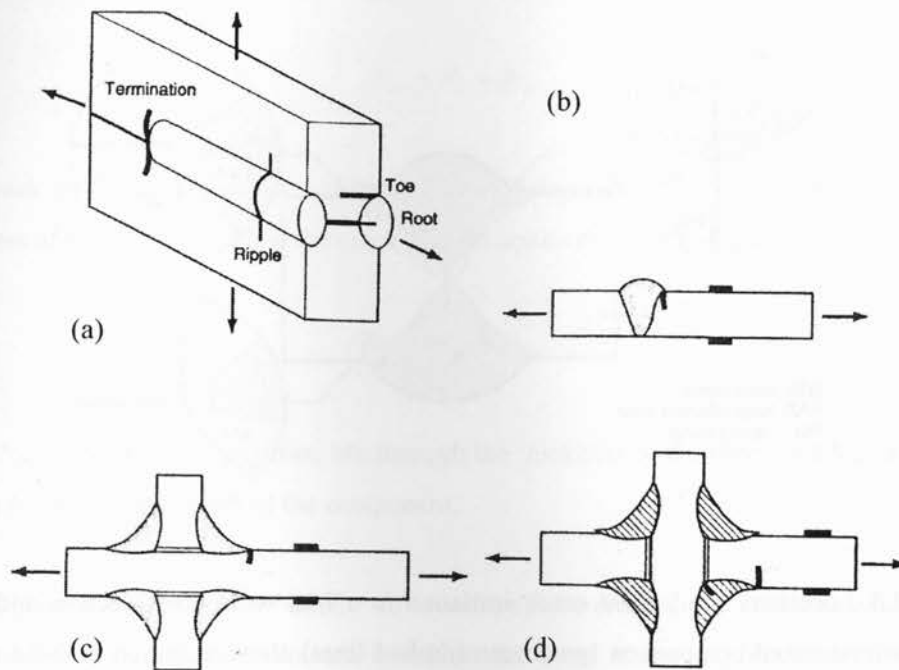
Figure 2.7 Failure locations in welded joints. The termination and ripple are fatigue crack initiation sites only when the applied load is longitudinal and the root and toe become crack initiation sites under transverse loading (a), single V-groove butt-welded joint with fatigue crack initiation at weld toe (b), non-load carrying cruciform joint with fatigue crack initiation at weld toe (applied axial stresses) (c), and load-carrying cruciform joint with failure happening at either the weld toe (applied bending stresses) or weld root (applied axial stresses) (d) [8].

2.4.2 Application of the notch strain approach

The notch strain approach is introduced to evaluate fatigue damage of welded joints, where cracks are more likely to initiate (see figure 2.8). Critical locations are found in an elastic maximum notch stress analysis performed on the cross sectional model. Different material zones are present in these sites.
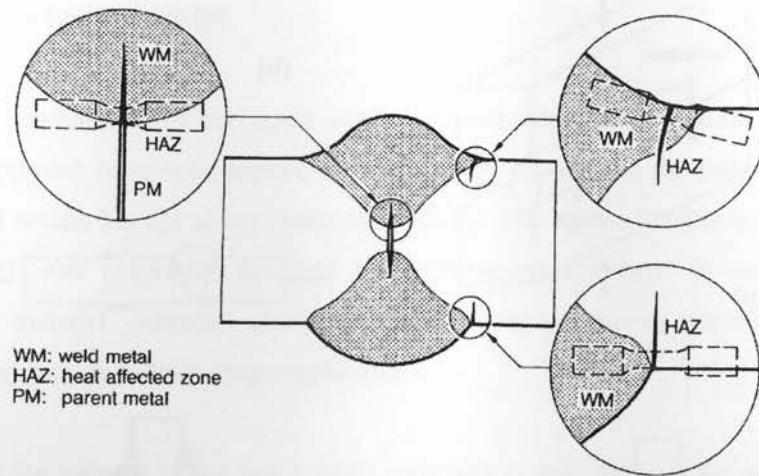
Figure 2.8 Locations for fatigue crack initiation in a butt weld cross section and related smooth miniaturized comparison specimens (dashed lines) show initiation in weld metal at weld root and in weld metal or heat affected zone at weld toe [3].

As shown in Figure 2.6, life cycles over 10^5 correspond to a dominant elastic deformation and for lives less than 10^5 cycles, cyclic plasticity is appreciable. Both the elastic and the plastic regimes are described by the Coffin-Manson equation.

Notch root stress and strain components are measures of the elastic and the plastic deformations of materials when the welded component is axially loaded. The notch stresses and strains which are the local stresses and strains at the crack initiation site are determined based on analysis of elastic-plastic stress-strain response at the notch root.

The cyclic stress-strain curve which is estimated by the Ramberg-Osgood relationship forms the hysteresis loops in the stress-strain diagram. In the low cycle fatigue regime ($N \leq 10^5$ cycles), hysteresis loops are wider, presenting a higher plastic deformation, while in the high

19

cycle fatigue regime ($N > 10^5$ cycles), the hysteresis loop reduces to a line with a dominant elastic deformation.

2.4.3 Notch analysis- life assessment

The total fatigue life, N_t, of welded joints, consists of the crack initiation life, N_i, and the crack propagation life, N_p, as:

$$N_T = N_i + N_p \tag{2.15}$$

The crack propagation life of welded joints is integrated from the propagation through thickness of the component and the crack growth across the width of the component as:

$$N_p = N_{pt} + N_{pw} \tag{2.16}$$

where N_{pt} is the crack propagation life through the thickness of the sheet and N_{pw} is the crack growth life across the width of the component.

In the high-cycle fatigue range of $N_i > 10^5$ cycles, elastic deformation is dominant. The crack initiation life can then be estimated based on the local stress amplitude using Basquin's equation including Morrow's mean stress correction as [3]:

$$\sigma_a = \frac{\Delta\sigma}{2} = (\sigma'_f - \sigma_m)(2N_i)^b \tag{2.17}$$

where σ_a is the local stress amplitude, $\Delta\sigma$ is the local stress range, σ'_f is the fatigue strength coefficient, σ_m is the local mean stress, b is the fatigue strength exponent and N_i is the crack initiation life.

The fatigue effective local stress amplitude at the weld toe, weld root, defect edge or weld location edge, which are all initiation sites for fatigue cracking, is expressed as:

$$\sigma_a = \frac{\Delta\sigma}{2} = \frac{1}{2}\Delta\sigma_n K_f \qquad (2.18)$$

where $\Delta\sigma_n$ is the nominal stress range and K_f is the fatigue notch factor.

The Ramberg-Osgood stress-strain relationship at the notch root [16], also known as the local stress-strain relationship, is expressed as:

$$\frac{\Delta\varepsilon}{2} = \frac{\Delta\sigma}{2E} + \left(\frac{\Delta\sigma}{2K'}\right)^{1/n'} \qquad (2.19)$$

where E is the elastic modulus, $\Delta\varepsilon$ is the total local strain range, $\Delta\sigma$ is the local stress range, K' is the cyclic strain hardening coefficient, and n' is the cyclic strain-hardening exponent.

The value for cyclic strain hardening exponent, n', is expressed as [3]:

$$n' = \frac{b}{c} \qquad (2.20)$$

where the fatigue strength exponent, b, and the fatigue ductility exponent, c, are obtained from the cyclic stress-strain properties table for the selected base metal.

The cyclic strain hardening coefficient, K', is expressed as [3]:

$$K' = \frac{\sigma'_f}{(\varepsilon'_f)^{n'}} \qquad (2.21)$$

where the axial fatigue strength coefficient, σ'_f, and axial fatigue ductility coefficient, ε'_f, are found from the cyclic stress-strain properties table for the selected base metal.

Neuber's equation relates the nominal cyclic stress range, ΔS (ΔS_n), and nominal strain range, Δe, to the local stress range, $\Delta\sigma$, and local strain range, $\Delta\varepsilon$, at the notch root. By substituting the stress concentration factor, K_t, with the fatigue notch factor, K_f, in Neuber's original

macro-structural formula[1], and stress and strain concentration factors (σ/S and ε/e) in the original equation, after manipulations we obtain [16]:

$$K_f^2 \frac{\Delta S \Delta e}{4} = \frac{\Delta \sigma \Delta \varepsilon}{4} \qquad (2.22)$$

After substituting the nominal and local stress-strain relationships with the nominal strain range, (Δe,), and the local strain range, ($\Delta \varepsilon$), based on the Ramberg-Osgood stress-strain relationship, the following equation is found, which is used to calculate the values of the local stresses at the weld toe for cyclic loading condition:

$$K_f^2 \times \frac{\Delta S}{2} \times [\frac{\Delta S}{2E} + (\frac{\Delta S}{2K'})^{1/n'}] = \frac{\Delta \sigma}{2} \times [\frac{\Delta \sigma}{2E} + (\frac{\Delta \sigma}{2K'})^{1/n'}] \qquad (2.23)$$

The strain-fatigue life relation by Coffin - Manson, including the mean stress effect is given by [16]:

$$\varepsilon_a = \varepsilon_{ael} + \varepsilon_{apl} = \frac{(\sigma'_f - \sigma_m)}{E}(2N)^b + \varepsilon'_f (2N)^c \qquad (N \leq N_E) \qquad (2.24)$$

The coefficients used in the stress-strain equation (2.19) and strain-fatigue life equation (2.24) are presented in table 2.1 for non-welded base metals, including steel alloys and aluminium alloys. The experimental data coefficients for base metals have been tabulated in Appendix B.

---

[1] Neuber's macro-structural formula: also known as Neuber's equation, states that the theoretical stress concentration, K_t, is the geometric mean or the square root of the product of the elastic-plastic stress concentration factor, K_σ, and the elastic-plastic strain concentration factor, K_ε, which is expressed as: $K_t^2 = K_\sigma K_\varepsilon$.

Table 2.1 Material and fatigue coefficients of base metals [3].

Material parameter	Steels, unalloyed and low-alloy	Aluminium and titanium alloys
σ'_f	$1.50\sigma_U$	$1.67\sigma_U$
b	-0.087	-0.095
ε'_f	0.59ψ	0.35
c	-0.58	-0.69
σ_E	$0.45\sigma_U$	$0.42\sigma_U$
ε_E	$0.45(\sigma_U/E)+(1.95\times10^{-4})\psi$	$0.42\sigma_U/E$
N_E	5×10^5	1×10^6
K'	$1.65\sigma_U$	$1.61\sigma_U$
n'	0.15	0.11
$\psi=1.0$ for $\sigma_U/E \leq 3\times10^{-3}$		
$\psi=(1.375-125\sigma_U/E) \leq 0$ for $\sigma_U/E > 3\times10^{-3}$		

2.5 Crack propagation approach

2.5.1 Principals

The strength and life assessment of a structural component including a welded joint based on the crack propagation approach involves notch root analysis and growth of a crack originating from the notch root. Stable crack propagation includes the cyclic growth of a micro-crack to a macro-crack with dimensions in the order of size of appropriate component dimensions, for example plate thickness. Thus, it is argued that structural components with welded joints include small initial cracks or weld flaws similar to cracks from the beginning, due to poor production situations, so that the component life can be decided based only on crack propagation.

The crack propagation rate is characterised based on the cyclic stress intensity factor, ΔK_I, for the mode I crack, or its comparable value, according to the Paris and Erdogan equation [17]. Cyclic crack propagation happens as soon as the threshold value of the stress intensity factor

is exceeded and ends as soon as a larger crack length results in reaching the load-carrying capacity of the remaining cross section. Generally, the crack path follows the pure mode I condition. The increase in crack length as the number of cycles progresses, is monitored, cycle by cycle, up to final fracture. Crack initiation life according to the notch stress or notch strain approach can be added up to the crack propagation life, found from the crack propagation approach, resulting in the total life [13].

2.5.2 Crack propagation equations; fatigue life assessment

To assess the fatigue strength and service life of welded joints, the Paris and Erdogan equation [15] is employed for estimating the crack propagation rate at the crack tip as [3,18]:

$$\frac{da}{dN} = C(\Delta K)^m \tag{2.25}$$

Fatigue life N is then calculated as:

$$N = \int_{a_0}^{a_c} \frac{da}{C(\Delta K)^m} \tag{2.26}$$

where a_0 and a_c respectively correspond to the crack size in initiation and failure stages, and ΔK corresponds to the mode I stress intensity factor range and is given as:

$$\Delta K = M_k Y \Delta \sigma \sqrt{\pi a} \tag{2.27}$$

Critical crack length, a_c, is characterised by the fracture toughness, K_{IC}, yield stress, σ_y, and crack geometry factor, Y, as:

$$a_c = \frac{1}{\pi} (\frac{K_{IC}}{Y\sigma})^2 \tag{2.28}$$

The constants C and m are material constants in equation 2.26, and the term M_k is the magnification factor related to a notch stress concentration.

Figure 2.9 schematically shows the crack growth rate versus stress intensity factor range.
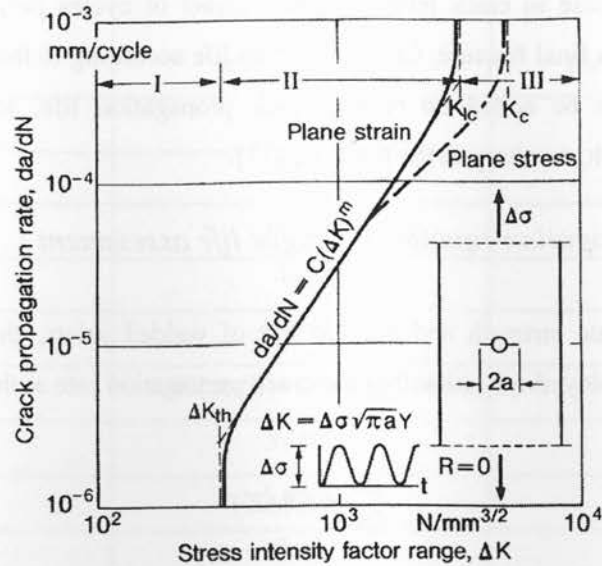
Figure 2.9 A schematic presentation for crack propagation rate under cyclic loading; typical of structural steels [3].

The following recommendation is given by the fatigue assessment code BS7608 [3] for structural steels tested in air at stress ratio=0:

$$m= 2.4\text{-}3.6, \quad C=\frac{1.315\times10^{-4}}{895.4^m}$$

The magnification factor M_k is given as (t = base plate thickness for parent metal, a = semi elliptical surface crack depth):

$$M_k = A\,(a/t)^I \tag{2.29}$$

where the coefficient A and the exponent I depend on weld toe radius, weld toe angle, attachment width and other factors. The factors recommended in BS7910 [3] are A = 0.4-0.8 and I = -0.2 to -0.3 for $a/t \lll 1.0$, and M_k = 1.0 for larger values of $a/t < 1.0$.

25

2.6 Notch stress intensity approach for welded joints

There has been no commonly approved fatigue assessment process for welded joints based on notch stress intensity factors until now, because the mentioned method is quite new. The method was applied to fillet welds until recently, when related examinations have been positively carried out on butt welds. Single groups of researchers, motivated by Lazzarin and Atzori [19,20], have developed the notch stress-intensity approach for seam-welded joints.

The weld toe and weld root notch in welded joints are important locations for fatigue crack initiation and propagation, modelled in the form of either a sharp notch or a curved notch. High stresses happen in this region that can be described by elastically established notch stress intensity factors or for higher stresses, by elastic-plastically established notch stress or strain intensity factors. In the notch stress intensity approach to the fatigue assessment of welded joints in which the weld toe is modelled as a sharp V-notch, the local stress distributions at the crack tip are given based on notch stress intensity factors related to crack modes. An averaged strain energy density at the notch corner is established using the notch intensity factors to derive a specific failure standard. This approach takes account of the notch (located at the weld toe) opening angle and the notch radius, resulting from the nominal stresses.

There is a stress field present close to corner notches just like stress fields close to crack tips, which can be described by stress intensity factors, named 'notch stress intensity factors', different from the typical stress intensity factors related to crack tips. The stress field at a sharp corner notch can be specified by three notch loading modes, similar to the crack opening modes; symmetric mode I stress, anti-symmetric mode II stress and mode III stress. The related notch loading stress modes are normal tension stress, σ_{nt}, transverse shear stress, $\tau_{n(per)}$, and longitudinal shear stress, $\tau_{n(par)}$. For the notch stress components, the following equations are derived [3]:

$$\sigma_\varphi(r,0) = \frac{1}{\sqrt{2\pi}} K_1 r^{\lambda_1-1} \quad \text{(mode I)} \tag{2.30}$$

$$\tau_{\varphi r}(r,0) = \frac{1}{\sqrt{2\pi}} K_2 r^{\lambda_2-1} \quad \text{(mode II)} \tag{2.31}$$

$$\tau_{\varphi z}(r,0) = \frac{1}{\sqrt{2\pi}} K_3 r^{\lambda_3-1} \quad \text{(mode III)} \tag{2.32}$$

For this purpose, a cylindrical coordinate system shown in figure 2.10 is used with the z axis normal to the r-φ plane.
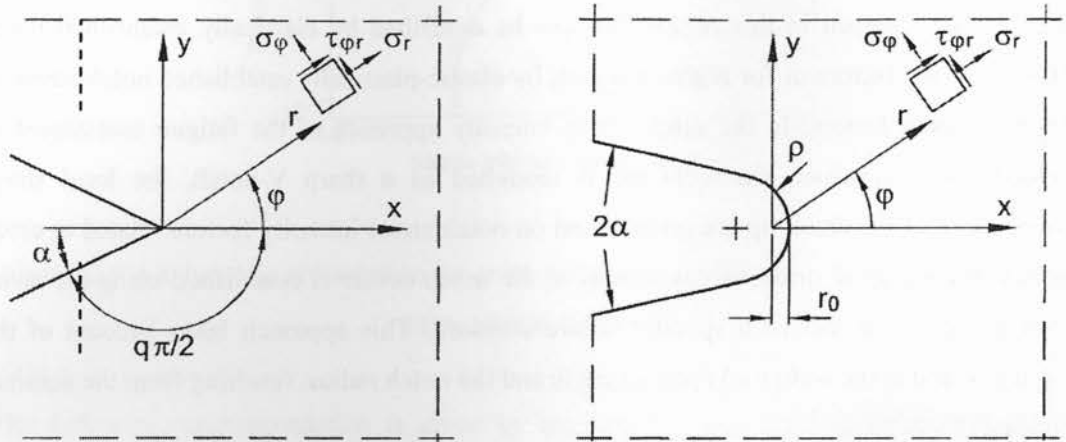
Figure 2.10 Coordinate systems, symbols and notch stresses [3].

The notch stress intensity factors K_1, K_2 and K_3 that refer to the loading modes I, II and III, depending on the geometrical parameters such as notch depth and loading condition (tension or bending) are established. The factor $\frac{1}{\sqrt{2\pi}}$ can be replaced by $(2\pi)^{\lambda_1-1}$, $(2\pi)^{\lambda_2-1}$ and $(2\pi)^{\lambda_3-1}$, respectively, in equations (2.30), (2.31) and (2.32). The parameters λ_1, λ_2 and λ_3 in the exponent show the first eigenvalue depending only on the notch opening angle. The value for λ is 0.5 for crack tips (sharpest notch), $2\alpha = 0$, and 1.0 for straight edges (no notch), $2\alpha = \pi$. The eigenvalues λ_1, λ_2 and λ_3 are shown in figure 2.11.
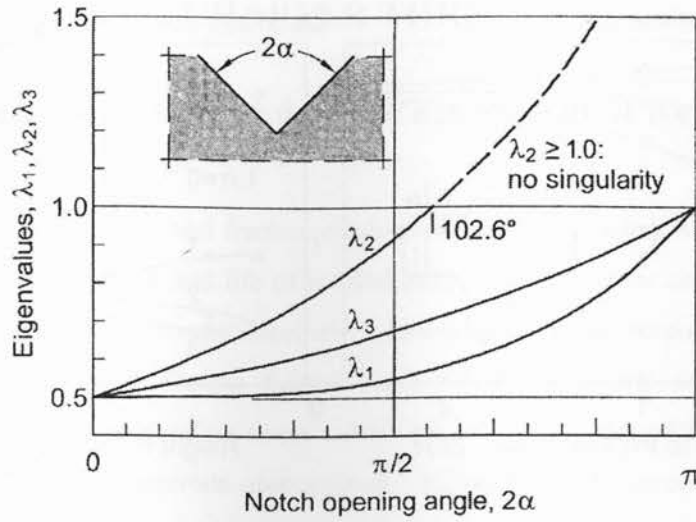
Figure 2.11 Eigenvalues λ_1, λ_2 and λ_3 versus notch opening angle diagram for mode I, II and III loading conditions [3].

The dimensions of the notch stress intensity factors K_1, K_2 and K_3 are $N/mm^{1+\lambda 1}$, $N/mm^{1+\lambda 2}$ and $N/mm^{1+\lambda 3}$, respectively. Considering a cross-section with net section width t in front of the notch, this width can be put identical to the plate thickness in a welded joint. The result of the notch stress intensity factors can thus be expressed in the following form [3]:

$$K_1 = k_1\,\sigma_{nt}\,t^{1-\lambda 1} \quad \text{(mode I)} \tag{2.33}$$

$$K_2 = k_2\,\tau_{n(per)}\,t^{1-\lambda 2} \quad \text{(mode II)} \tag{2.34}$$

$$K_3 = k_3\,\tau_{n(par)}\,t^{1-\lambda 3} \quad \text{(mode III)} \tag{2.35}$$

where k_1, k_2, and k_3 are non-dimensional geometry coefficients depending on the shape and dimension ratios of the notch. These coefficients can be determined from figure 2.12.

28
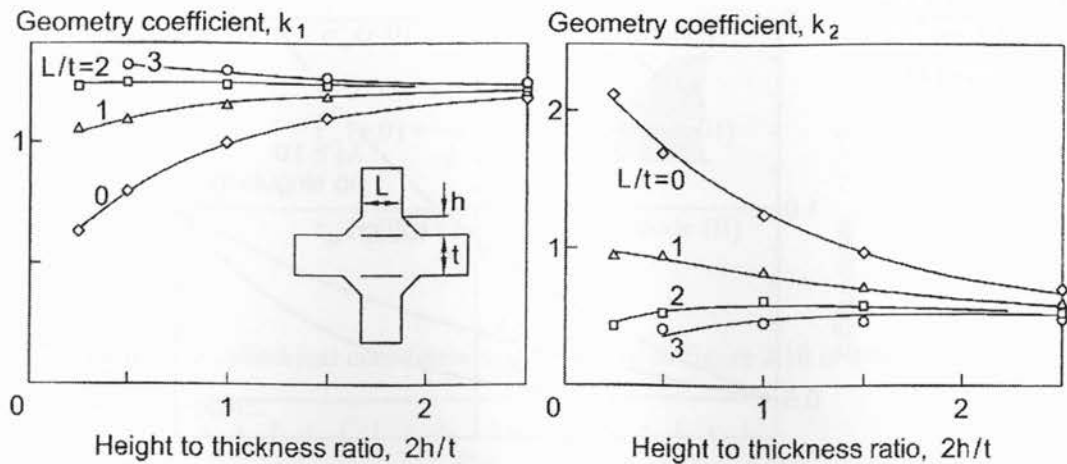
Figure 2.12 Geometry coefficients for weldments subjected to tension load [3].

The next chapter focuses on the strain energy density averaged in a small volume around the notch tip or fillet weld toe with a material dependant radius as a fatigue relevant parameter, with changing notch or weld toe opening angles and with varying stress ratios, under conditions of local yielding at the notch tip. In this regard and for the means of evaluating the total strain energy, the definitions defined through the equations in this section, such as the notch stress-intensity factors, will be used again in the strain energy method equation that will be further explained in the related energy method approach.

CHAPTER THREE

Energy methods in fatigue damage assessment of welded joints

The strain-based, stress-based, and fracture mechanics-based approaches were evaluated for assessment of fatigue strength and life of welded joints in the previous chapter. Stress and strain-based criteria lack in comprehensively addressing materials response required for fatigue damage assessment. During fatigue cycles, both the elastic and plastic strain components and their corresponding stress values are involved to describe fatigue damage phenomena on the tested materials appropriately. Accordingly, the stress-based or strain based approaches cannot adequately evaluate the fatigue response of materials. To modify damage approaches and to construct precise continuum mechanics fundamentals, the fatigue approach should include both the stress and the strain components. Energy-based approaches were introduced for this purpose. These approaches incorporate both stress and strain in damage assessment of materials.

In applying energy-based failure approaches it has been found that energy-based damage parameters can combine the damage caused by different types of loading. In addition, it is possible to analyze the damage accumulation of notched components through the energy approach [21]. It has been confirmed that in the case of large numbers of cycles, the stress and energy models are the best for explaining fatigue, and for a small number of cycles the strain and energy models are superior. Thus, the energy model seems to be universal [22].

In each category of welded joint, varying from butt welded joint to cruciform joint, the weld toe geometry is mainly comparable to an open notch. The energy approaches describe the simultaneous stress-strain situation in the area near to the weld toe, concerned by the fatigue damage progress. In this regard, in welded joints subjected to cyclic loading, the highly stressed regions where cracks initiate and spread are normally located at weld toes and roots. Studying the stress-strain regions near the crack initiation locations is an interesting problem, especially when the goal of the study is to create direct relations between energy values, fatigue strength, and factors influencing fatigue, of the structural welded components [23].

This chapter discusses energy-based methods available in the literature for fatigue assessment

of welded joints. Energy-based approaches are described in detail in the present chapter and will be employed for fatigue assessment of welded joints in the following chapters. Energy approaches examined in this chapter, chosen to be the most popular, and different in methodology, are:

- Hysteresis loop energy method
- Fracture mechanics energy approach; known as notch stress-intensity method
- Critical plane/energy method

The Masing material type hysteresis loop energy method is estimated from stress-strain hysteresis loops, generated by a symmetric doubling of Masing's rule. This energy method has been evaluated to assess fatigue damage of welded joints with low alloy steels and carbon steels as parent metals [24]. The energy-based fracture mechanics approach is a notch stress-intensity based method developed lately [25]. This approach was evaluated by means of the numerical simulations and the experimental verifications are yet to fully support the method to assess fatigue damage in butt-joint welds. The critical plane/energy damage model accounts for states of stress through combining the normal and shear strain and stress ranges acting on the critical plane, and has shown success in evaluating fatigue damage of notched metallic specimens. The model will be used to assess the fatigue of welded joints in this study. Energy-based approaches will be discussed for their parameters, formulations and applicabilities.

3.1 Hysteresis loop energy method

As previously mentioned structures and components are often subjected to cyclic loads leading to deformation. In addition, many structures and components that include welded joints are severe stress raisers. At these stressed sites, the local stress and strain will exceed the elastic limit. Such situations are very common; resulting in early failures in parts planned for long life applications. The basic fatigue curve for a specific material provides the designer the pertinent material data required to design against failure under dynamic loads. Since fatigue damage is usually caused by elastic-plastic cyclic strain, the dissipated elastic-plastic strain energy is important, and the difference between different life ranges is related to the amount of dissipated strain energy.

Many empirical studies show that most materials show a certain degree of cyclic softening and hardening during cyclic loading tests. The cyclic hardening and softening response is presented by comparing stress-strain response of materials subjected to the tensile monotonic load and the fatigue cycles. It has been found that the cyclic deformation resistance varies for the welded joints [26]: the weld metal, the heat affected zone and the base metal. For weld metals, cyclic softening happens during initial cycles; then the material achieves its stabilized stress-strain after 100-200 cycles. The heat affected zone softens slightly under cyclic loading. The base metal is clearly different from the other two zones, which are more similar in mechanical behaviour to one another. The base metal cyclically softens at low strain amplitudes. At higher strain amplitudes the material first softens and then hardens as the cyclic loading progresses [26].

The calculation of notch stresses and strains is based on the stabilized cyclic stress-strain curve. The cyclic stress-strain curve is generated by the Ramberg-Osgood equation (2.19). The stabilized cyclic stress-strain hysteresis loop diagram is estimated by Masing's hypothesis by doubling the amplitudes of the cyclic stress-strain curve for each cycle. Masing's theory allows the stabilized loop to be estimated for a material that shows symmetric behaviour in tension and compression. Figure 3.1 schematically presents a hysteresis loop generated based on Masing's theory.
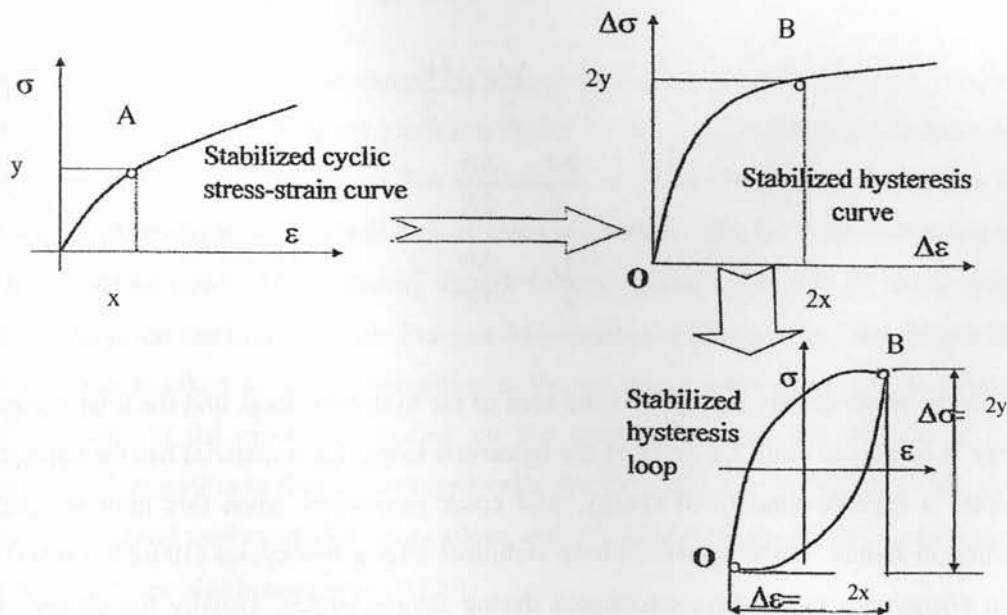
Figure 3.1 Cyclic stress-strain curve development for Masing's theory [27].

The area within the loop corresponds to the dissipated plastic energy per cycle (per unit volume of the material), representing a measure of the plastic deformation work/energy done on the material. Figure 3.2 shows the cyclic stress-strain energy area in the hysteresis loop.
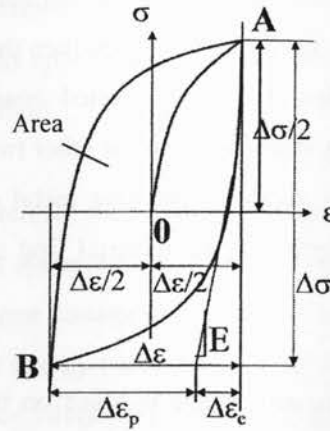
Figure 3.2 Cyclic stress-strain stabilized curve and energy area in the hysteresis loop for Masing material [17].

The Ramberg-Osgood equation (2.19) relates the local stress range and the local strain range for Masing materials, and its terms are expressed in equations 3.1 – 3.3:

$$\frac{\Delta\varepsilon}{2} = \frac{\Delta\varepsilon_e}{2} + \frac{\Delta\varepsilon_p}{2} \tag{3.1}$$

$$\frac{\Delta\varepsilon_e}{2} = \frac{\Delta\sigma}{2E} \tag{3.2}$$

$$\frac{\Delta\varepsilon_p}{2} = (\frac{\Delta\sigma}{2K'})^{1/n'} \tag{3.3}$$

The plastic strain energy per cycle is the area of the hysteresis loop, and the total dissipated energy is computed from the areas of the hysteresis loops. Each material has the capacity to dissipate a specific amount of energy, and crack propagates when this limit is reached, resulting in failure. If the hysteresis loop stabilizes after a few cycles (100-200 cycles), the strain energy per cycle stays unchanged during fatigue cycles. Usually the plastic strain energy is calculated from the hysteresis loop at half-life [28]. The plastic energy range, ΔW_p,

is calculated based on components of the stress range ($\Delta\sigma$) and the plastic strain range ($\Delta\varepsilon_p$) extracted from stabilized stress-strain hysteresis loops as [24]:

$$\Delta W_p = (\frac{1-n'}{1+n'})\Delta\sigma\Delta\varepsilon_p \tag{3.4}$$

where n' is the cyclic hardening exponent.

Substituting for the plastic strain range and the stress range from the Coffin-Manson equation, equation 3.4 is rewritten as:

$$\Delta W_p = 4\frac{1-n'}{1+n'}\sigma'_f\,\varepsilon'_f\,(2N_f)^{b+c} \tag{3.5}$$

The results of calculations for the life of welded joints, N_f, for joints made of low-alloy steels and pearlitic steels, welded by means of covered electrodes, submerged arc welding and electroslag welding, agree well with experimental test results justifying the usage of the above-mentioned equation for plastic strain energy in welded joints [24].

3.2 Fracture mechanics energy method

The geometry of the weld bead cannot be accurately defined because the weld bead shape and toe radius change in different joints due to the nature of the welding procedure even in well controlled welding operations. The weld toe is an important location for fatigue crack initiation and propagation in which high stresses are present. The local stresses at the crack tip are based on notch stress intensity factors related to mode I, II and III notch intensity factors. Based on the Linear Elastic Fracture Mechanics (LEFM) method, the fatigue life of welded joints is taken as crack propagation at the toe of the weld seam. LEFM relates the applied stress to the crack propagating on the welded joints as the number of cycles progresses. The goal is to find an averaged value for the strain energy density in the welded joints of structural steels and aluminium alloys with a V notch (angle of 135°) at the weld toe, where stresses are highly concentrated [29].

Fatigue damage includes damages generated due to failure stage. Sharp notches and the cracks emanating from the notch root, severely reduce the life of components under fatigue cycles. Lazzarin et al. [29] have introduced a strain energy density approach to estimate fatigue failure of welded joints. Based on this approach, fatigue failure occurs when the average value of the total or plastic strain energy density reaches a critical value in a cylindrical volumetric region around the notch tip with a radius R_c, independent of the loading mode. The deviatoric strain energy density ($\overline{W}_d$) components were averaged over a cylindrical sector with radius R_c, and resulted in equations 3.6 – 3.8 as [3]:

$$\overline{W}_{d1} = \frac{e_{d1}}{E}(K_1)^2(R_c)^{2(\lambda_1-1)} \quad \text{(mode I crack)} \tag{3.6}$$

$$\overline{W}_{d2} = \frac{e_{d2}}{E}(K_2)^2(R_c)^{2(\lambda_2-1)} \quad \text{(mode II crack)} \tag{3.7}$$

$$\overline{W}_{d3} = \frac{e_{d3}}{E}(K_3)^2(R_c)^{2(\lambda_3-1)} \quad \text{(mode III crack)} \tag{3.8}$$

where E is the elastic modulus, e_{d1}, e_{d2}, e_{d3} are angular function integrals depending on the notch opening angle and are determined from figure 3.3. In equations 3.6 – 3.8, λ_1, λ_2, λ_3 are the eigenvalues and K_1, K_2, K_3 are the notch stress intensity values introduced earlier in section 2.6.
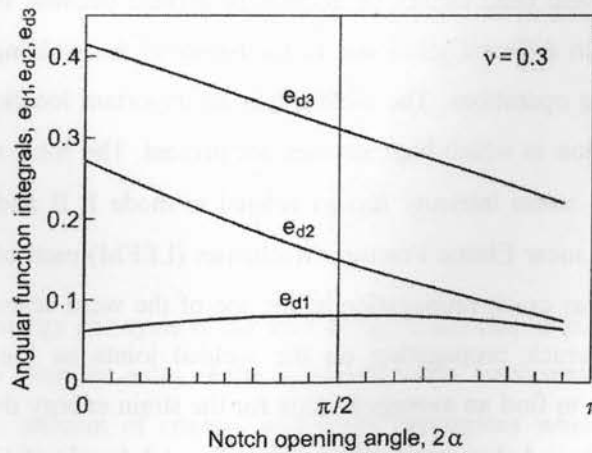
Figure 3.3 Angular function integrals e_{d1}, e_{d2}, e_{d3} (related to mode I, II, III cracks) for notch opening angle 2α [3].

An appropriate expression for the cylindrical sector radius R_c is given as [28]:

$$R_c = (\frac{(\sqrt{2e_{d1}})\Delta K_1}{\Delta \sigma})^{\frac{1}{1-\lambda_1}}$$ (3.9)

It has been found that for welded joints using the average value of the strain energy density range existing in a control volume with a radius R_c at the weld toe, R_c turns out to be 0.28 mm for welded joints made of structural steels and 0.12 mm for aluminium alloys [29].

The total strain energy ($\overline{\Delta W}$) averaged over the circular sector with its center at the weld toe and radius R_c shown in figure 3.4 turns out to be [3,29]:

$$\overline{\Delta W} = \frac{e_{d1}}{E}(K_1)^2(R_c)^{2(\lambda_1-1)} + \frac{e_{d2}}{E}(K_2)^2(R_c)^{2(\lambda_2-1)} + \frac{e_{d3}}{E}(K_3)^2(R_c)^{2(\lambda_3-1)}$$ (3.10)
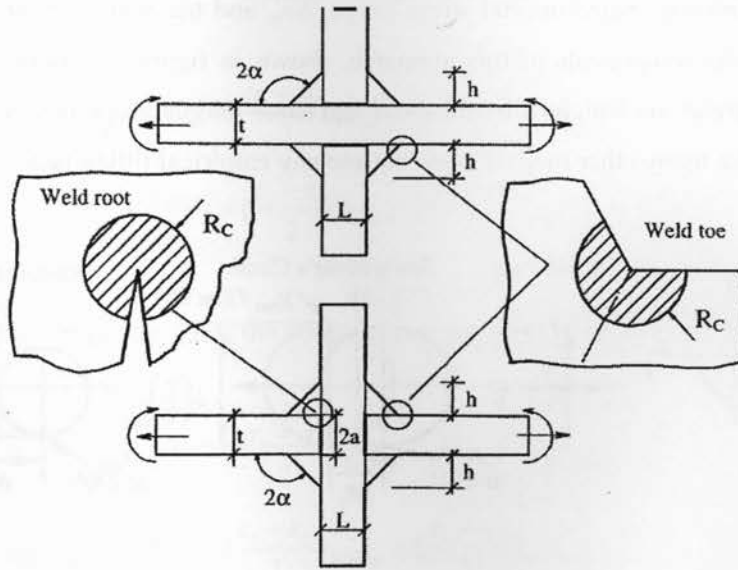
Figure 3.4 Schematic presentation of weld angle, weld root, toe position and critical volume (area) at the weld toes [30].

Equation 3.12 is referred to as Lazzarin's energy model hereafter.

3.3 Critical plane/energy method

In the critical plane-energy fatigue damage model, both the normal and the shear energies are computed on the most damaging plane of materials, referred to as the critical plane, introduced first by Varvani [31]. The critical plane/energy parameter is defined on specific planes and accounts for states of stress through combining the normal and shear strain and stress ranges. This damage approach depends upon the choice of the critical plane and the stress and strain ranges acting on that specific plane.

In Varvani's fatigue damage approach, the critical plane is defined by the largest shear strain and stress Mohr's circles during the reversals of a cycle, and the model consists of tensorial stress and strain range components acting on this critical plane. The model addresses in-phase and out-of phase fatigue and where the additional strain hardening is concerned. The range of maximum shear stress, $\Delta\tau_{max}$, and shear strain, $\Delta(\gamma_{max}/2)$, found from the largest stress and strain Mohr's circles for loading and unloading during the first and the second reversals of a loading cycle and the related normal stress range, $\Delta\sigma_n$, and the normal strain range, $\Delta\varepsilon_n$, on that plane are the components of this approach, shown in figure 3.5. Both the normal and shear strain energies are weighted by the axial and shear fatigue properties, respectively, and the model, unlike many other models, does not use any empirical fitting factor [31].
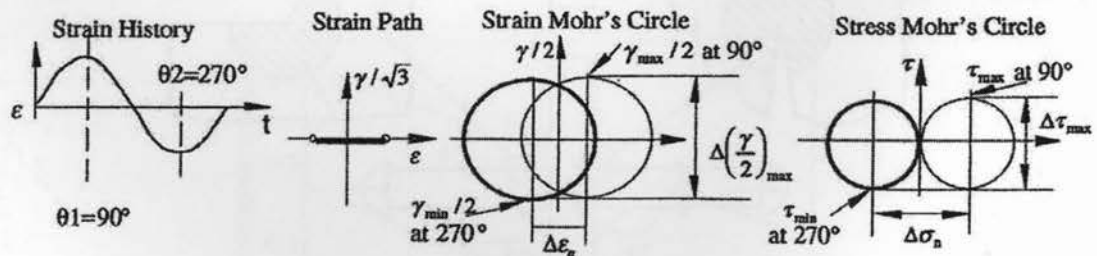
Figure 3.5 Strain Mohr's circle and stress Mohr's circle with stress and strain components of the critical plane-energy model [31].

Varvani's fatigue damage model contributes to both the normal and the shear energies acting on the most damaging plane, and it is expressed as [31]:

$$W = \frac{1}{(\sigma'_f \, \varepsilon'_f)}(\Delta\sigma_n \Delta\varepsilon_n) + \frac{1}{(\tau'_f \, \gamma'_f)}(\Delta\tau_{max}\Delta(\frac{\gamma_{max}}{2})) \qquad (3.11)$$

where σ'_f and ε'_f are the axial fatigue strength and ductility coefficients, respectively, and τ'_f and γ'_f are the shear fatigue strength and ductility coefficients, respectively.

The axial fatigue strength coefficient, σ'_f, and axial fatigue ductility coefficient, ε'_f, are found from the cyclic stress-strain properties table for selected metals. The shear fatigue strength and ductility coefficients τ'_f and γ'_f are found from σ'_f and ε'_f respectively from:

$$\tau'_f = \frac{\sigma'_f}{\sqrt{3}} \qquad (3.12)$$

$$\gamma'_f = \sqrt{3} \times \varepsilon'_f \qquad (3.13)$$

The range of maximum shear stress, $\Delta\tau_{max}$, and shear strain, $\Delta(\gamma_{max}/2)$, are calculated as:

$$\Delta\tau_{max} = (\frac{\sigma_1 - \sigma_3}{2})_{loading} - (\frac{\sigma_1 - \sigma_3}{2})_{unloading} \qquad (3.14)$$

$$\Delta(\frac{\gamma_{max}}{2}) = (\frac{\varepsilon_1 - \varepsilon_3}{2})_{loading} - (\frac{\varepsilon_1 - \varepsilon_3}{2})_{unloading} \qquad (3.15)$$

The normal stress range, $\Delta\sigma_n$, and the normal strain range, $\Delta\varepsilon_n$, are defined as:

$$\Delta\sigma_n = (\frac{\sigma_1 + \sigma_3}{2})_{loading} - (\frac{\sigma_1 + \sigma_3}{2})_{unloading} \qquad (3.16)$$

$$\Delta\varepsilon_n = (\frac{\varepsilon_1 + \varepsilon_3}{2})_{loading} - (\frac{\varepsilon_1 + \varepsilon_3}{2})_{unloading} \qquad (3.17)$$

where σ_1 and σ_3 are the maximum and minimum principal stresses and ε_1 and ε_3 are the maximum and minimum principal strains calculated from loading (90°) and unloading (270°) reversals of a cycle.

CHAPTER FOUR

Cyclic stress-fatigue life data assortment, calculations based on energy models and numerical analysis of K_t for welded joints

The available experimental data are first converted to terms required in energy approaches, and the model and the values are used accordingly to assess damage of welded joints using energy-based approaches. This chapter provides details of experimental data and testing procedures conducted by various authors and laboratories followed by the methodology of calculations for energy-based models. In addition, a numerical analysis for notch stress-concentration factor, K_t, has been carried out using finite element analysis.

4.1 Fatigue data for welded joints

To evaluate the energy based fatigue damage analysis proposed in this study, fatigue data of different types of seam-welded joints have been extracted from the available literature. Appendix A, Appendix B and Appendix C tabulate experimental data including; S-N data, stress-strain data for the material properties of the base metals of the welded joints, and specimen geometry and dimensions. The S-N tables present the nominal stress range or the maximum stress values in MPa applied to a specific welded joint versus fatigue endurance life in number of cycles. The nominal applied stresses will be used to calculate the local stresses and the fatigue lives, based on Neuber's notch analysis. It must be noted that because all welded joints selected from the literature are laboratory prepared welds, they have been considered as an 'ideal weldment' in which the fatigue crack is assumed to initiate at the weld toe, probably in the weld metal [8].

4.1.1 Chapetti et al. data

Chapetti et al. [32] performed fatigue tests on steel butt-welded specimens under transverse stress loading conditions. Simple double-sided butt-welded joints of 12.5 mm thickness were made using conventional manual metal arc welding (MMAW). Figure 4.1 (a) represents the butt-welded joint fatigue tested by Chapetti et al. The parent metal for the welded joints was a low carbon steel En2b (0.2 weight percentage carbon, 0.8 weight percentage Manganese). All

specimens were fully stress relieved at 600° C immediately and then fatigue tested with a frequency of 50 Hz and stress ratio of R=0.1. The weld cap height of h=2 mm from the base metal and the weld angle of θ=135° were held constant in their experiments. The fatigue tests on the welded specimens were performed based on uniaxial loading conditions. The S-N data generated from these experiments were extended over low and high cycle fatigue regimes. The nominal stress range versus fatigue life addressing the low and the high cycle fatigue regimes are tabulated in Appendix A. The cyclic stress-strain properties of AISI 1025 structural steel as the base metal of the welded joints are presented in Appendix B. The geometric and dimensional specifications of the welded joints are presented in Appendix C.

4.1.2 Livieri and Lazzarin data with reference to steel welded cruciform structure

Livieri and Lazzarin [30] performed fatigue tests on cruciform steel joints with non-load carrying double-fillet welds with base metal and attachment of 13 mm × 10 mm, 25 mm × 32 mm, and 38 mm × 220 mm in dimension. Figure 4.1 (b) represents the cruciform joint fatigue tested by Livieri and Lazzarin. The parent metal for the welded joint was a low carbon type steel BS 4360:50D. All specimens were 'as-welded', made using conventional MMAW. Failures systematically originated from the weld toes. The weld heights from the base metal and the weld angles on the four sides were held constant; h=8 mm and θ=135°, h=9 mm and θ=135°, and h=15 mm and θ=135° respectively. The fatigue tests on the welded specimens were performed based on a uniaxial loading condition, with stress ratio of R=0. The S-N data generated from these experiments were extended over low and high cycle fatigue regimes. The nominal stress range versus fatigue life addressing the low and the high cycle fatigue regimes are tabulated in Appendix A. The cyclic stress-strain properties of AISI 1025 structural steel as the base metal of the welded joints are presented in Appendix B. The geometric and dimensional specifications of the welded joints are presented in Appendix C.

4.1.3 Livieri and Lazzarin data with reference to aluminium butt-welded structure

Livieri and Lazzarin [30] performed fatigue tests on aluminium alloy butt-welded specimens under transverse stress loading conditions. Single sided butt-ground welded joints (removed weld caps) with a thickness of 9.5 mm were used. Figure 4.1 (c) represents the butt-ground

welded joint fatigue tested by Livieri and Lazzarin. The parent metal for the welded joint was 5083-H113 aluminium alloy. This alloy is a strong magnesium-manganese-chromium-aluminium alloy (AlMg4.5Mn), with a very good weld-ability and a high ductility property. The fatigue tests on the welded spedimens were performed based on a uniaxial loading condition, with stress ratio of $R=0$. The S-N data generated from these experiments were extended over low and high cycle fatigue regimes. The nominal stress range versus fatigue life addressing the low and the high cycle fatigue regimes are tabulated in Appendix A. The cyclic stress-strain properties of AlMg4.5Mn aluminium alloy as the base metal of the welded joints are presented in Appendix B. The geometric and dimensional specifications of the welded joints are presented in Appendix C.

4.1.4 Reemsnyder data

Reemsnyder [33] performed fatigue tests on steel butt-welded specimens under transverse stress loading conditions with different weld cap heights of $h=1.5$ mm, $h=2.3$ mm, and $h=3.8$ mm. Simple double-sided butt-welded steel joints with a thickness of 19.1 mm were used. Figure 4.1 (a) represents the butt-welded joint fatigue tested by Reemsnyder. The parent metal for the welded joint was quenched and tempered carbon steel. The fatigue tests on the welded specimens were performed based on a uniaxial loading condition, with stress ratio of $R=0$. The S-N data generated from these experiments were extended over low and high cycle fatigue regimes. The nominal stress range versus fatigue life addressing the low and the high cycle fatigue regimes are tabulated in Appendix A. The cyclic stress-strain properties of 10B21 carbon steel as the base metal of the welded joints are presented in Appendix B. The geometric and dimensional specifications of the welded joints are presented in Appendix C.

4.1.5 Webber data

Webber [34] performed fatigue tests on aluminium alloy double butt-strap fillet (lap) load carrying welded specimens under transverse stress loading conditions. Welded joints with a base metal thickness of 12 mm were used. Figure 4.1 (d) represents the butt-strap fillet welded joint fatigue tested by Webber. The parent metal for the welded joint was DGFVE 232A aluminium alloy. This alloy is a strong magnesium-manganese-zinc-aluminium alloy (Al-Zn-Mg), with a very good weld-ability property, with fatigue characteristics in between 7075-T6 and 2024-T3 aluminium alloys [35]. All specimens were 'as-welded', made using

the metal-inert-gas (MIG) process using 5.2Mg-0.7Mn welding wire with argon as the shielding gas. The weld height and weld angle in the experiments were h=12 mm and θ=135° respectively. The fatigue tests on the welded specimens were performed based on a uniaxial loading condition, with a frequency of 33 Hz and stress ratio of R=0. The S-N data generated from these experiments were extended over low and high cycle fatigue regimes. The nominal stress range versus fatigue life addressing the low and the high cycle fatigue regimes are tabulated in Appendix A. The cyclic stress-strain properties of Al-Zn-Mg aluminium alloy as the base metal of the welded joints are presented in Appendix B. The geometric and dimensional specifications of the welded joints are presented in Appendix C.
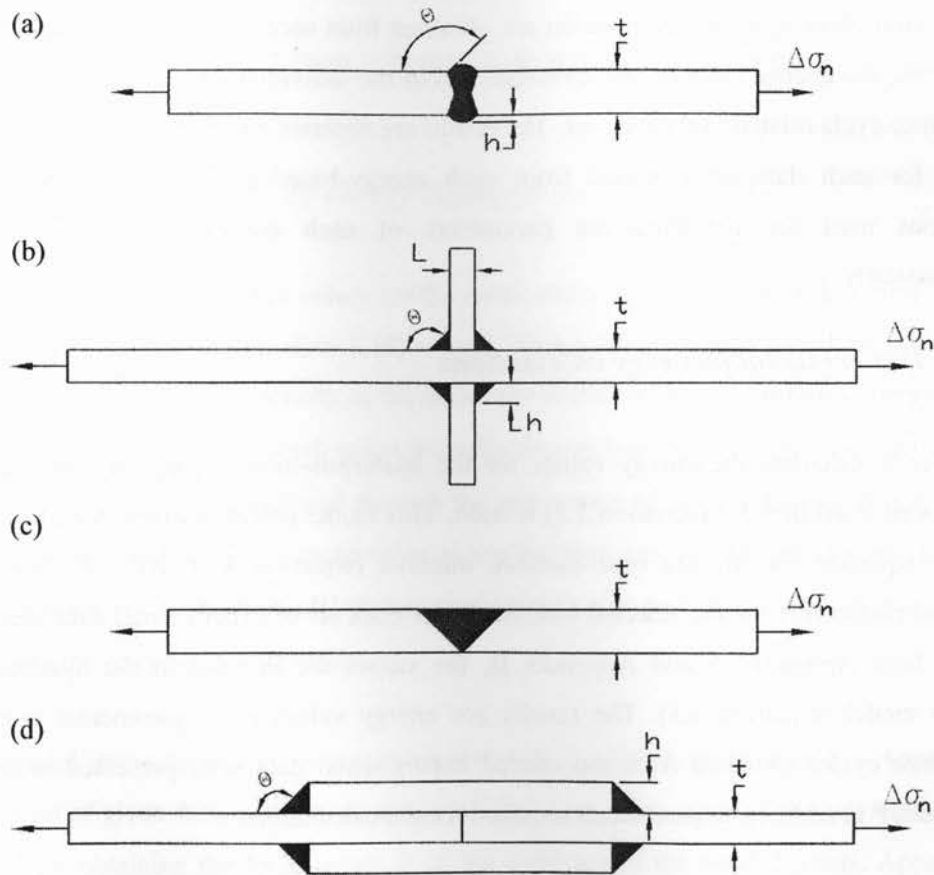
Figure 4.1 Drawings (not to scale) representing welded joints fatigue tested by: Chapetti et al. and Reemsnyder (a), Livieri and Lazzarin (cruciform joint) (b), Livieri and Lazzarin (butt joint) (c), and Webber (d).

4.2 Energy calculations for welded joints

In order to perform the calculations presented in this part, the parameters in the three energy based models introduced in chapter three are calculated separately for each model from the original experimental data obtained from the literature related to each weld joint. The data used as a basis for the calculations of the three energy based models for different weld joints include: cyclic stress-strain properties related to the base metal material type of the weld joints, dimensional and geometrical information on the weld joints, and stress versus endurance cycle tables obtained from the tests performed on the welded joints. All the mentioned variables are parameters influencing the fatigue life of a welded joint. After the terms required in each energy equation are obtained from each data set and submitted in the equations, the energy amounts are calculated from the individual energy equations for each endurance cycle related to the data set. The results are separate energy versus endurance cycle tables for each data set obtained from each energy-based equation. The methods and equations used for obtaining the parameters of each energy model are explained systematically.

4.2.1. Hysteresis loop energy calculations

In order to calculate the energy values for the hysteresis-loop energy method, the model introduced in section 3.1 (equation 3.5) is used. This model originates from the plastic strain energy equation for Masing type metallic material (equation 3.4). After finding all the required parameters for the selected base metal for each set of experimental data used in this study, from Appendix A and Appendix B, the values are inserted in the hysteresis-loop energy model (equation 3.5). The results are energy values for experimental number of endurance cycles obtained from the related experimental data sets, presented in tables in Appendix F in addition to parameters required for the calculations.

Figure 4.2 shows a general algorithm for the determination of hysteresis-loop energy values using the related criterion.
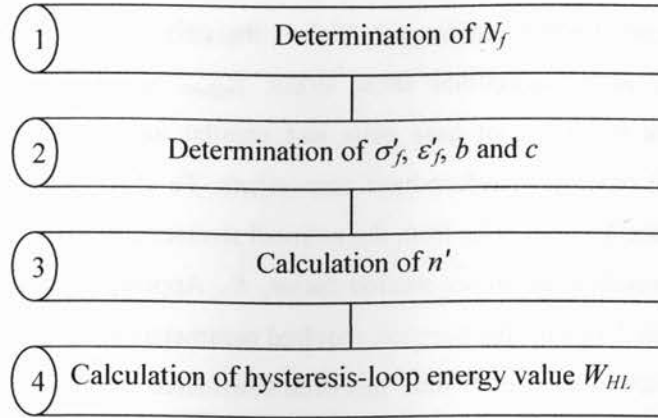
Figure 4.2 Steps in hysteresis-loop energy calculation.

4.2.2. Notch stress- intensity energy calculations

In order to calculate the energy values for the notch stress-intensity method, Lazzarin's model introduced in section 3.2 (equation 3.10) is used. This model, which is based on an averaged value for the strain energy density at the notch tip at the weld toe, combines energy values related to mode I, II and III notch stress intensity factors based on local stresses at the notch tip. The total energy value is found through the summation of mode I, II and III notch stress intensity factor energies. For a cyclic uniaxial applied load, the second and third energy terms related to the mode II and mode III stresses are equal to zero leaving the mode I stress energy as the only present energy expression.

The nominal stress range, ΔS, or maximum stress, S_{max}, which can be found in Appendix A for each set of given data, is the stress range or maximum stress, applied to each welded joint, required for obtaining the local stress, σ, at the weld toe of the welded joints. Appendix B provides all the required cyclic stress-strain properties used for some of the parameters needed for the calculations. Appendix C is used for calculating the geometry factor, k_1, required for the notch stress-intensity factor, K_1, with the assumption that the notch-opening angle has been held constant and equal to 135°. The related notch loading stress modes; normal tension stress, σ_n, transverse shear stress, $\tau_{n(per)}$, and longitudinal shear stress, $\tau_{n(par)}$, used for calculating the notch stress intensity factors, K_1, K_2 and K_3, are actually local stresses

44

at the weld toe. It must be noted that in the case of cyclic uniaxial applied stress, the local stress, S, is the normal tension stress, σ_{nt}, which is the only stress present. The transverse shear stress, $\tau_{n(per)}$, and longitudinal shear stress, $\tau_{n(par)}$, which are the shear stresses perpendicular to the welded joint base plate and parallel to the welded joint base plate respectively, are not present, therefore have zero values. To obtain the fatigue notch factor needed for finding the local stresses from the nominal stresses (equation 2.23), it is required to find the elastic notch stress-concentration factor, K_t. Appendix D is used to obtain K_t, needed for K_f (figure 2.4). For this purpose, required parameters are given in Appendix E. In this regard, a weld toe radius of 0.5 mm[1] has been considered for all joints. In addition, for the double fillet joint, a root face to base metal thickness ratio[2] of 0.5 has been considered.

After obtaining all the required parameters for each set of experimental data used in this study, the values are inserted in Lazzarin's notch stress-intensity energy model resulting in energy values related to the experimental number of endurance cycles. The local stresses obtained from the experimental nominal stresses, the calculated energy values for each local stress and the experimental numbers of endurance cycles for the nominal stresses, in addition to all of the calculated parameters in this section, for each set of experimental data used in this study, are presented in tables in Appendix F.

Figure 4.3 shows a general algorithm for the determination of notch stress-intensity energy values using the related criterion.

---

[1] The weld toe radius ranges from 0 to 1. A value of 0.5 is the average value [3].
[2] The root face thickness at the welded joint is reduced before welding in order to decrease stress concentration factor. The root face to plate thickness ratio ranges from 0 to 1; 1 resulting in the highest stress concentration factor (see Appendix D) [3].

1. Determination of e_{d1}, λ_1, E, and R_c [1]

2. Determination of K_t

3. Determination of K_f

4. Calculation of n' and K'

Notch analysis

5. Determination of nominal stress range ΔS

6. Calculation of local stress range (at the weld toe) $\Delta\sigma$

7. Determination of k_1 and t

8. Determination of K_1

9. Calculation of notch stress-intensity energy value W_{NS}
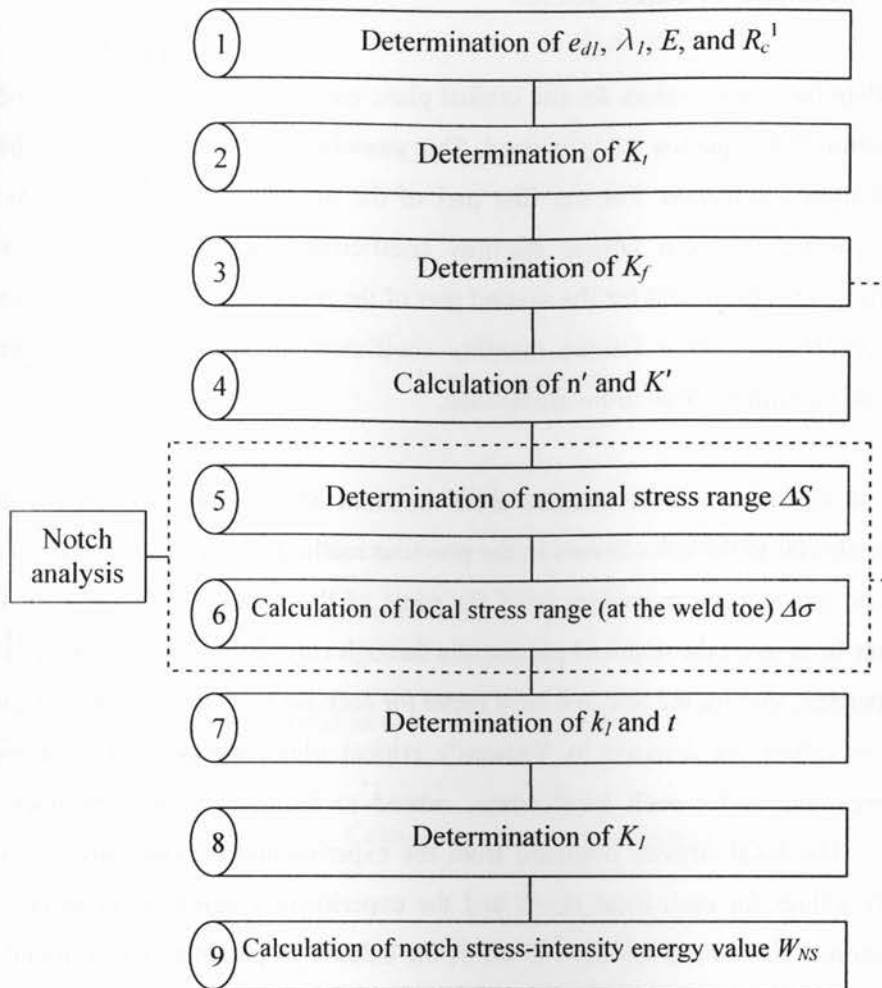
Figure 4.3 Steps in notch stress-intensity energy calculation.

[1] Cylindrical sector radius, Rc, turns out to be 0.28 mm for welded joints made of structural steels and 0.12 mm for aluminium alloys.

4.2.3. Critical plane energy calculations

In order to calculate the energy values for the critical plane/energy method, Varvani's model introduced in section 3.3 (equation 3.11) is used. This model combines the axial and shear energies through their summation. For the first part of the model, the axial energy, axial fatigue strength coefficient, axial fatigue ductility coefficient, normal stress range, and normal strain range are needed; and for the second part of the model, the shear energy, shear fatigue strength coefficient, shear fatigue ductility coefficient, range of maximum shear stress, and range of maximum shear strain are needed.

The procedure of calculating local stresses from nominal stresses and finding K_t and calculating K_f are similar to the calculations in the previous method. Appendix B provides all the required cyclic stress-strain properties used for some of the parameters needed for the calculations. After finding all the required parameters through calculations or from the cyclic stress-strain properties table for the selected base metal for each set of experimental data used in this study, the values are inserted in Varvani's critical plane/energy model equation resulting in energy values for each local stress, related to the experimental number of endurance cycles. The local stresses obtained from the experimental nominal stresses, the calculated energy values for each local stress and the experimental numbers of endurance cycles for the nominal stresses, in addition to all of the calculated parameters mentioned in this section, for each set of experimental data used in this study, are presented in tables in Appendix F.

Figure 4.4 shows a general algorithm for the determination of critical plane/energy values using the related criterion.

1. Determination of σ'_f, ε'_f and E
2. Calculation of τ'_f and γ'_f
3. Determination of K_t
4. Determination of K_f
5. Calculation of n' and K'
6. Determination of nominal stress range ΔS
7. Calculation of local stress range (at the weld toe) $\Delta\sigma$

Notch analysis

8. Calculation of principal stresses
9. Calculation of principal strains (Ramberg-Osgood equation)
10. Calculation of normal stress range $\Delta\sigma_n$ ($\Delta\tau_{max}$ is the same for uniaxial load)
11. Calculation of normal strain range $\Delta\varepsilon_n$ ($\Delta(\gamma_{max}/2)$ is the same for uniaxial load)
12. Calculation of critical plane/energy value W_{CP}

Figure 4.4 Steps in critical plane/energy calculation.

4.3 Numerical analysis of K_t for welded joints

The notch stress-concentration factor, K_t, at the weld toes of the welded joints is defined as the ratio of the local stress at the weld toe and the nominal stress applied to the welded part (equation 2.14). The nominal stress corresponds to the load applied to the gross cross sectional area of the structure, while the maximum notch stress corresponds to the peak stress at the weld toe. The maximum notch stress can be obtained based on numerical methods such as the finite element method. The stress concentration factor depends on geometric parameters of the welded joint such as the width and height of the reinforcement (in the case of butt joints), the weld length (in the case of fillet joints), weld angle of the reinforcement, base plate thickness, and the radius of the weld toe. Not all geometric data of weldments needed for the notch stress analysis are included in the welded joint design specifications. Some data such as the width and height of the weld cap, the weld toe angle, and the weld toe radius depend on the welding procedure and quality [3]. The stress concentration factor was numerically evaluated using ANSYS finite element software [36] for various welded joints. The fatigue notch factor, K_f, was then evaluated based on notch sensitivity factor, q;

$q = \dfrac{K_f - 1}{K_t - 1}$ (equation 2.14), and Peterson's equation [37]:

$$ q = \frac{1}{(1 + \dfrac{a}{r})} \tag{4.1} $$

$$ K_f = 1 + \frac{K_t - 1}{(1 + \dfrac{a}{r})} \tag{4.2} $$

where a is a material constant known as Peterson's constant and is defined as $a = [300/S_{UTS}(ksi)]^{1.8} \times 10^{-3}$ (inch) and r corresponds to the weld toe radius (inch).

The investigated welded joints are the steel butt joint of Chapetti et al. [32], the 13×10 mm steel cruciform joint of Livieri and Lazzarin [30], the carbon steel butt joint of Reemsnyder ($h=1.5$ mm) [33] and the aluminium alloy double butt-strap fillet joint of Webber [34]. The critical site in the welded joints is defined as the node experiencing maximum stress based on

finite element (FE) analysis. This node is also the most likely location for emanating a fatigue crack at the weld toe.

4.4 FE modeling and element specifications

The welded joints have been modeled in a structural two-dimensional plane strain condition. The local geometry and related dimensions for the weldments were considered in the two-dimensional FE model. These local dimensions include the width/length and height of the weld cap, weld angle of the reinforcement, base plate thickness, and the radius of weld toes.

Eight-node finite element (PLANE82) has been utilized for the welded joint models. The eight-node structural solid element is a high order two-dimensional eight-node element. It offers precise results for the mixed quadrilateral-triangular automatic meshes and can accept asymmetrical shapes without much loss of precision. PLANE82 has a quadratic dislocation performance, and well-matched displacement shapes, and is appropriate to model uneven and unequal meshes and curved boundaries, which are common in welded joints. The eight-nodes with two degrees of freedom in each node describe this element moving along the nodal x and y directions.

For modeling of the welded joints, a solid two-dimensional model with very fine triangular mesh element size 1 has been employed. The modeled welded joints have been considered as isotropic and linearly elastic materials, with allowable relative displacement, U_x, in X-direction at which the maximum applied stress (nominal stress) was applied. The value of Poisson's ratio (v), employed for FE models of the steel joints and aluminium joint has been 0.30 and 0.35 respectively. The elastic modulus (E) values used for the FE models of the welded joints have been obtained from Appendix B. Corresponding local stresses were calculated at the critical site where the weld toe experiences the highest stress concentration.

A two-dimensional solid model was utilized to numerically determine the local stress at the weld toe of the welded joints reported by Chapetti et al. [32], Livieri and Lazzarin [30], Reemsnyder [33] and Webber [34] for both steel and aluminium alloy. Figures 4.5–4.8 present two-dimensional solid meshed models developed for butt-welded, cruciform welded and double butt-strap fillet welded joints. For the models in figures 4.6 and 4.8, boundary conditions were located, preventing displacements parallel to the Y-axis (U_x) and parallel to

the X-axis (U_y). For the model in figure 4.7, boundary conditions prevented displacements parallel to the X-axis (U_y).
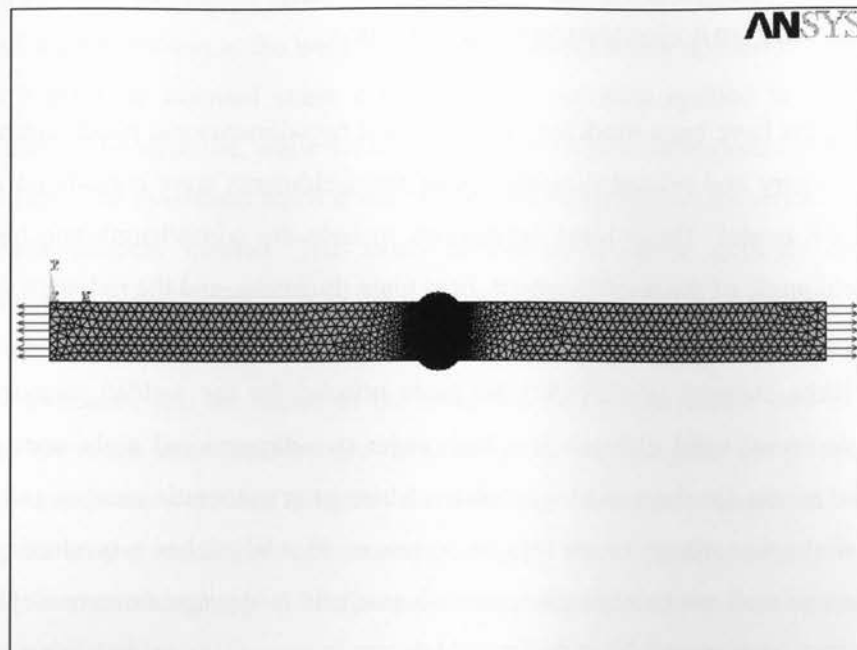
Figure 4.5 Two-dimensional solid FE model for a butt-welded joint.
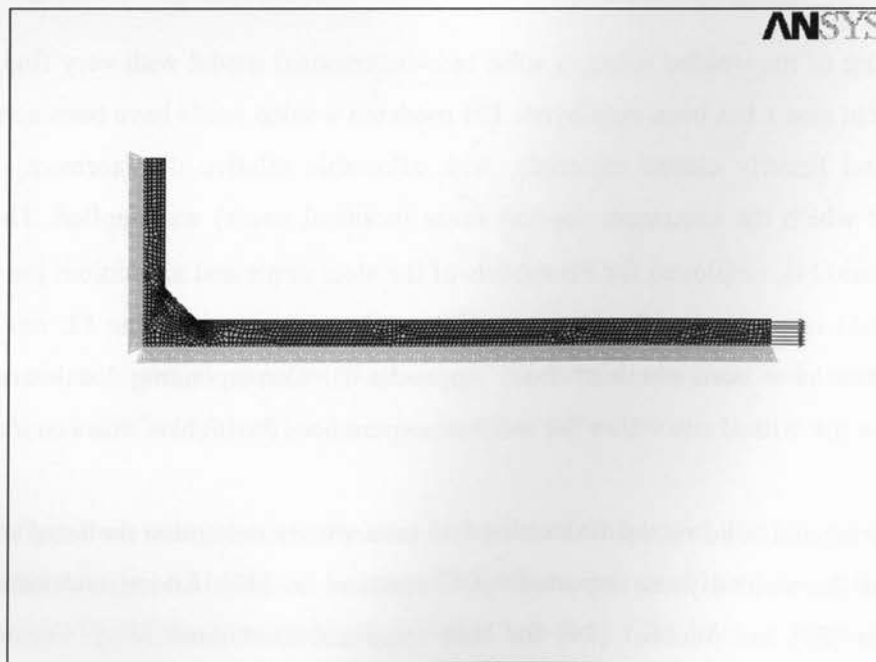
Figure 4.6 Two-dimensional solid FE model (quarter symmetry) for a cruciform welded joint.
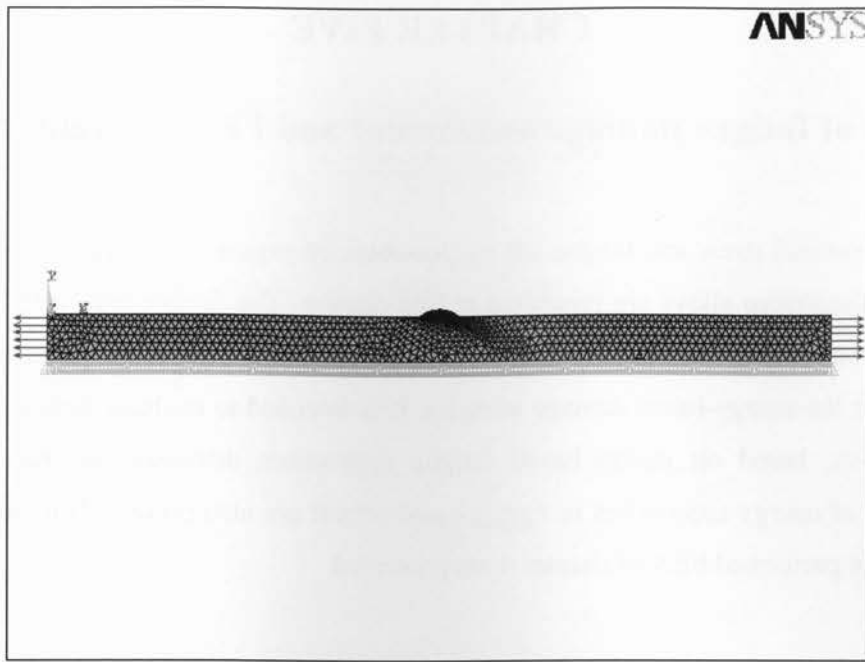
Figure 4.7 Two-dimensional solid FE model (half symmetry) for a butt-welded joint.
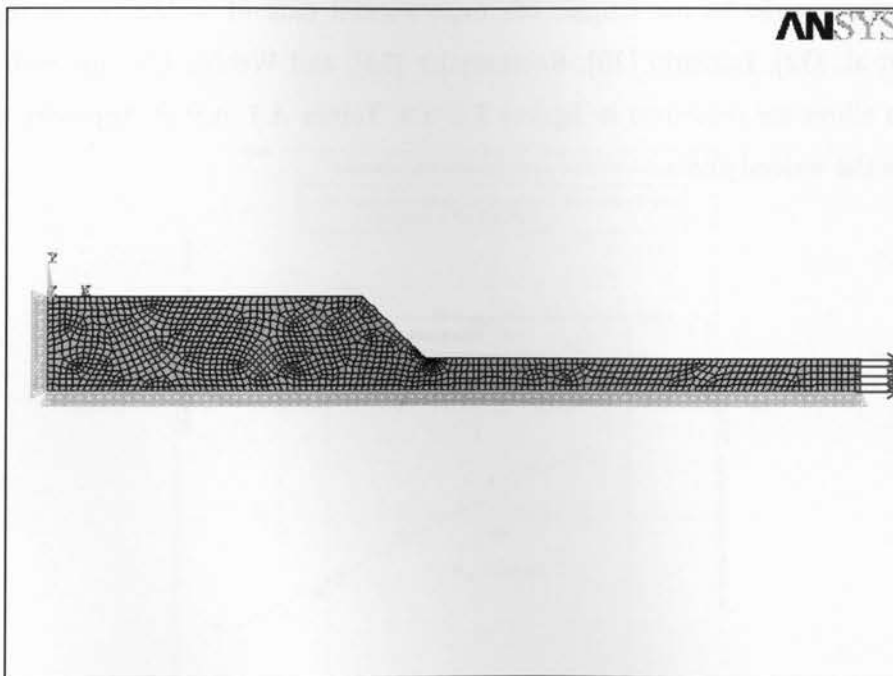
Figure 4.8 Two-dimensional solid FE model (quarter symmetry) for a double butt-strap

fillet welded joint.

The results of the FEA for the welded joints have been presented in chapter 5. The results
include the maximum local stresses at the weld toes where stress is highly concentrated.

CHAPTER FIVE

Results of fatigue damage assessment and FEA for welded joints

Results of nominal stress and fatigue life cycles obtained experimentally in welded joints of steels and aluminium alloys are presented in this chapter. The fatigue tests were performed under uniaxial loading conditions and reported in the literature. The results presented here are the basis for the energy-based damage analysis. It is intended to evaluate fatigue damage of welded joints, based on energy-based fatigue approaches discussed in chapter 3. The capabilities of energy approaches in damage assessment are also presented. In addition, the results of the performed FEA of chapter 4 are presented.

5.1 Presentation of S-N curves related to data sets

Nominal stress range versus fatigue life experimental data of welded joints reported by Chapetti et al. [32], Lazzarin [30], Reemsnyder [33], and Webber [34] for both steel and aluminium alloys are presented in figures 5.1–5.9. Tables A.1–A.9 of Appendix A tabulate S-N data of the welded joints.
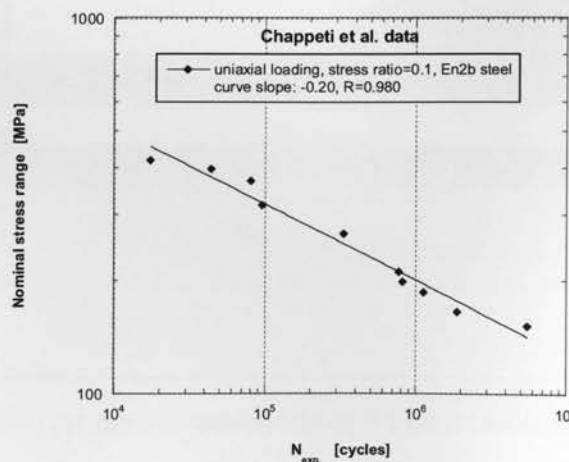
Figure 5.1 Nominal stress range versus fatigue life data for butt-welded joints conducted by Chapetti et al. [32].
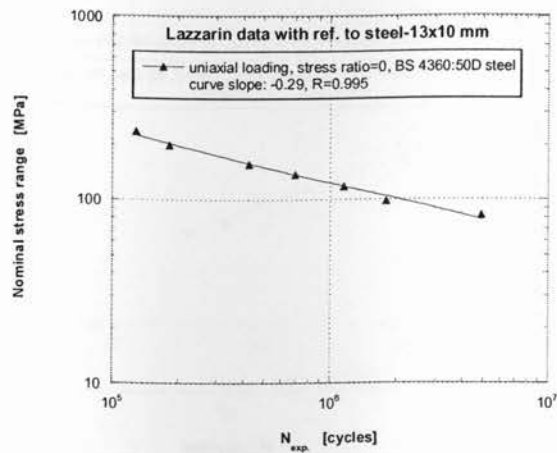
Figure 5.2 Nominal stress range versus fatigue life data for cruciform structural steel welded joints (13×10 mm) conducted by Lazzarin for [30].
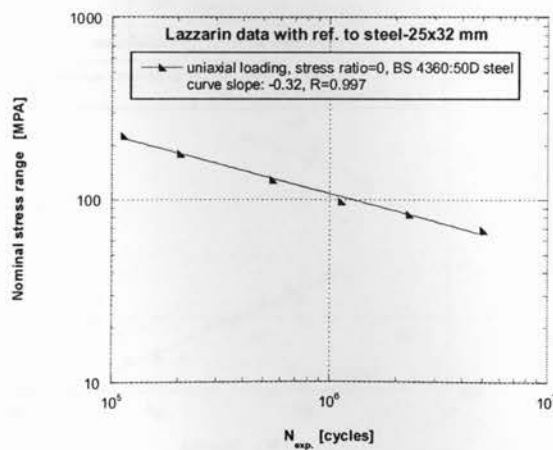
Figure 5.3 Nominal stress range versus fatigue life data for cruciform structural steel welded joints (25×32 mm) conducted by Lazzarin for [30].
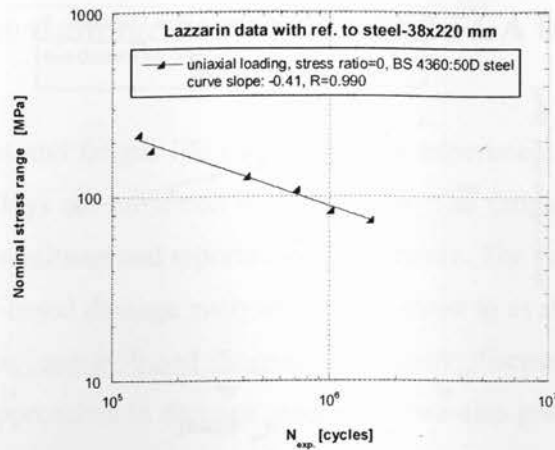
Figure 5.4 Nominal stress range versus fatigue life data for cruciform structural steel welded joints (38×220 mm) conducted by Lazzarin for [30].
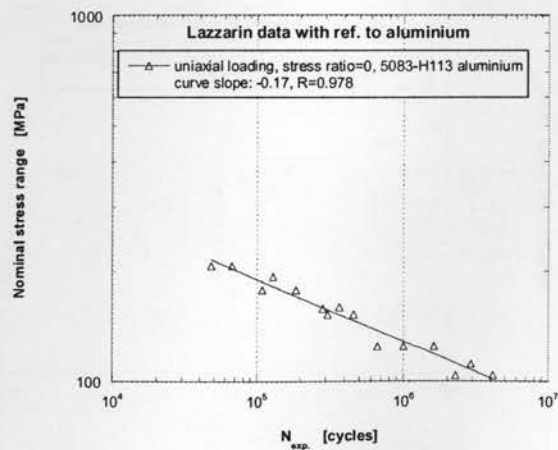
Figure 5.5 Nominal stress range versus fatigue life data for aluminium butt-welded joints conducted by Lazzarin [30].
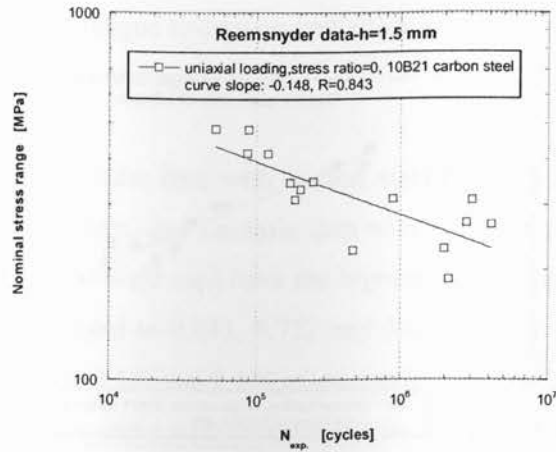
Figure 5.6 Nominal stress range versus fatigue life data for butt-welded joints conducted by Reemsnyder (h=1.5 mm) [33].
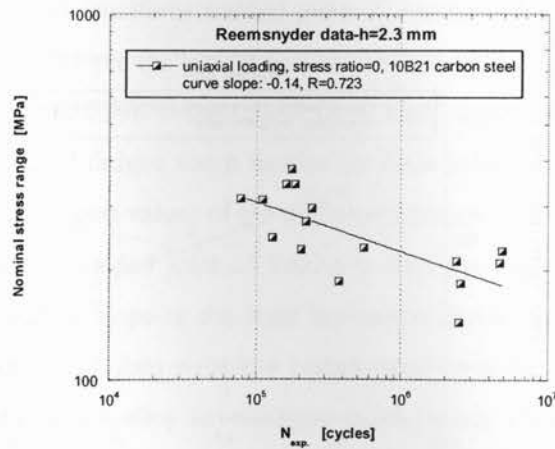
Figure 5.7 Nominal stress range versus fatigue life data for butt-welded joints conducted by Reemsnyder (h=2.3 mm) [33].
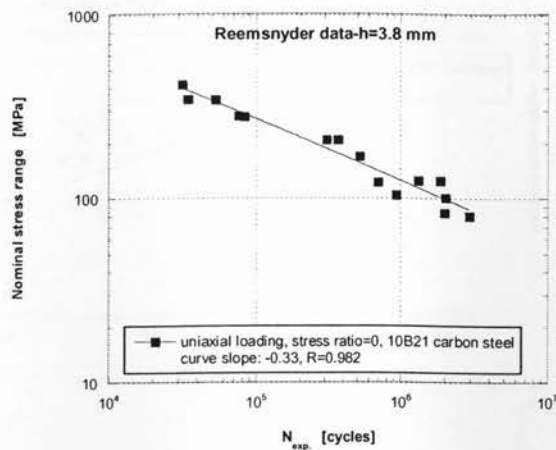
Figure 5.8 Nominal stress range versus fatigue life data for butt-welded joints conducted by Reemsnyder (*h*=3.8 mm) [33].
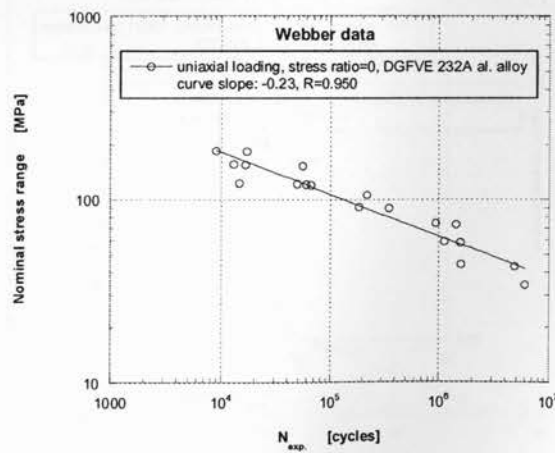
Figure 5.9 Nominal stress range versus fatigue life data for load-carrying double butt-strap fillet aluminium alloy welded joints conducted by Webber [34].

For curve-fitted *S-N* data, the slope is presented in these figures. The *S-N* curves help significantly to estimate the fatigue resistance and stress raising effect of the tested welded joints through the scatter index and curve slope.

The welded joints in Reemsnyder data with carbon steel base metal of 10B21 (weld cap heights ranging from 1.5-2.3 mm) and Lazzarin data with reference to aluminium alloy base metal of 5083-H113 (removed weld cap) have the highest scatter indexes. Their curve fitted line regression values[1] are equal to 0.843, 0.722 and 0.978 respectively (in addition to the lowest slope values of: 0.148, 0.140 and 0.170 respectively). Although the aluminium joint of Lazzarin has the weakest base metal with ultimate tensile strength of 363 MPa, it follows the joint of Reemsnyder, having the strongest base metal with ultimate tensile strength of 814 MPa, in terms of low slope and high scatter. The calculated fatigue notch factors for the carbon steel joints of Lazzarin are equal to $K_f=2.15$ and for the aluminium butt joint of Lazzarin it is equal to $K_f=1$, which is the smallest value of the calculated fatigue notch factors. The welded joint in Reemsnyder data with a weld cap of 3.8 mm has a low scatter index, with a curve fitted line regression value equal to 0.982 and a high slope value of 0.33. The calculated fatigue notch factor for this joint is equal to $K_f=2.15$, a relatively small value[2]. The 25×32 and 38×220 mm cruciform welded joints in Lazzarin data with reference to steel base metal of BS 4360:50D have the lowest scatter indexes, with curve fitted line regression values equal to 0.997 and 0.990 respectively (and high slope values of 0.32 and 0.41 respectively). The calculated fatigue notch factors for these joints are equal to $K_f=3.585$ and $K_f=4.4$, very high values (largest values of the calculated fatigue notch factors). In this regard the 38×220 mm cruciform welded joint of Lazzarin with the highest fatigue notch factor ($K_f=4.4$) also has the highest slope or the least horizontal curve (slope value of 0.41). The welded joints in Chapetti et al. data with low carbon steel base metal of En2b and Webber data with Al-Zn-Mg aluminium alloy have fatigue notch factors equal to $K_f=2$ and $K_f=1.95$. Their curve slope values are 0.20 and 0.23 respectively, which stand in between the curve slopes of other welded joints.

---

[1] A regression value of R=1 represents fatigue data fallen on the fitted straight line.
[2] Fatigue notch factor, K_f, of 1.8 to 2.5 is considered a relatively small value and 3.0 to 4.5 is considered a very high value [8].

5.2 Energy-fatigue life (W-N) response

Calculated energy values based on three energy-based approaches are plotted versus fatigue life data in figures 5.10–5.12. Experimental life data for different weldments were extracted from available literature and energy values are tabulated in tables F2.1–F2.27 of Appendix F.

The mean regression values for the data sets related to the hysteresis loop energy model, the notch stress-intensity energy model, and the critical plane/energy model are R=0.910, R=0.972, and R=0.944, respectively. In addition, the mean curve slope absolute values for the data sets related to the hysteresis-loop energy model, the notch stress-intensity energy model, and the critical plane/energy model are 0.64, 0.46, and 0.98, respectively. The maximum convergence of the energy value scatter-points belongs to the notch stress-intensity energy model, whereas the maximum curve slope of the energy value belongs to the critical plane/energy model. It must be noted that in terms of scatter, the critical plane/energy model follows the notch stress-intensity model closely, whereas in terms of curve slope value, the critical plane/energy model is more than twice the notch stress-intensity model.
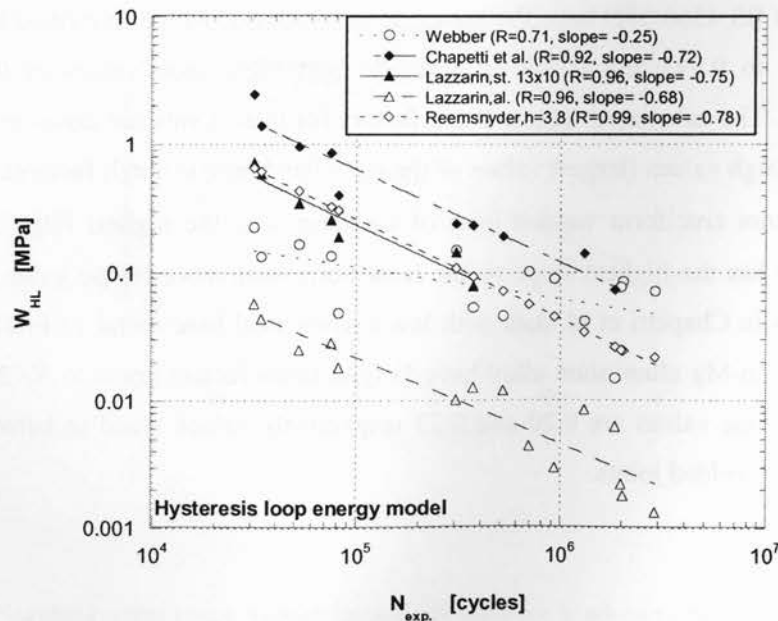
Figure 5.10 Hysteresis loop energy versus fatigue life data.
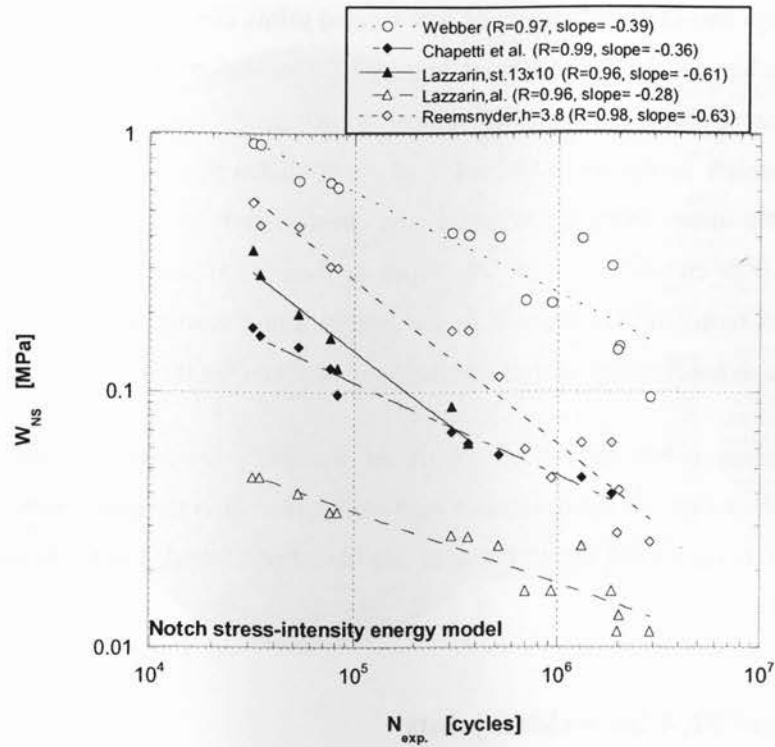
Figure 5.11 Notch stress intensity energy versus fatigue life data.
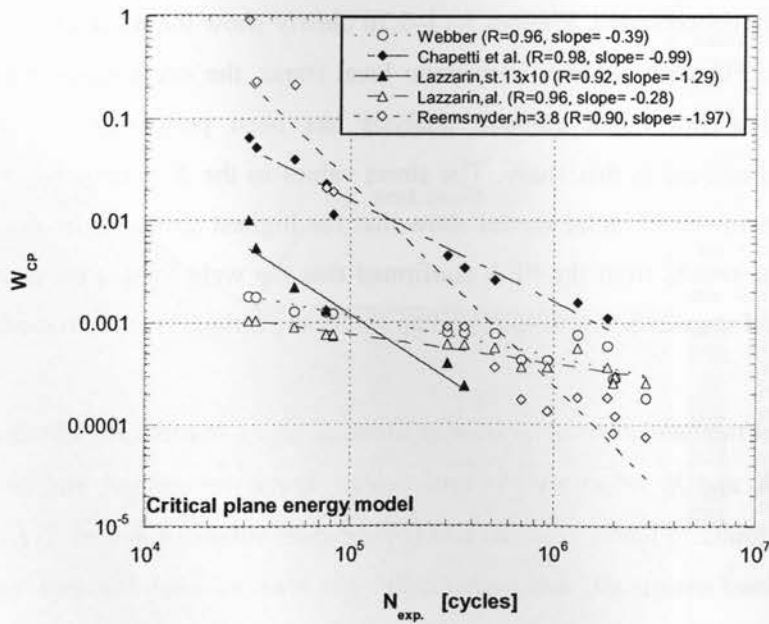
Figure 5.12 Critical plane energy versus fatigue life data.

Fatigue damage and life assessments of butt-welded joints can be evaluated based on energy-based approaches for sets of different materials presented in figures 5.10–5.12 using the scatter and curve slope criteria. The critical plane/energy approach and the notch stress-intensity approach in figures 5.11 and 5.12 show different slopes of W-N curves as the welded joint's data changes, whereas the hysteresis-loop energy approach fails to differentiate W-N curves, as values of slopes in figure 5.10, except for one data set, stay unchanged. In terms of convergence of the energy value scatter-points, the hysteresis-loop energy approach has the least scatter convergence between the three energy models.

The mean energy values have been calculated separately for each data set for the energy models, and the values for the hysteresis loop model, the notch stress-intensity model, and the critical plane/energy model for all the data sets have been found. These values are presented in Appendix G.

5.3 Results of FEA for welded joints

The present section discusses the numerical results of finite element analysis for various welded joints. The results include the maximum local stresses at the weld toes where the stress is highly concentrated. Figures 5.13–5.20 clearly show the local stress contours in the welded joints. For each obtained maximum local stress, the stress concentration factor, K_t, has been calculated. Finite element analysis has been performed for various welded components discussed in this study. The stress values in the X direction acquired from the nodal solution of the FE solid model show that the highest stress values are located at the weld toes. The results from the FEA confirmed that the weld toes as the nodal points with maximum local stresses are most likely locations for the fatigue crack initiation.

Tables 5.1–5.4 tabulate maximum nominal stress, $S_{nom(max)}$, numerically obtained local stress, $\sigma_{loc(FE)}$, and K_t and K_f values for the butt-welded, cruciform welded, and double butt-strap fillet welded joints. Figures 5.21 (a) and (b) compare values of K_t and K_f for various weld joints determined analytically and numerically. The obtained analytical and numerical values are in close agreement.
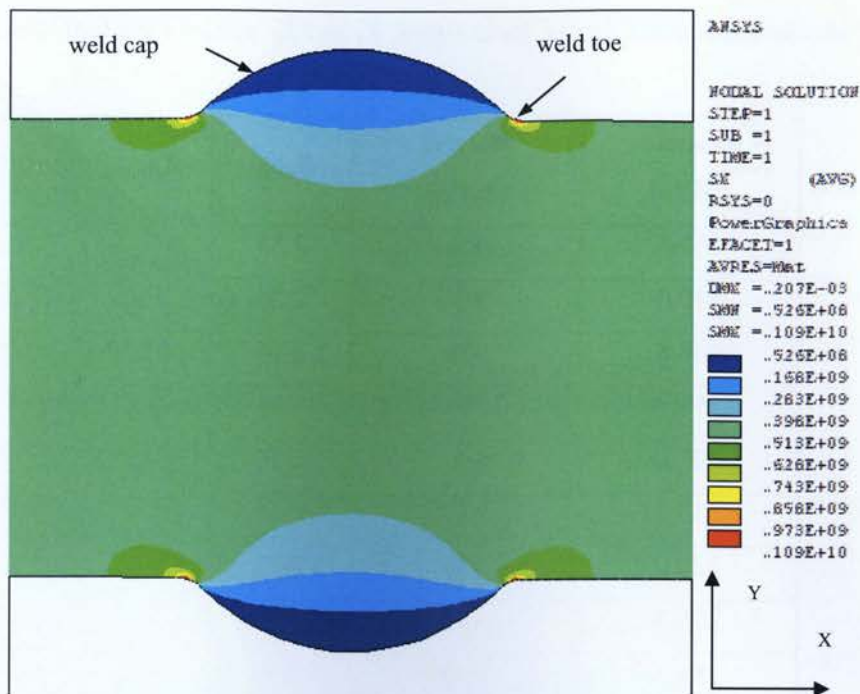
Figure 5.13 Stress contour generated by ANSYS (nodal solution) along X-axis for a double-sided butt-welded joint.
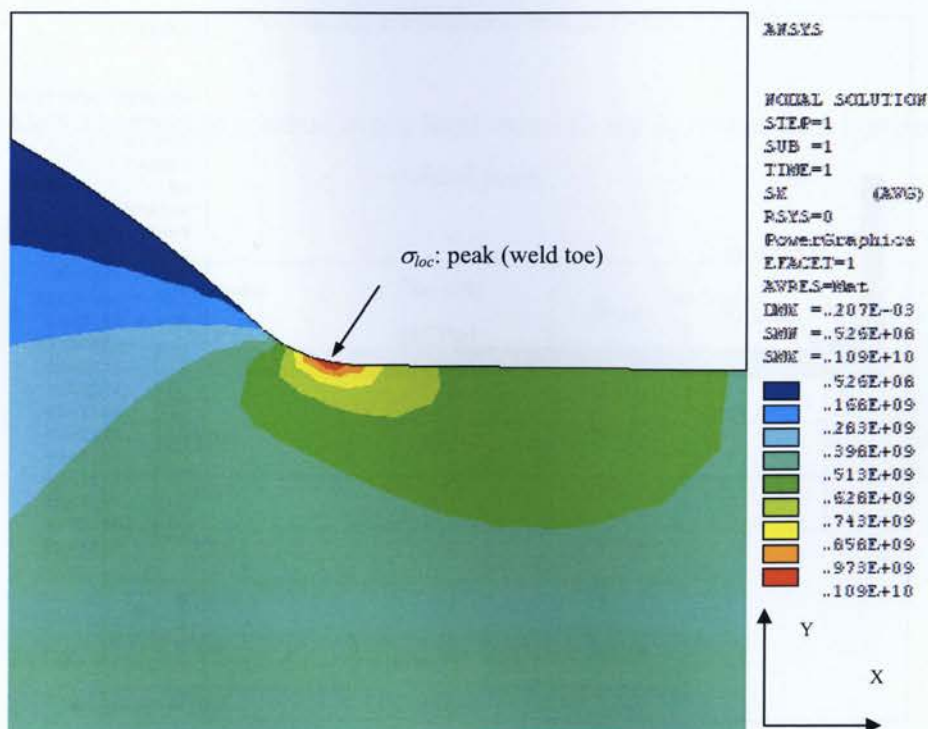
Figure 5.14 Stress contour in weld toe vicinity, generated by ANSYS (nodal solution) along X-axis for a butt-welded joint.

Table 5.1 Maximum nominal stress, local stress, K_t and K_f values for a butt-welded joint.

$S_{nom(max)}$ [MPa]	$\sigma_{loc\ (FE)}$ [MPa]	$K_{t(FE)}$	$K_{f(num)}$ r=0.020" a=0.011"
464.4	1090	2.35	
440.0	1030	2.34	
408.8	959	2.35	1.870
353.3	828	2.34	
295.5	693	2.35	
234.4	550	2.35	
220.0	516	2.35	
206.6	484	2.34	
183.3	430	2.35	
168.8	396	2.35	
---	$K_{t(FE)}$ average = 2.347		
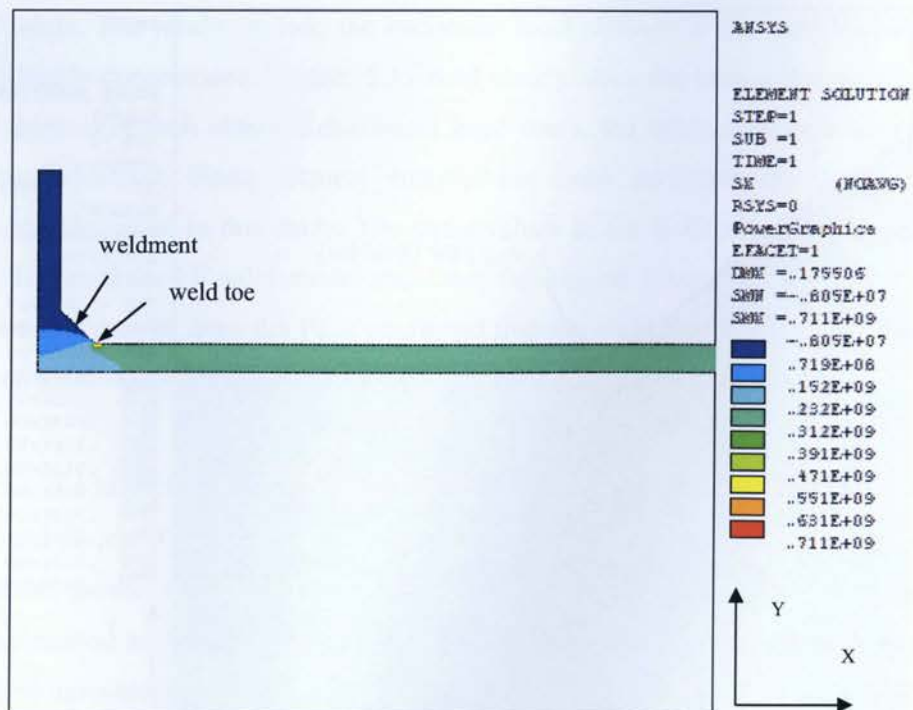
Figure 5.15 Stress contour generated by ANSYS (nodal solution) along X-axis for a cruciform welded joint (¼-symmetry model).

63
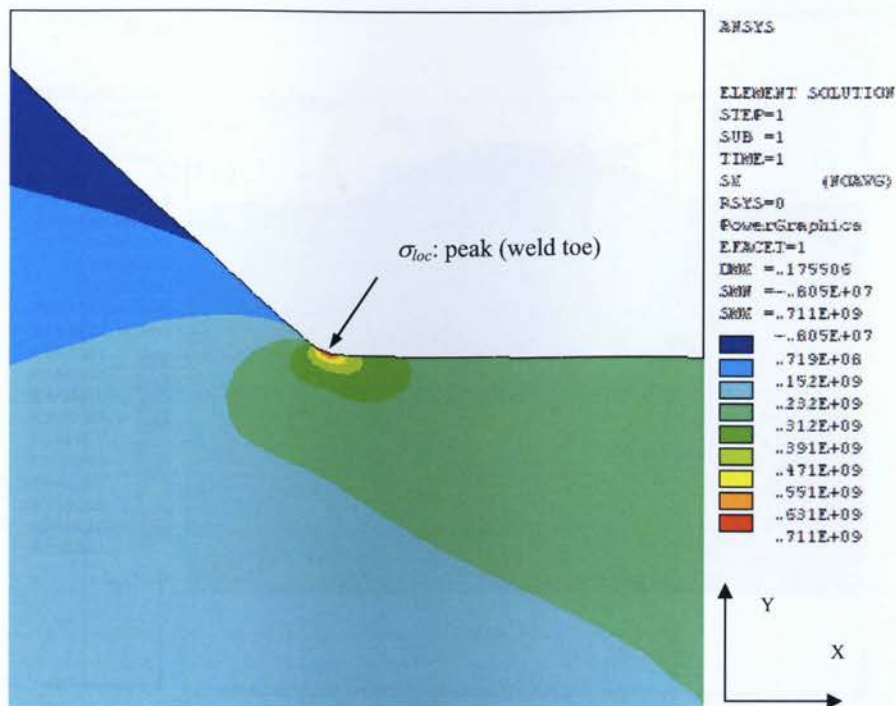
Figure 5.16 Stress contour in weld toe vicinity, generated by ANSYS (nodal solution) along X-axis for a cruciform welded joint.

Table 5.2 Maximum nominal stress, local stress, K_t and K_f values for a cruciform welded joint.

$S_{nom(max)}$ [MPa]	$\sigma_{loc\ (FE)}$ [MPa]	$K_{t(FE)}$	$K_{f(num)}$ r=0.020" a=0.011"
236	711	3.01	
199	597	3.00	
157	471	3.00	2.291
138	414	3.00	
118	354	3.00	
98	294	3.00	
82	246	3.00	
---	$K_{t(FE)}$ *average* = 3.001		
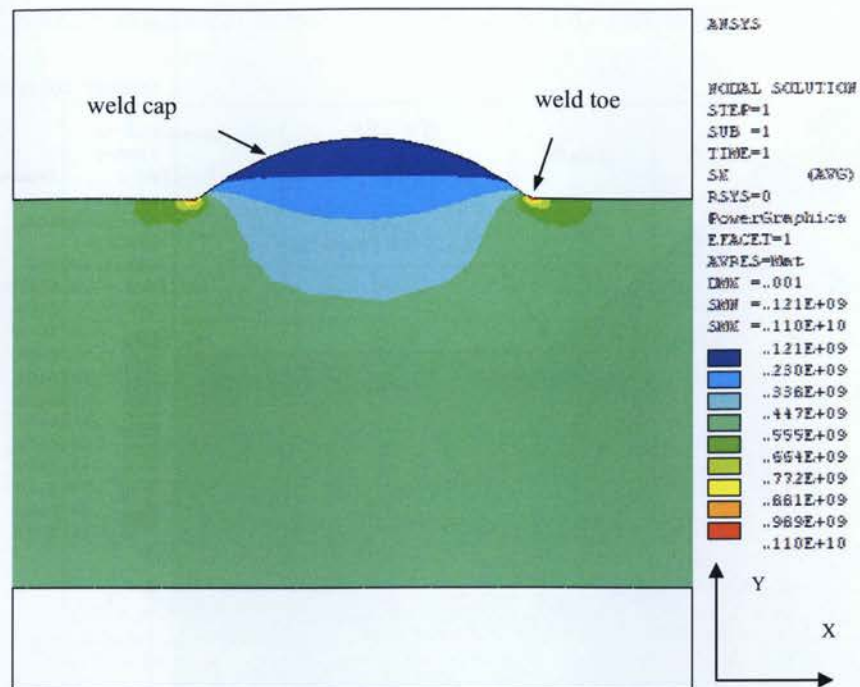
Figure 5.17 Stress contour generated by ANSYS (nodal solution) along X-axis for a double-sided butt-welded joint (½-symmetry model).
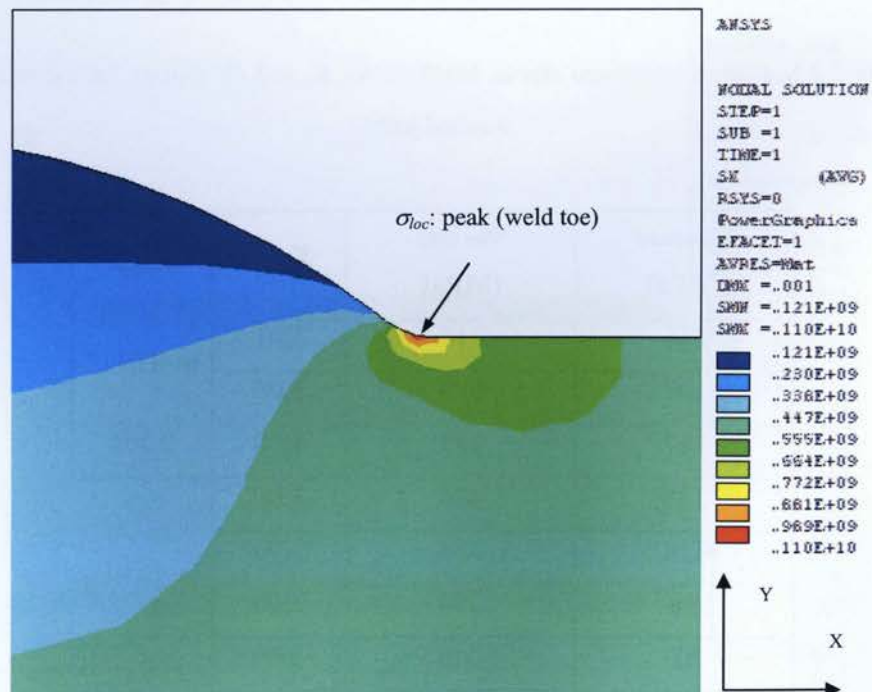
Figure 5.18 Stress contour in weld toe vicinity, generated by ANSYS (nodal solution) along X-axis for a butt-welded joint.

Table 5.3 Maximum nominal stresses, local stress, K_t and K_f values for a butt-welded joint.

$S_{nom(max)}$ [MPa]	$\sigma_{loc\ (FE)}$ [MPa]	$K_{t(FE)}$	$K_{f(num)}$ r=0.020" a=0.005"
486	1100	2.26	
484	1090	2.25	
418	944	2.26	2.010
416	940	2.26	
350	790	2.26	
347	784	2.26	
333	752	2.26	
312	705	2.26	
311	702	2.26	
309	698	2.26	
268	605	2.26	
265	598	2.25	
228	515	2.26	
226	510	2.25	
188	425	2.26	
---	$K_{t(FE)}$ *average* = 2.258		
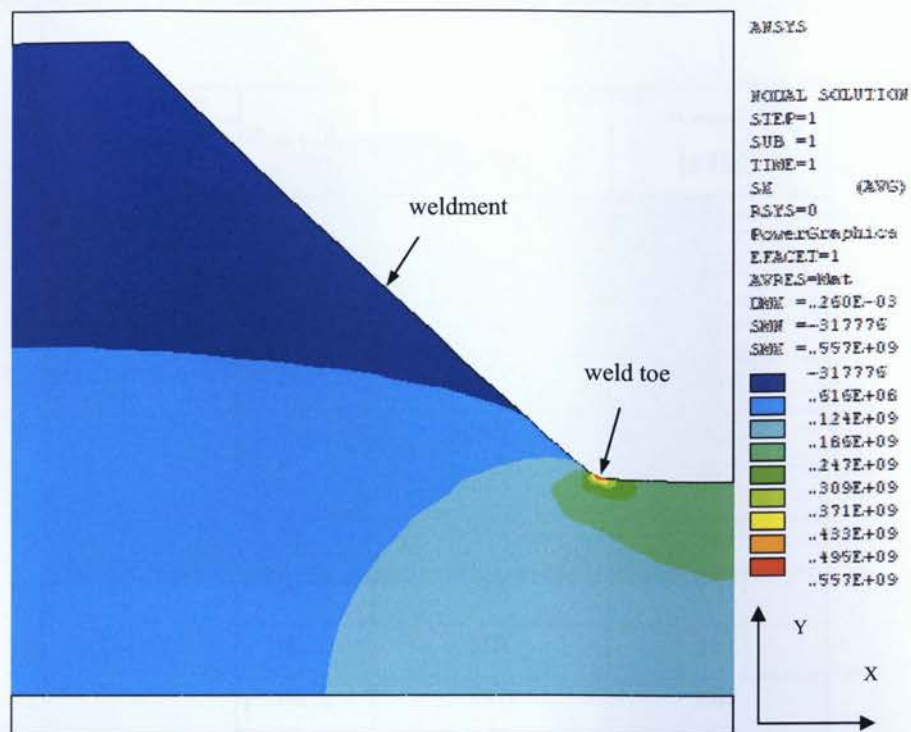
Figure 5.19 Stress contour generated by ANSYS (nodal solution) along X-axis for a double butt-strap fillet welded joint (¼-symmetry model).
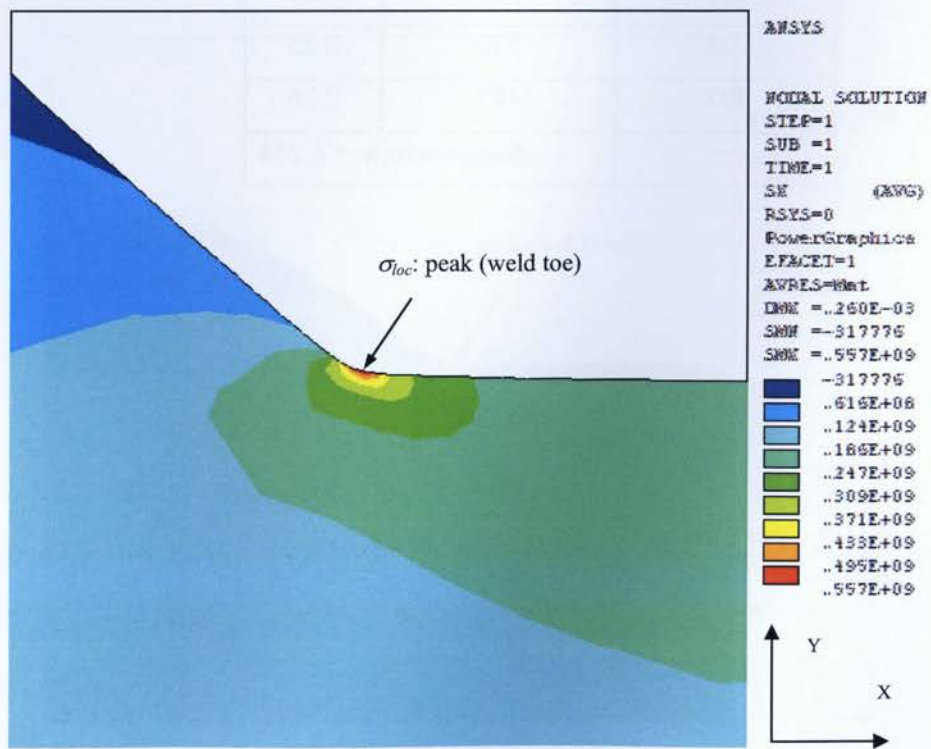
Figure 5.20 Stress contour in weld toe vicinity, generated by ANSYS (nodal solution) along X-axis for a double strap butt-welded fillet joint (¼-symmetry model).

Table 5.4 Maximum nominal stresses, local stress, K_t and K_f values for a double butt-strap fillet welded joint.

$S_{nom(max)}$ [MPa]	$\sigma_{loc\,(FE)}$ [MPa]	$K_{t(FE)}$	$K_{f(num)}$ r=0.020" a=0.021"
184	557	3.03	
183	554	3.03	
156	472	3.03	1.998
155	469	3.03	
152	460	3.03	
123	372	3.02	
122	369	3.02	
121	366	3.02	
121	366	3.02	
120	363	3.03	
106	321	3.03	
91	276	3.03	
90	273	3.03	
74	224	3.03	
73	221	3.03	
59	179	3.03	
58	176	3.03	
44	133	3.02	
43	130	3.02	
34	103	3.03	
---	$K_{t(FE)}$ *average* = 3.027		
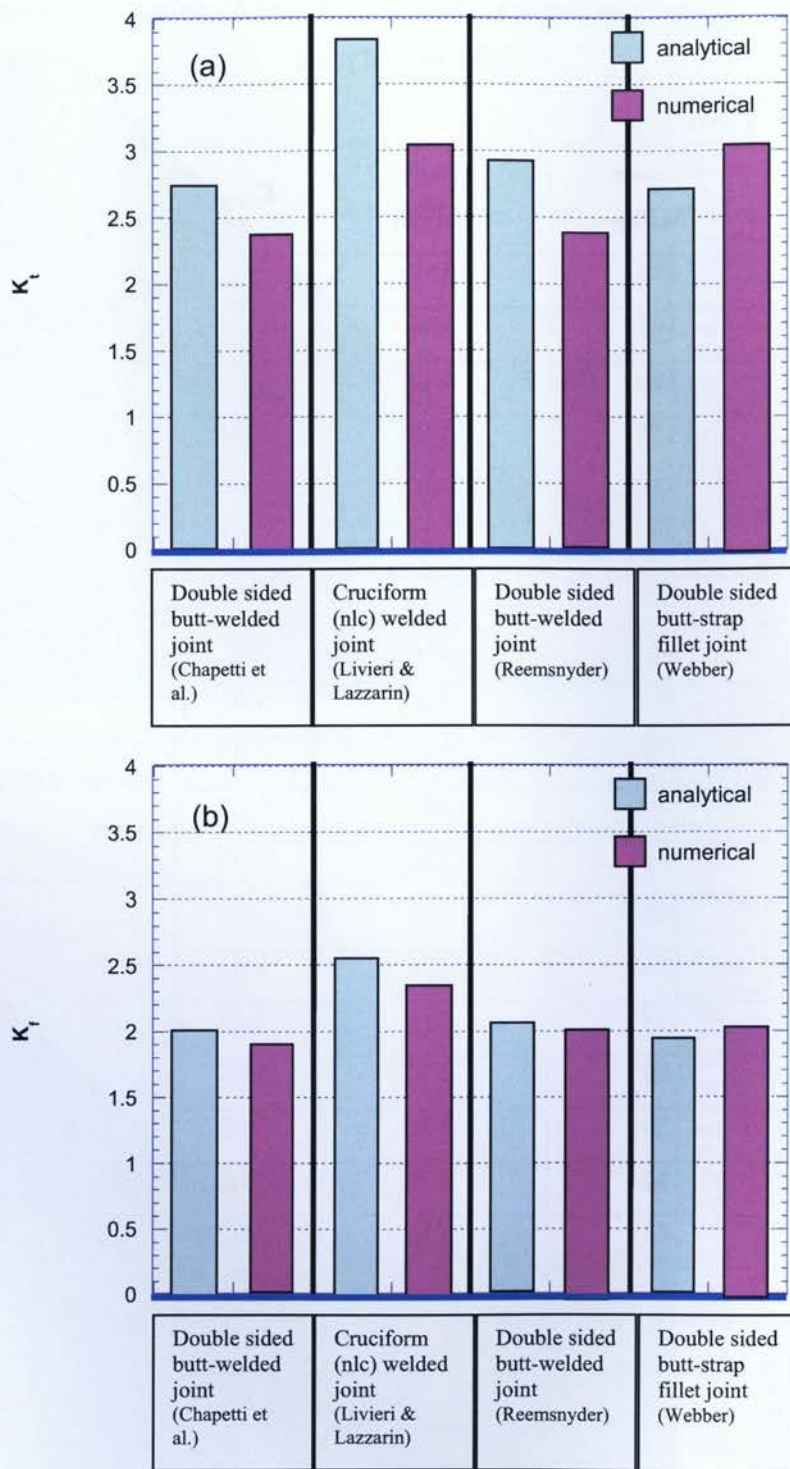
Figure 5.21 Numerical and analytical values of K_t (a), and K_f (b) for various welded joints.

CHAPTER SIX

Discussion

This chapter carries out discussions based on the obtained results of the energy models, already presented in the previous chapter and compares the energy-lifetime curves with each other, including their slopes and their ability to unify fatigue data. The nominal stress-fatigue life data sets and the effects of the fatigue variables on the energy-based models, welded joint material, and joint types, are discussed in detail. In addition, W-N diagrams generated based on energy based models for welded joints are compared and discussed for butt welded joints, cruciform welded joints, and a double butt-strap fillet welded joint with different materials.

The relation between factors influencing fatigue; applied stress amplitude, material properties, geometrical stress concentration effects, and energy values can be studied based on the energy values presented in the W-N diagrams, which do not primarily reflect the effect of ultimate tensile strength of the base metal on the welded joints. On the other hand, fatigue assessment based on the S-N approach, does not reflect the main parameters influencing fatigue.

In the energy approaches, the fatigue notch factor, K_f, has an affect on the energy values through increasing the local stress, which results in the increase in energy. In addition, for the notch stress-intensity energy approach, the mean energy values for each data set have a direct positive correlation with the fatigue notch factor obtained for that specific data set. For the notch stress-intensity and critical plane/energy approaches, the lowest energy values belong to Lazzarin data (aluminium joint reference), with the lowest fatigue notch factor, while the energy values belonging to other data sets do not have any specific relation with their related fatigue notch factors. The stress raising effect of the welded joint is directly applied to the notch stress-intensity energy model and critical plane/energy model through the calculated local stress. No apparent direct link between the fatigue notch factor and the hysteresis-loop energy model can be found.

The stress raising effect of the weld, represented through the fatigue notch factor K_f of the welded joints, somehow shows an effect on the induced damage through the obtained energy

values in this study. In this regard, the fatigue notch factor, K_f, of the weldment, can be reduced through a technique that has been applied in industry for some time with great success, for fatigue strength improvement of butt and fillet welded joints through applying weld grinding. This can result in lower energy values indicating less damage in the welded joint.

It must be noted that the S-N diagrams presented in the previous chapter clearly show that the main parameter designating fatigue resistance in welded joints is not principally the ultimate tensile strength of the base metal, but the fatigue notch factor, K_f, of the specific joint, resulting from the joint geometry and welding procedure. In this regard, it was shown that the welded joints with the lowest fatigue notch factors, such as Reemsnyder's butt-joints (h^1=1.5 mm and h=2.3 mm) and Lazzarin's aluminium butt-joint, with K_f=2.10, K_f=2.30 and K_f=1, respectively, have the lowest S-N curve slope values (0.148, 0.140 and 0.170, respectively), while the welded joints with the highest fatigue notch factors, such as Lazzarin's steel cruciform joints (25×32, 38×220 mm) and Reemsnyder's butt-joint (h=3.8 mm), with K_f=3.585, K_f=4.4 and K_f=2.35, respectively, have the highest S-N curve slope values (0.32, 0.41 and 0.33, respectively). This reiterates the theory already mentioned that welded joints with greater fatigue resistance have S-N diagrams that are more nearly horizontal [8]. This will be further investigated in comparing W-N curves of butt versus cruciform joints and different butt joints (figures 6.10–6.15). It must be noted that the reason for the high curve slope in the case of the butt joint of Reemsnyder with h=3.8 mm, although having a fatigue notch factor of K_f=2.35, could only be its high weld cap; contributing to a decrease in fatigue strength in the welded joint.

For the cruciform steel joint of Lazzarin with three different sizes (13×10, 25×32, 38×220 mm), the presented S-N diagrams show an increase in curve slope values (0.30, 0.32 and 0.41, respectively), with the increase in base plate thickness, indicating decrease in fatigue strength of the welded joints. This reiterates the theory that the fatigue strength of a cruciform welded joint decreases greatly as both the main plate thickness ratio, and the attachment thickness, increase, especially for large variations, which could occur with non-load-carrying attachments in cruciform joints [38,39].

---

[1] h: weld cap or weld reinforcement height.

For the butt joint of Reemsnyder with three different weld cap heights (1.5, 2.3 and 3.8 mm) the presented *S-N* diagrams show an increase in curve slope values (0.13, 0.14 and 0.33, respectively) in addition to an increase in scatter index value from 0.882 to 0.982 as the weld cap height increases from 1.5 mm to 3.8 mm. This indicates a decrease in fatigue strength of the welded joints reiterating the theory that the fatigue strength of a butt-welded joint decreases with the increase in the height of the reinforcement cap and the increase of weld angle [4,40] and that lower fatigue strengths are related to welds that have a meager shape; welds with excess weld reinforcement [5]. This issue was observed in the case of the butt joint of Reemsnyder with weld cap height of 3.8 mm, possessing a high curve slope value of 0.33, being categorized with the joints with high K_f values ranging from 2.55-4.4 and curve slope values ranging from 0.3-0.41. This will be further investigated in comparing W-N curves of butt joints with different weld cap heights (figures 6.13–6.15).

The *W-N* diagrams presented for all data sets in the previous chapter (figures 5.10–5.12), clearly show distinctive curve slopes for different types of joints in both the notch stress-intensity and critical plane/energy approach (ranging from 0.28-0.66 and 0.28-1.80, respectively). The critical plane/energy approach shows considerably higher slopes (average slope value of 0.95) compared to the notch stress-intensity approach (average slope value of 0.46). In this regard, the hysteresis loop energy approach does not show great difference in curve slope for different types of joints (ranging from 0.68-0.78) except for the joint of Webber (K_f=1.95) showing the least curve slope value of 0.254.

The *W-N* curves were generated based on energy-based fatigue models, for separate data sets, showing maximum convergence by the notch stress-intensity model and maximum slope by the critical plane/energy model. Comparison of energy-based models for assessing fatigue life of welded joints of different joints/materials is presented in figures 6.1–6.9.

These figures show that the critical plane/energy model possesses the highest slope of *W-N* curves. A higher slope of *W-N* curves provides less variation of life data along life-axis at any given energy value resulting in a better fatigue life prediction. The lowest slopes in *W-N* diagrams belong to Lazzarin's energy model of welded joints under axial loading conditions.
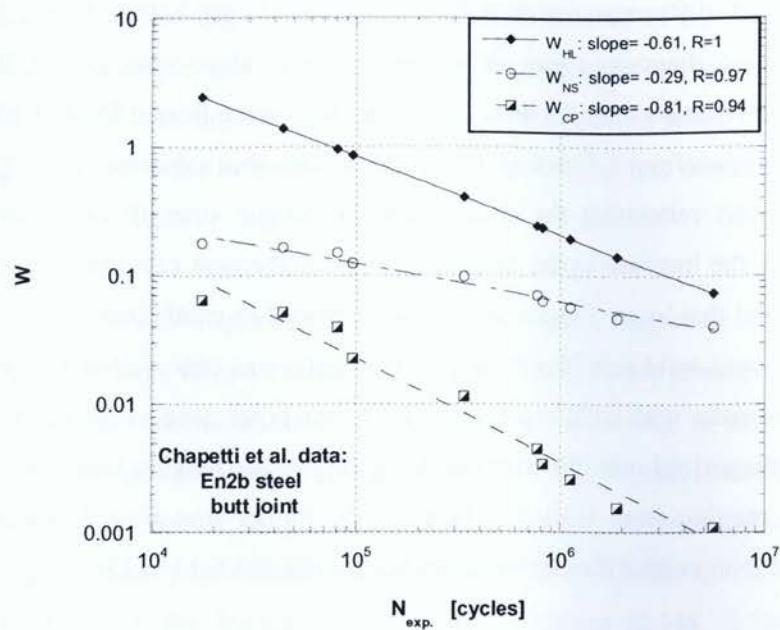
Figure 6.1 Energy versus fatigue life data for all energy models for Chapetti et al. data.
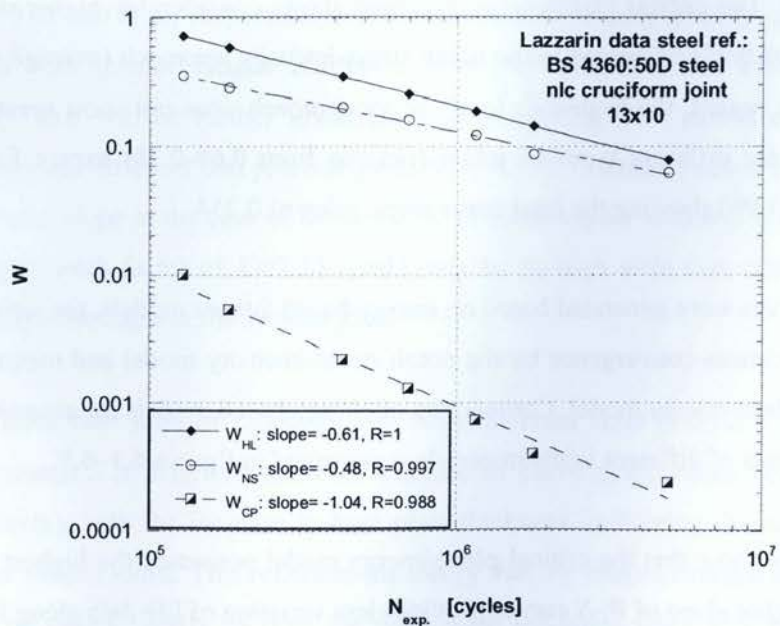
Figure 6.2 Energy versus fatigue life data for all energy models for Lazzarin data

(steel joint) - 13×10 mm.
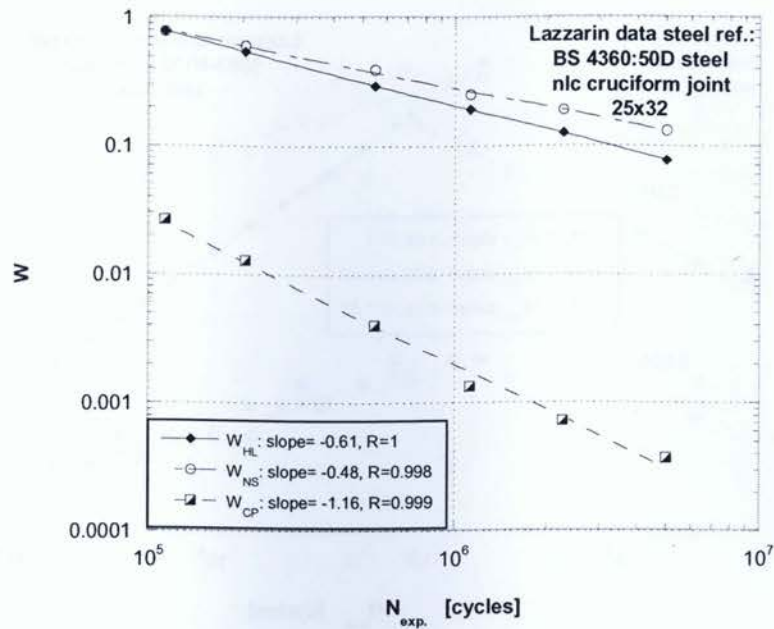
Figure 6.3 Energy versus fatigue life data for all energy models for Lazzarin data (steel joint) - 25×32 mm.
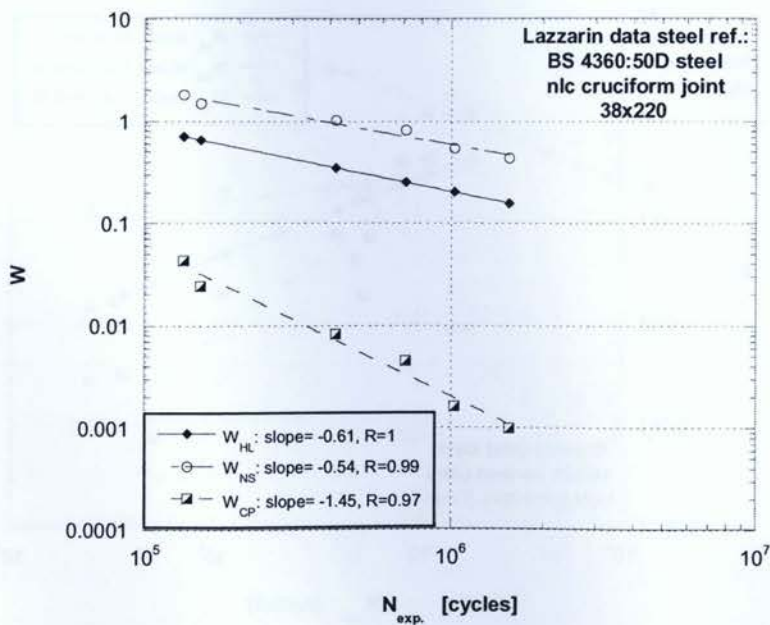
Figure 6.4 Energy versus fatigue life data for all energy models for Lazzarin data (steel joint) - 38×220 mm.

74
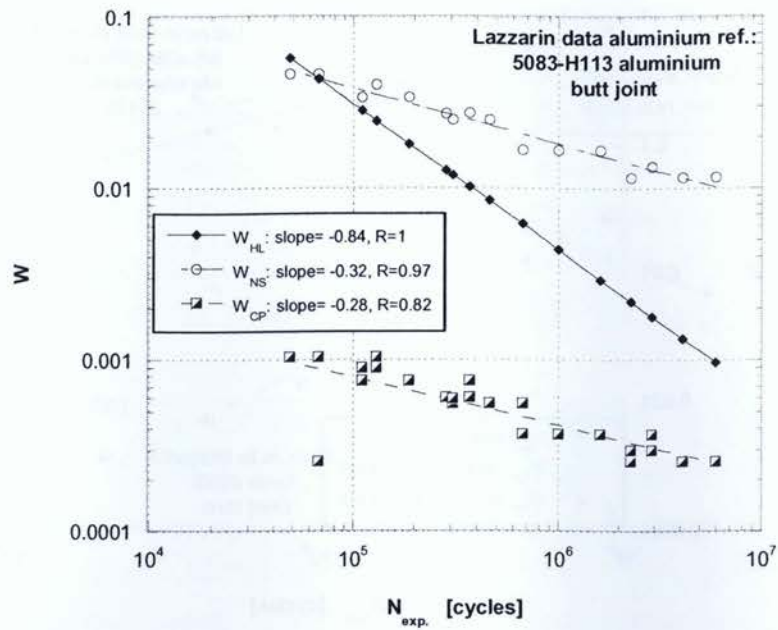
Figure 6.5 Energy versus fatigue life data for all energy models for Lazzarin data (aluminium joint).
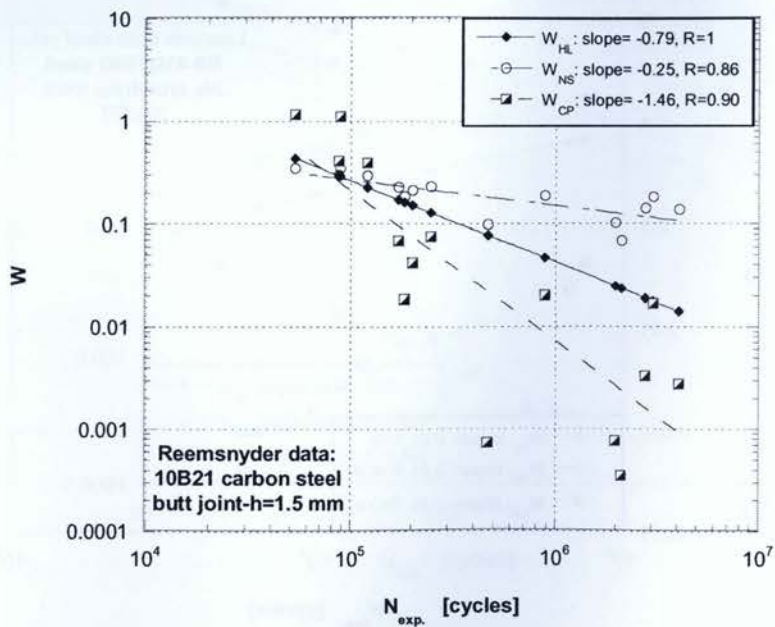
Figure 6.6 Energy versus fatigue life data for all energy models for Reemsnyder data-
h=1.5 mm.
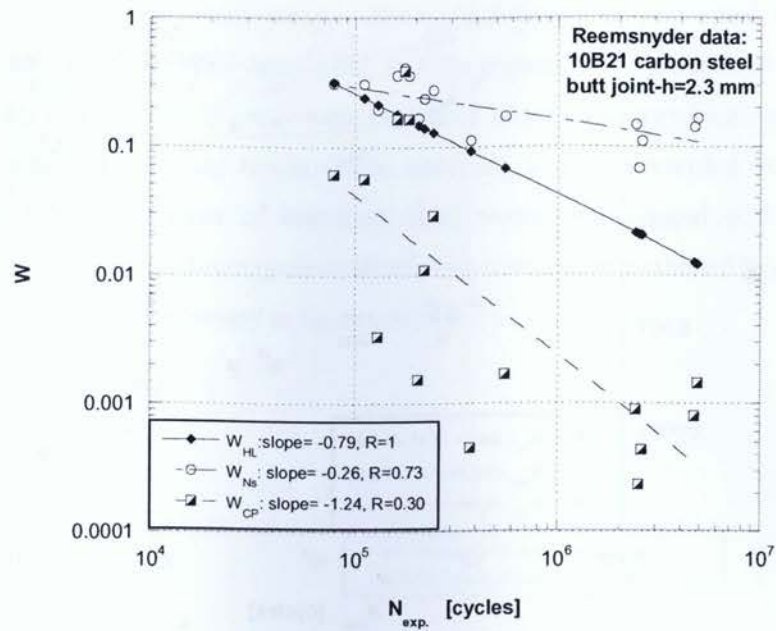
Figure 6.7 Energy versus fatigue life data for all energy models for Reemsnyder data-
h=2.3 mm.
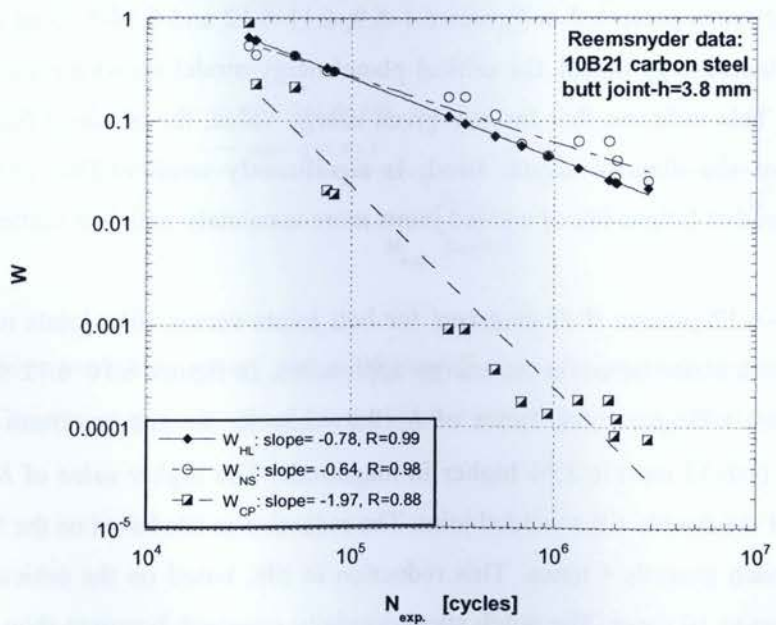
Figure 6.8 Energy versus fatigue life data for all energy models for Reemsnyder data-
h=3.8 mm.
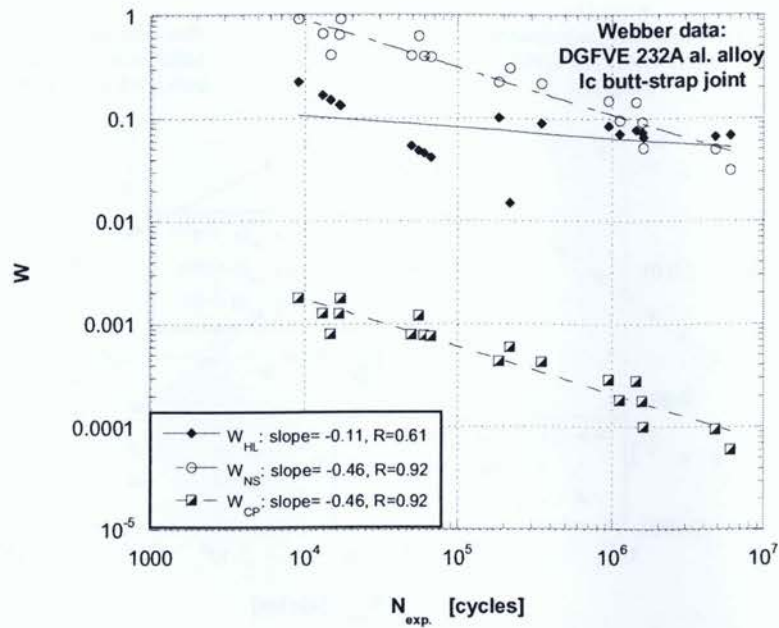
Figure 6.9 Energy versus fatigue life data for all energy models for Webber data.

While the notch stress-intensity energy model shows slightly better scatter convergence for butt and fillet joints presented in figures 6.1–6.9, 6.11–6.12 and 6.14–6.15 as compared with the critical plane/energy model, the critical plane/energy model shows a considerably higher curve slope. This indicates that for any given energy value, the obtained fatigue life range resulting from the diagram scatter band, is significantly smaller. This enables a design engineer to predict fatigue life of welded joints more accurately with less scatter.

Figures 6.10–6.12 present *W-N* diagrams for butt joints versus fillet joints made from low carbon steel calculated based on the energy approaches. In figures 6.10–6.12 the butt-welded joint possesses a fatigue notch factor of K_f=2.0 while K_f for the cruciform (double-fillet) welded joint (10×13 mm) is 25% higher in magnitude. The higher value of K_f shortens the fatigue life of the double-fillet welded joint. The reduction in life based on the hysteresis-loop energy approach exceeds 4 times. This reduction in life, based on the critical plane/energy approach is up to 10 times. The notch stress-intensity approach however shows no reduction in life (figure 6.11). The hysteresis loop energy approach in figure 6.10 fails to introduce the weaker double-fillet welded joint of Lazzarin (13×10 mm) in terms of curve slope (curve slope=0.61) compared to the stronger butt-welded joint of Chapetti (curve slope=0.67).

Fatigue life assessments of butt versus fillet-welded joints for the same material were evaluated based on energy-based approaches and are presented in figures 6.10–6.12. Fatigue life assessments of butt-welded joints were evaluated based on energy-based approaches for three sets of different weld cap height (same material), and are presented in figures 6.13–6.15. Fatigue life assessments of butt-strap fillet versus butt-ground welded joints for aluminium alloys (magnesium-manganese-aluminium alloy) were evaluated based on energy-based approaches and are presented in figures 6.16–6.18.
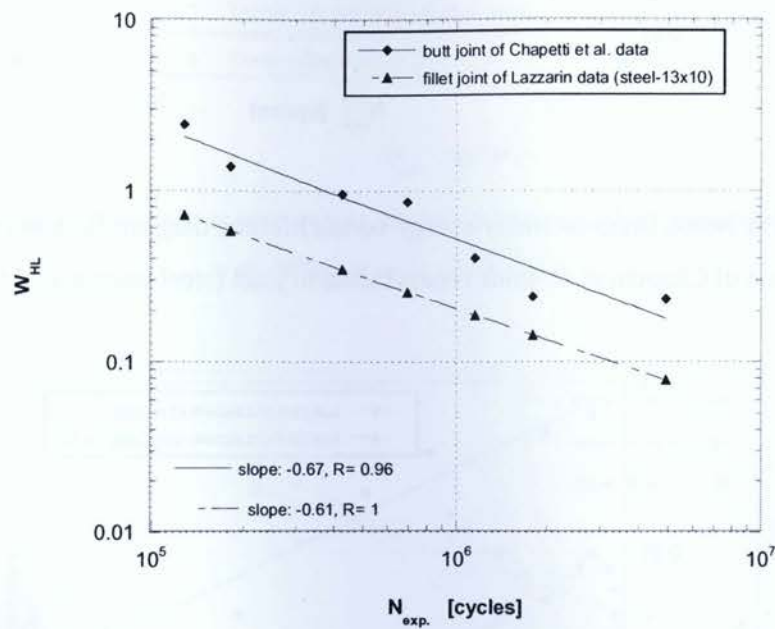
Figure 6.10 Hysteresis loop energy versus lifetime diagram for low carbon steel comparison of Chapetti et al. joint versus Lazzarin joint (steel reference) - 13×10 mm.
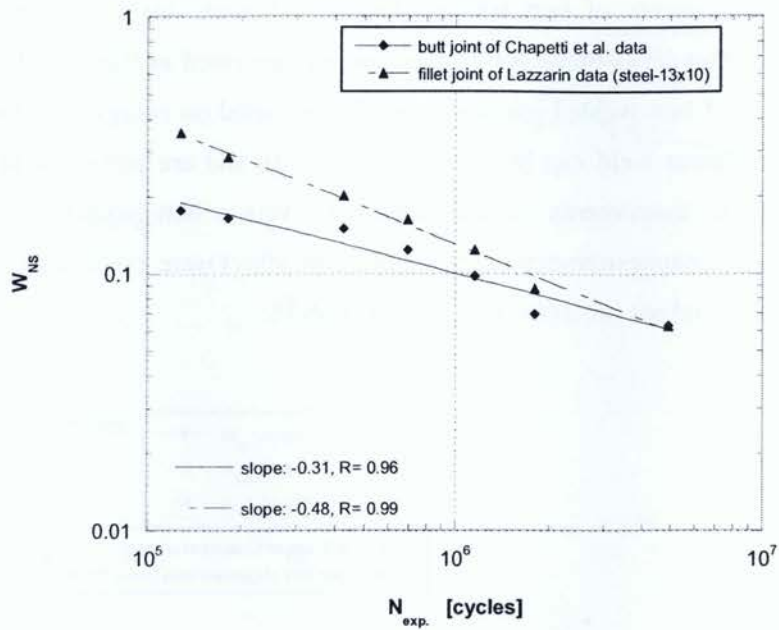
Figure 6.11 Notch stress-intensity energy versus lifetime diagram for low carbon steel comparison of Chapetti et al. joint versus Lazzarin joint (steel reference) - 13×10 mm.
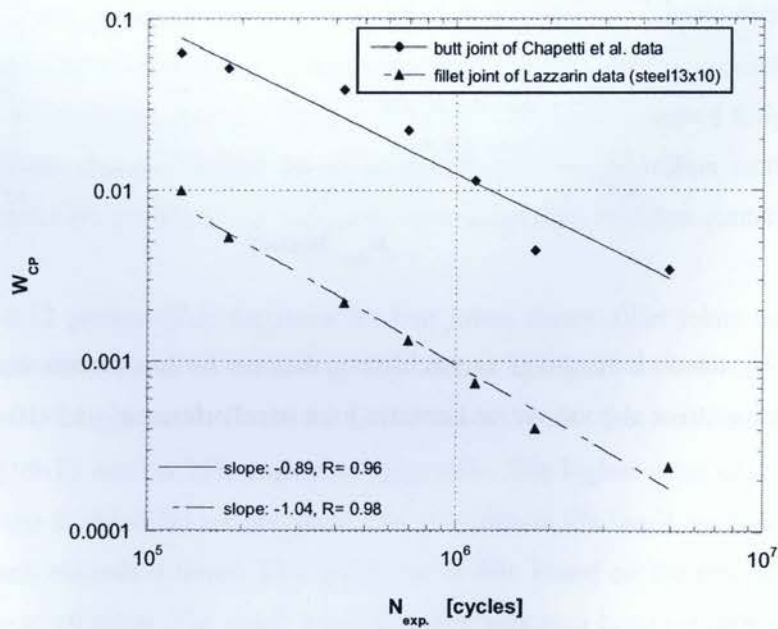
Figure 6.12 Critical plane/energy versus lifetime diagram for low carbon steel comparison of Chapetti et al. joint versus Lazzarin joint (steel reference) - 13×10 mm.
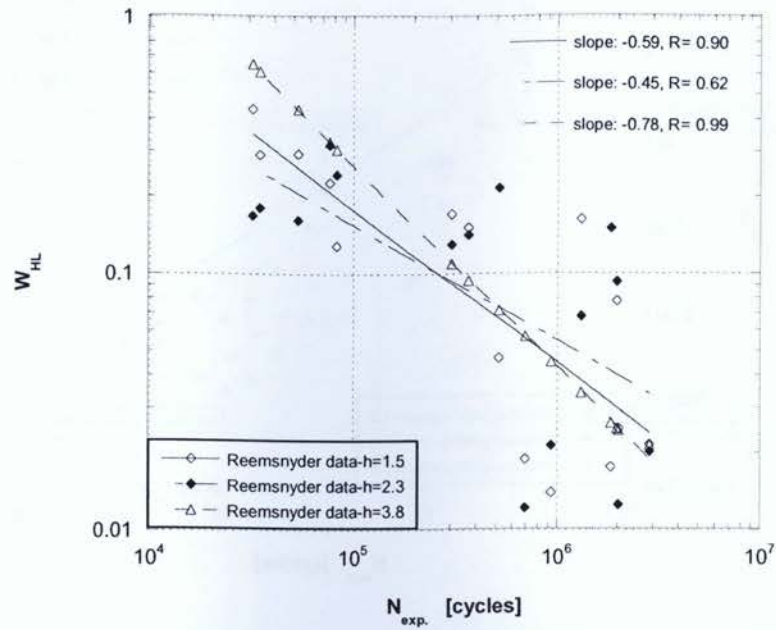
Figure 6.13 Hysteresis loop energy versus lifetime diagram for butt joints of Reemsnyder with different weld cap heights.
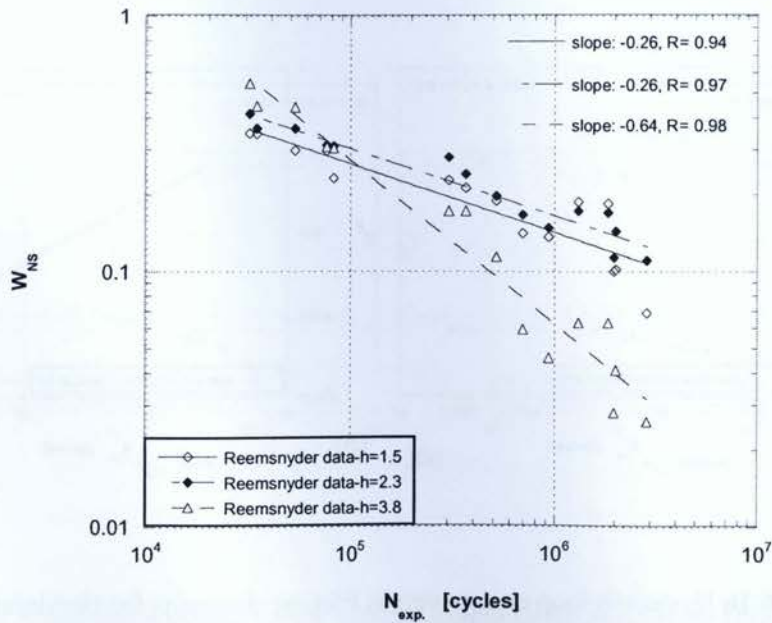
Figure 6.14 Notch stress-intensity energy versus lifetime diagram for butt joints of Reemsnyder with different weld cap heights.
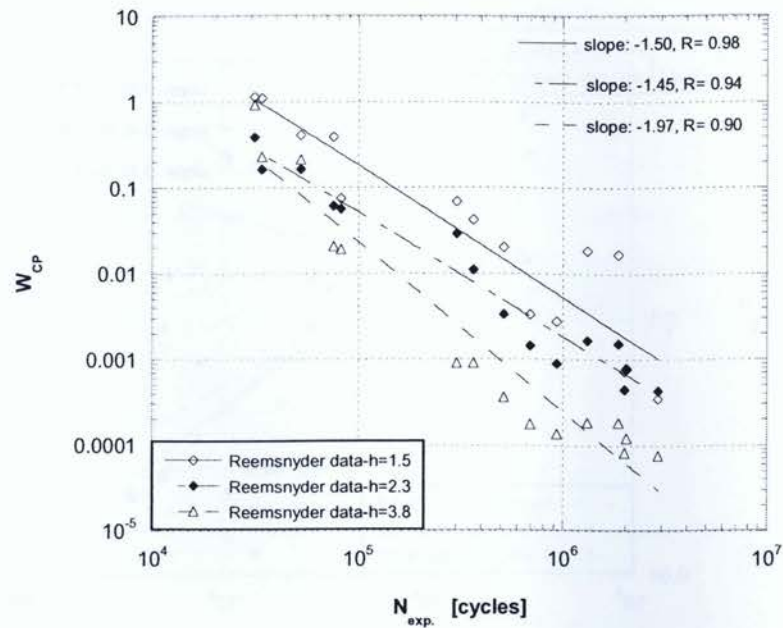
Figure 6.15 Critical plane/energy versus lifetime diagram for butt joints of Reemsnyder with different weld cap heights.
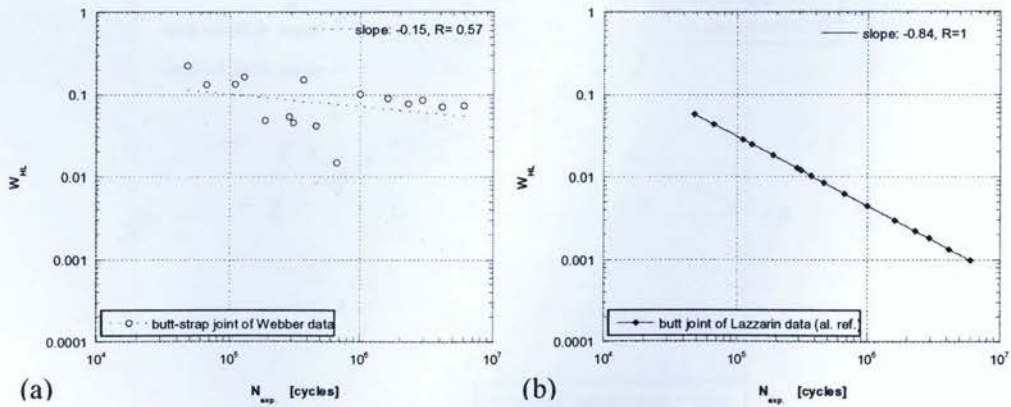
Figure 6.16 Hysteresis loop energy versus lifetime diagrams for aluminium alloys comparison of Webber joint (a), versus Lazzarin joint, aluminium reference (b).
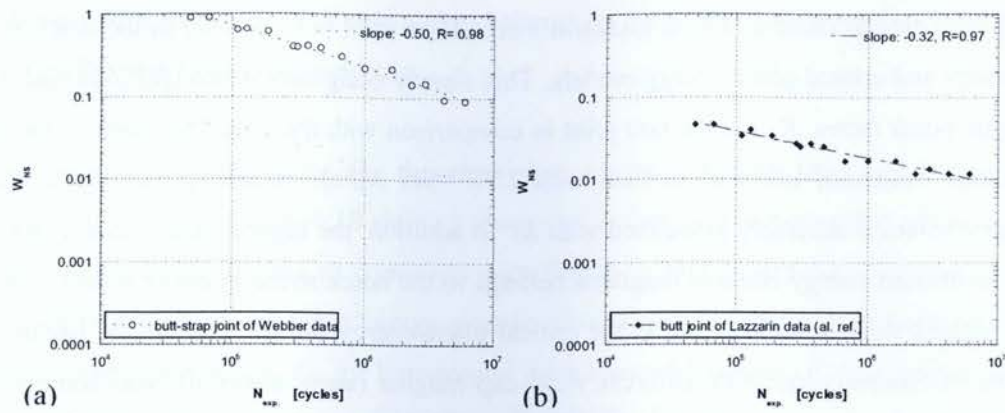
Figure 6.17 Notch stress-intensity energy versus lifetime diagrams for aluminium alloys comparison of Webber joint (a), versus Lazzarin joint, aluminium reference (b).
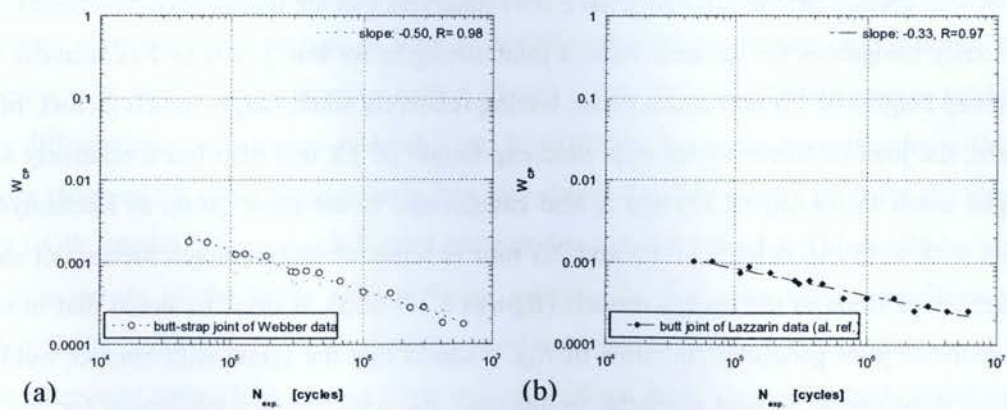
Figure 6.18 Critical plane/energy versus lifetime diagrams for aluminium alloys comparison of Webber joint (a), versus Lazzarin joint, aluminium reference (b).

Comparison of *W-N* diagrams for the low carbon steel butt and cruciform welded joints in figures 6.10–6.12 shows a lower curve slope and higher scatter of energy-life for Chapetti's butt-joint data as compared with Lazzarin's cruciform joint (13×10 mm) in the notch stress-intensity and critical plane/energy models. This clearly designates a stronger joint and lower fatigue notch factor, K_f, for the butt joint in comparison with the cruciform joint of the same material (structural low carbon steel with UTS^1=547 MPa), indicating that the scatter in energy values is inversely associated with K_f. In addition, the highest scatter convergence in the mentioned energy-lifetime diagrams belongs to the notch stress-intensity model, whereas the highest slope values belong to the critical plane/energy model. The fatigue life of butt-joints of Reemsnyder, with different weld cap heights (same material), was compared as energy based models were employed (figures 6.13–6.15), and it was found that no relation between scatter index and K_f can be seen.

The butt joints of Reemsnyder with weld cap height of 1.5 mm (K_f =2.10) and weld cap height of 2.3 mm (K_f=2.30) show similar response with the lowest slope values compared to the other butt joint of Reemsnyder with weld cap height of 3.8 mm (K_f =2.35), in the notch stress-intensity and critical plane/energy models in figures 6.13–6.15. This shows that welded joints with greater fatigue resistance have *W-N* diagrams that are more nearly horizontal. This obviously designates the greatest welded-joint strengths for butt joints of Reemsnyder with weld cap heights of 1.5 mm and 2.3 mm, having relatively small fatigue notch factors. In this regard, the joint of Reemsnyder with weld cap height of 3.8 mm also has a relatively small fatigue notch factor (K_f =2.35) and is also categorized in the same group as Reemsnyder's joints with weld cap heights of 1.5 and 2.3 mm in terms of fatigue notch factor, but shows higher curve slope in the energy models (figures 6.13–6.15). It must be noted that in equal situations of joint geometry (in terms of K_f), it seems that the joints with smaller weld cap heights show greater fatigue strengths. In this case, the comparison is performed for one type of base metal (quenched and tempered carbon steel with UTS=814 MPa).

Comparison of *W-N* diagrams for different butt-welded joints in all three energy models in figures 6.13–6.15, shows that the highest curve slope belongs to the joint of Reemsnyder with weld cap height of 3.8 mm (K_f=2.35). Although this joint is in the same category as the other

---

[1] Ultimate tensile strength.

two butt joints of Reemsnyder (h=1.5 and h=2.3 mm), in terms of fatigue notch factor, it shows a sudden decrease in fatigue strength. This shows that up to 2.3 mm weld cap height, a similar response can be expected in the W-N curves. In this regard, the weakest butt joint of the three compared joints of Reemsnyder, belongs to the joint of Reemsnyder with h=3.8 mm, possibly due to its large weld cap.

Comparison of W-N diagrams for the aluminium alloys butt-strap fillet and butt-ground welded joints in figures 6.16–6.18 shows a lower curve slope and higher scatter of energy-life for Lazzarin's butt-joint data as compared with Webber's butt-strap fillet joint in the notch stress-intensity and critical plane/energy models. This clearly designates a stronger joint and lower fatigue notch factor, K_f, for butt-ground joint type of Lazzarin (K_f =1) in comparison with butt-strap fillet joint type of Webber (K_f =1.95), for aluminium alloys, once again indicating that the scatter in energy values is inversely associated with K_f. In addition, both the notch stress-intensity and critical plane/energy models show the same scatter convergence and slope values in the mentioned energy-lifetime diagrams.

In evaluating the W-N diagrams, it was found that the hysteresis-loop energy model fails to differentiate the stronger welded joints from the weaker welded joints using either the scatter index or the curve slope criteria. The comparison was made for different types of joints with the same material, the same type of joint with different weld cap heights, and different types of joints with similar alloys (figures 6.10, 6.13 and 6.16). The critical plane/energy model not only differentiates the stronger welded joints from the weaker welded joints using either the scatter index or the curve slope criteria, but also shows a higher energy level for the stronger joint (with smaller fatigue notch factor) compared to the weaker joint. This could be seen in the comparison of the joints with different geometries; butt joint versus cruciform joint (figure 6.12), and butt joints with different weld cap heights (figure 6.15). In the case of butt-strap fillet joint versus butt-ground joint of similar alloys, both having relatively small values of fatigue notch factor, indicating strong joints, the critical plane/energy model differentiates the stronger welded joint from the weaker welded joint and shows energy levels with close proximity (figure 6.18).

In evaluating fatigue damage of welded joints through the mentioned energy models, another important comparison that must be considered is how readily coefficients/constants are determined and employed in the energy parameters. In the hysteresis-loop energy model, no

local stress analysis and fatigue notch factor were required. The fatigue assessment was determined from the nominal stress versus fatigue life data and coefficients of n', b, c, σ'_f, ε'_f from the fatigue properties table of the joint base metal. In the notch stress-intensity energy model, variables such as e_d and λ are obtained from diagrams. Constants such as R_c and E are available and found from the fatigue properties table of the joint base metal. In order to obtain the stress intensity factor, K, the geometry coefficient, k, is obtained from a diagram through geometric specifications of the joint. Plate thickness is obtained from the geometric specifications of the joint. The eigenvalue, λ, is obtained from a diagram, and for normal tension stress σ_{nt}, the local stress amplitude is calculated. In order to find the local stress amplitude, the local stress must be calculated using the fatigue notch factor, K_f; the stress concentration factor, K_t, and the fatigue notch factor, K_f, are determined from standard diagrams. Constants such as K' and n' are used for calculating the local stress, which are obtained from the fatigue properties table of the joint base metal. In the critical plane/energy model, constants such as σ'_f and ε'_f are obtained from the fatigue properties table of the joint base metal. Coefficients such as τ'_f and γ'_f are calculated using the obtained constants. In order to calculate $\Delta\sigma_n$, $\Delta\varepsilon_n$, $\Delta\tau_{max}$, and $\Delta(\gamma_{max}/2)$, principal stresses and strains are calculated. For the calculation of principal stresses, the local stress is calculated using Neuber's rule. Once the principal stresses are found, the principal strains are calculated from the Ramberg-Osgood equation.

CHAPTER SEVEN

Conclusions and future recommendations

7.1 Conclusions

In order to achieve the most reliable welded joint, under cyclic loading, the state of local stress and strain at the notch root (weld toe) is to be determined. A welded joint is a stress raiser, causing a reduction in fatigue strength of the welded component or structure. Although today fatigue failure of welded joints remains the most common type of failure, unfortunately recognizing this problem at the design stage, before the manufacturing procedure, is not complete yet, and affecting parameters are still unknown due to the complicated nature of the fatigue of weldments. Thus, it is very important that design engineers have sufficient knowledge and information on recent fatigue damage-assessment methods of welded joints.

Fatigue in weldments is a complicated issue due to the nature of the welding process. Considering the complication of the subject and its wide application, it is common to have different approaches for fatigue analysis of welded joints. Fatigue failures in welded joints occur at the weld toe region where the stress is highly localized. In this regard, local approaches can be used based on local stress and strain calculations.

Stress or strain based weld fatigue-assessment methods were reviewed. Stress or strain based criteria are limited to assess fatigue life in the low-cycle or the high-cycle fatigue regimes. The fatigue phenomenon involves cyclic plastic deformation. Energy-based fatigue assessment methods, which are categorized as local approaches, however, involve both the stress and strain components in damage assessment of materials.

Three energy-based methods were employed to assess fatigue of welded joints. These energy-based methods consist of the hysteresis-loop energy method, the fracture-mechanics energy-method or notch stress-intensity method, and the critical plane/energy method. Of these methods, only the notch stress-intensity method has been recently developed and applied to welded joints. The purpose was to evaluate the energy-based approaches for fatigue damage assessment of welded joints.

Energy versus fatigue life data diagrams (*W-N* diagrams) were evaluated based on different approaches and compared for different joint/material types: (i) butt versus fillet joint for the same base metal, (ii) butt joints with different weld cap heights (same base metal), and (iii) butt versus butt-strap fillet joint of aluminium alloys.

The values of K_f factor for welded joints, which indicate their fatigue strength, are highly influenced by welded joint type. Other parameters such as base plate thickness, weld toe radius, and weld angle were also found to influence the K_f factor value.

The calculated values of K_f factor for various welded joints were evaluated with K_t factor values determined by finite element analysis used in the equation resulting from Peterson's equation (equation 4.2) to determine K_f factor required for the energy models.

Energy-based fatigue models of the hysteresis-loop energy method, notch stress-intensity energy method, and the critical plane/energy method have corresponded differently as they were plotted versus fatigue lives. Of these models, the critical plane/energy model possessed a steeper *W-N* curve slope. This suggests that the critical plane/energy approach has correlated fatigue data of welded joints with less scatter in fatigue life range.

Both approaches of the notch stress-intensity and the critical plane/energy methods are dependant on K_f factor and they incorporate the effect of weld joint types in the fatigue analysis, while the hysteresis-loop energy approach fails to correspond to various joint types as the K_f factor is not used in the analysis.

The availability of the coefficients/constants and how readily they are determined and employed in the energy approaches are essential in the damage assessment of welded joints. The critical plane/energy approach is more readily used compared with other energy-based approaches. In addition, it is not based on geometrical specifications of the welded joint, thus reducing the error probability due to dimensional measurements.

Energy approaches were employed to evaluate the fatigue damage of various weld joints under uniaxial loading conditions. Energy-fatigue life (*W-N*) curves were further discussed and comported for their capabilities in assessing fatigue life of various joints through different parameters including curve slope, life data scatter, and how readily

coefficients/constants are determined and employed in the energy methods. The critical plane/energy approach was found to be the most suitable energy-based approach for fatigue damage and life assessment of welded joints by offering sharper W-N curves and less life scatter. This approach also allowed employing readily available material coefficients/properties as compared with notch stress-intensity energy approach.

7.2 Future recommendations

In spite of vast information on the fatigue of weldments and their various joint types and loading spectrum, the present work reviews three distinct welded joint types under uniaxial fatigue loading conditions. In the current study, only fusion welded joints were considered and the performance of other welded joint types such as spot welded joints, which are mostly applied to thin-walled components, requires further investigation. It is also recommended to investigate fatigue of welded joints at different stress ratios, loading spectrum including multi-axial loading, and variable amplitude loading conditions.

APPENDICES

Appendix A - Stress versus lifetime tables (extracted from literature) related to the welded joints of data sets

Appendix A tabulates the nominal stress [MPa] versus endurance lifetime [cycles] for the tested welded joints extracted from the literature.

Tables A.1 through A.9: present fatigue test results performed for different welded joint types.

Table A.1 Nominal stress range versus fatigue life experimental data by Chapetti et al. [32].

ΔS_{nom} [MPa]	$N_{exp.}$ [cycles]
418	17,338
396	43,804
368	80,475
318	95,748
266	332,669
211	770,535
198	816,488
186	1,122,831
165	1,891,166
152	5,522,534

Table A.2 Nominal stress range versus fatigue life experimental data by Livieri and Lazzarin
(with reference to steel joint) - 13×10 mm [29].

ΔS_{nom} [MPa]	$N_{exp.}$ [cycles]
236	127,355
199	180,896
157	424,910
138	694,501
118	1,148,496
98	1,791,364
82	4,898,879

Table A.3 Nominal stress range versus fatigue life experimental data by Livieri and Lazzarin
(with reference to steel joint) - 25×32 mm [29].

ΔS_{nom} [MPa]	$N_{exp.}$ [cycles]
226	111,978
179	203,345
129	549,624
98	1,121,938
83	2,263,558
68	5,000,000

Table A.4 Nominal stress range versus fatigue life experimental data by Livieri and Lazzarin
(with reference to steel joint) - 38×220 mm [29].

ΔS_{nom} [MPa]	$N_{exp.}$ [cycles]
218	131,904
179	150,018
129	419,968
109	710,941
84	1,021,705
74	1,538, 647

Table A.5 Nominal stress range versus fatigue life experimental data by Livieri and Lazzarin
(with reference to aluminium joint) [29].

ΔS_{nom} [MPa]	$N_{exp.}$ [cycles]
208	47,863
208	66,681
194	129,420
178	109,648
178	187,068
160	369,828
159	285,759
153	307,610
153	461,318
125	666,807
125	1,000,000
125	1,614,359
112	2,910,717
104	2,290,868
104	4,130,475
104	5,970,353

Table A.6 Nominal maximum stress versus fatigue life experimental data by
Reemsnyder-h=1.5 mm [33].

$S_{nom(max)}$ [MPa]	$N_{exp.}$ [cycles]
486	52,445
484	87,902
418	86,402
416	119,832
350	246,934
347	172,019
333	200,846
312	882,738
311	184,281
309	3,048,810
268	2,797,361
265	4,085,348
228	1,982,536
226	466,880
188	2,123,863

Table A.7 Nominal maximum stress versus fatigue life experimental data by Reemsnyder-h=2.3 mm [33].

$S_{nom(max)}$ [MPa]	$N_{exp.}$ [cycles]
379	175, 006
344	160,572
344	184,282
314	77,923
312	109,949
295	242,719
272	218, 900
246	128,374
230	554,587
228	204,334
226	4,852,800
212	2,395,859
209	4,688,562
186	373,361
184	2,566,650
144	2,479,784

Table A.8 Nominal maximum stress versus fatigue life experimental data by
Reemsnyder-h=3.8 mm [33].

$S_{nom(max)}$ [MPa]	$N_{exp.}$ [cycles]
418	31,290
348	34,103
346	52,445
281	75,285
279	82,052
209	303,596
209	366,890
170	517,683
126	1,311,560
126	1,850,613
123	693,685
105	929,524
102	2,016,961
84	1,982,536
81	2,895,351

Table A.9 Nominal stress range versus fatigue life experimental data by Webber [34].

ΔS_{nom} [MPa]	$N_{exp.}$ [cycles]
184	9,060
183	16,812
156	12,934
155	16,500
152	54,726
123	14,472
122	48, 908
121	58,984
120	66,002
106	218,907
91	184,942
90	349,670
74	943,770
73	1,425,141
59	1,117,095
58	1,565,085
44	1,594, 681
43	4,816,114
34	6,030,155

Appendix B – Cyclic stress-strain properties tables related to the welded joints' base metals of data sets

Appendix B tabulates the monotonic and cyclic properties for welded joints extracted from the literature.

Tables B.1 through B.9: present monotonic and cyclic properties for different base metals/ welded joints.

Table B.1 Monotonic and fatigue properties of low carbon structural steel 1025 AISI used as base metal of welded joint (data by Chapetti et al. - extracted from ASM Handbook [41]).

Material	Product condition	UTS[1] MPa	TYS[2] MPa	E MPa	n'	K MPa	σ'_f MPa	b	ε'_f	c
1025 AISI	Hot-rolled	547	306	204,000	0.20	1082	961	-0.10	0.56	-0.51

Table B.2 Monotonic and fatigue properties of low carbon structural steel 1025 AISI used as base metal of welded joint (data by Livieri and Lazzarin-13×10 mm - extracted from ASM Handbook [41]).

Material	Product condition	UTS MPa	TYS MPa	E MPa	n'	K MPa	σ'_f MPa	b	ε'_f	c
1025 AISI	Hot-rolled	547	306	204,000	0.20	1082	961	-0.10	0.56	-0.51

---

[1] Ultimate tensile strength.
[2] Tensile yield strength.

Table B.3 Monotonic and fatigue properties of low carbon structural steel 1025 AISI used as base metal of welded joint (data by Livieri and Lazzarin-25×32 mm - extracted from ASM Handbook [41]).

Material	Product condition	UTS MPa	TYS MPa	E MPa	n'	K MPa	σ'_f MPa	b	ε'_f	c
1025 AISI	Hot-rolled	547	306	204.000	0.20	1082	961	-0.10	0.56	-0.51

Table B.4 Monotonic and fatigue properties of low carbon structural steel 1025 AISI used as base metal of welded joint (data by Livieri and Lazzarin-38×220 mm - extracted from ASM Handbook [41]).

Material	Product condition	UTS MPa	TYS MPa	E MPa	n'	K MPa	σ'_f MPa	b	ε'_f	c
1025 AISI	Hot-rolled	547	306	204,000	0.20	1082	961	-0.10	0.56	-0.51

Table B.5 Monotonic and fatigue properties of AlMg4.5Mn aluminium alloy plate used as base metal of welded joint (data by Livieri and Lazzarin - extracted from ASM Handbook [41].

Material	Product condition	UTS MPa	TYS MPa	E MPa	n'	K MPa	σ'_f MPa	b	ε'_f	c
AlMg4.5Mn	STA[1]	363	298	71,500	0.125	693	654	-0.089	0.450	-0.755

---

[1] STA: Solution Treated and Aged.

Table B.6 Monotonic and fatigue properties of 10B21 carbon steel used as base metal of welded joint (data by Reemsnyder-h=1.5 - extracted from ASM Handbook [41].

Material	Product condition	UTS MPa	TYS MPa	E MPa	n'	K MPa	σ'_f MPa	b	ε'_f	c
10B21	QT[1]	814	742	200,000	0.08	876	833	-0.05	1.42	-0.74

Table B.7 Monotonic and fatigue properties of 10B21 carbon steel used as base metal of welded joint (data by Reemsnyder-h=2.3 - extracted from ASM Handbook [41].

Material	Product condition	UTS MPa	TYS MPa	E MPa	n'	K MPa	σ'_f MPa	b	ε'_f	c
10B21	QT	814	742	200,000	0.08	876	833	-0.05	1.42	-0.74

Table B.8 Monotonic and fatigue properties of 10B21 carbon steel used as base metal of welded joint (data by Reemsnyder-h=3.8 - extracted from ASM Handbook [41].

Material	Product condition	UTS MPa	TYS MPa	E MPa	n'	K MPa	σ'_f MPa	b	ε'_f	c
10B21	QT	814	742	200,000	0.08	876	833	-0.05	1.42	-0.74

Table B.9 Monotonic and fatigue properties of Al-Zn-Mg aluminium alloy plate used as base metal of welded joint (data by Webber - extracted from ASM Handbook [41].

Material	Product condition	UTS MPa	TYS MPa	E MPa	n'	K MPa	σ'_f MPa	b	ε'_f	c
Al-Zn-Mg	---	385	330	70,000	0.068	752	965	-0.095	0.532	-0.828

---

[1] QT: Quenched and Tempered.

Appendix C – Dimensional specifications of the welded joints

Appendix C tabulates the dimensional specifications of the tested welded joints extracted from the literature.

Tables C.1 through C.9: present dimensional specifications for different welded joint types.

Table C.1 Dimensional specifications of welded joint (data used by Chapetti et al. [32]).

Load	Joint-type	t^1	h^2	L^3	L/t	$2h/t$
transverse	butt-joint	12.5	2	0	0	0.32

Table C.2 Dimensional specifications of welded joint for data used by Livieri and Lazzarin (with reference to steel joint-13×10 mm) [30].

Load	Joint-type	t	h	L	L/t	$2h/t$
transverse	nlc cruciform joint	13	8	10	0.769	1.231

Table C.3 Dimensional specifications of welded joint for data used by Livieri and Lazzarin (with reference to steel joint-25×32 mm) [30].

Load	Joint-type	t	h	L	L/t	$2h/t$
transverse	nlc cruciform joint	25	9	32	1.280	0.720

Table C.4 Dimensional specifications of welded joint for data used by Livieri and Lazzarin (with reference to steel joint-38×220 mm) [30].

Load	Joint-type	t	h	L	L/t	$2h/t$
transverse	nlc cruciform joint	38	15	220	5.789	0.789

---

[1] t: base plate thickness in welded joint.
[2] h: weld cap (reinforcement) height.
[3] L: transverse plate (attachment) thickness in fillet or cruciform welded joint.

Table C.5 Dimensional specifications of welded joint for data used by Livieri and Lazzarin (with reference to aluminium joint) [30].

Load	Joint-type	t	h	L	L/t	$2h/t$
transverse	butt-joint	9.5	0	0	0	0

Table C.6 Dimensional specifications of welded joint for data used by Reemsnyder-h=1.5 mm [33].

Load	Joint-type	t	h	L	L/t	$2h/t$
transverse	butt-joint	19.1	1.5	0	0	0.157

Table C.7 Dimensional specifications of welded joint for data used by Reemsnyder-h=2.3 mm [33].

Load	Joint-type	t	h	L	L/t	$2h/t$
transverse	butt-joint	19.1	2.3	0	0	0.240

Table C.8 Dimensional specifications of welded joint for data used by Reemsnyder-h=3.8 mm [33].

Load	Joint-type	t	h	L	L/t	$2h/t$
transverse	butt-joint	19.1	3.8	0	0	0.398

Table C.9 Dimensional specifications of welded joint for data used by Webber [34].

Load	Joint-type	t	h	L	L/t	$2h/t$
transverse	double butt-strap lc fillet joint	12	12	0	0	2

Appendix D – Stress concentration factor diagrams for welded joints

Appendix D presents cross sectional models of joints used for finding stress concentration factors of welded joints under axial and bending loading. Stress concentration factor diagrams of tensile loaded welded joints are also presented.

(a)

(b)
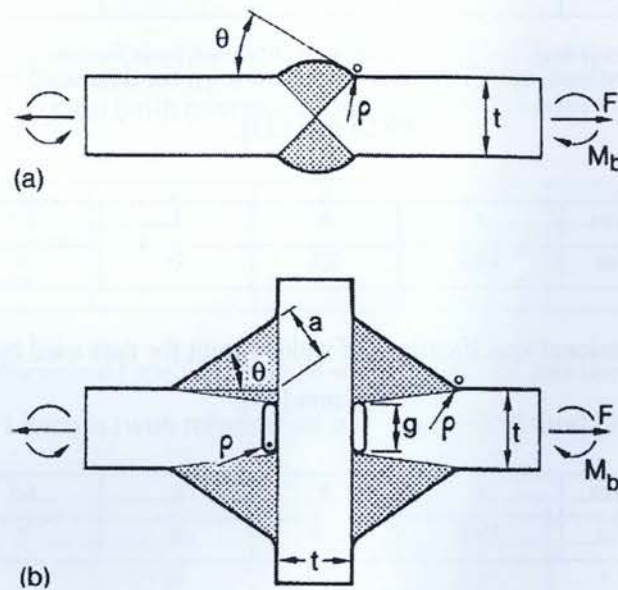
Figure D.1 Cross sectional models of butt-welded joint (a) and cruciform joint (b) for finding the stress concentration factor under tensile loading [3]. The weld-toe angle θ is the acute angle.
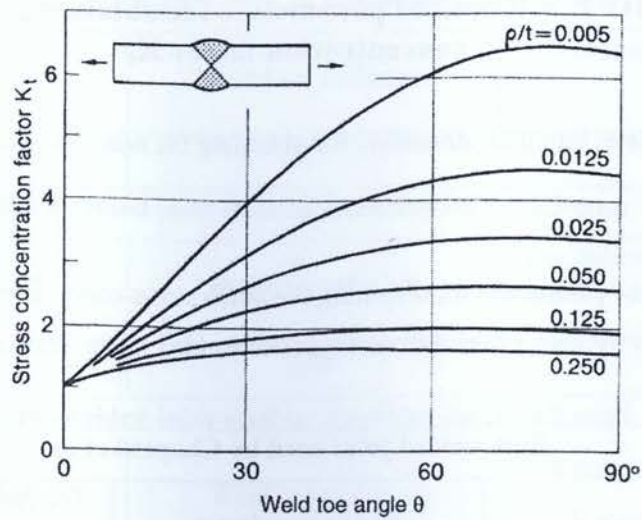
Figure D.2 Stress concentration factor diagram of tensile loaded butt joint as the weld toe angle changes [3].
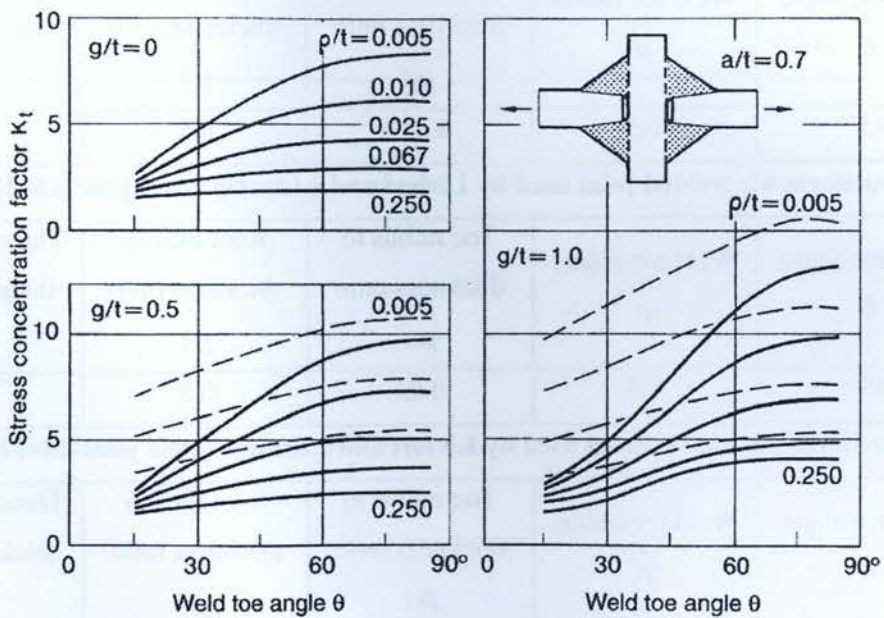
Figure D.3 Stress concentration factor diagrams at weld toe (solid curves) and weld root (dashed curves) of tensile loaded cruciform joint as the weld toe angle of the fillet weld changes [3].

Appendix E – Required parameters for obtaining notch stress-concentration factor K_t

Appendix E tabulates required parameters for obtaining the notch stress-concentration factor (Appendix D).

Table E.1 Required parameters for obtaining the notch stress-concentration factor, K_t, from standard diagrams for each of the different types of welded joints related to the data sets.

Butt-welded joint used by Chapetti et al.		
Weld toe angle θ	Weld toe radius ρ	Toe radius to thickness ratio ρ/t
45°	0.5	0.040

Cruciform nlc welded joint used by Livieri and Lazzarin (steel joint-13×10 mm)				
Weld toe angle θ	Weld toe radius ρ	Toe radius to thickness ratio ρ/t	Root face to thickness ratio g/t	Throat length to thickness ratio a/t
45°	0.5	0.039	0.5	0.7

Cruciform nlc welded joint used by Livieri and Lazzarin (steel joint-25×32 mm)				
Weld toe angle θ	Weld toe radius ρ	Toe radius to thickness ratio ρ/t	Root face to thickness ratio g/t	Throat length to thickness ratio a/t
45°	0.5	0.02	0.5	0.7

Cruciform nlc welded joint used by Livieri and Lazzarin (steel joint-38×220 mm)				
Weld toe angle θ	Weld toe radius ρ	Toe radius to thickness ratio ρ/t	Root face to thickness ratio g/t	Throat length to thickness ratio a/t
45°	0.5	0.013	0.5	0.7

Butt-welded joint used by Livieri and Lazzarin (aluminium joint)		
Weld toe angle θ	Weld toe radius ρ	Toe radius to thickness ratio ρ/t
0°	Not applicable	Not applicable

Butt-welded joint used by Reemsnyder (h=1.5 mm)		
Weld toe angle θ	Weld toe radius ρ	Toe radius to thickness ratio ρ/t
40°	0.5	0.026
Butt-welded joint used by Reemsnyder (h=2.3 mm)		
Weld toe angle θ	Weld toe radius ρ	Toe radius to thickness ratio ρ/t
55°	0.5	0.026
Butt-welded joint used by Reemsnyder (h=3.8 mm)		
Weld toe angle θ	Weld toe radius ρ	Toe radius to thickness ratio ρ/t
70°	0.5	0.026
Double butt-strap lc fillet welded joint used by Webber		
Weld toe angle θ	Weld toe radius ρ	Toe radius to thickness ratio ρ/t
45°	0.5	0.042

Appendix F – Calculated parameters and energy values of experimental data sets for three energy models

Appendix F tabulates the calculated parameters and energy values for experimental data sets for three energy approaches.

Tables F1.1 through F1.18: present calculated parameters related to experimental data sets for the energy models.

Tables F2.1 through F2.27: present calculated energy values related to experimental data sets for three energy models.

Table F1.1 Calculated parameters used in the notch stress-intensity energy method (Chapetti et al. data).

K'	K_t	K_f	
1076.7	2.75	2	
k_1	λ_1	ed_1	R_c
0.65	0.675	0.075	0.28
$\Delta\sigma_{loc}$ [MPa]	σ_{nt} [MPa]	K_1	$K_1{}^2$
621	310.5	458.8	210,450
599	299.5	442.5	195,803
571	285.5	421.8	177,925
519	259.5	383.4	146,994
461	230.5	340.5	115,976
389	194.5	287.4	82,578
370	185.0	273.3	74,708
351	175.5	259.3	67,233
317	158.5	234.2	54,838
295	147.5	218.0	47,491

Table F1.2 Calculated parameters used in the notch stress-intensity energy method - Livieri and Lazzarin data (with reference to steel joint) - 13×10 mm.

K'	K_t	K_f	
1076.7	3.8	2.55	
k_1	λ_1	ed_1	R_c
1.14	0.675	0.075	0.28
$\Delta\sigma_{loc}$ [MPa]	σ_{nt} [MPa]	K_1	K_1^2
495	247.5	649.5	421,862
443	221.5	581.3	337,884
372	186.0	488.1	238,257
335	167.5	439.6	193,219
292	146.0	383.2	146,800
246	123.0	322.8	104,191
208	104.0	272.9	74,488

Table F1.3 Calculated parameters used in the notch stress-intensity energy method - Livieri and Lazzarin data (with reference to steel joint) - 25×32 mm.

K'	K_t	K_f	
1076.7	5	3.585	
k_1	λ_1	ed_1	R_c
1.15	0.675	0.075	0.28
$\Delta\sigma_{loc}$ [MPa]	σ_{nt} [MPa]	K_1	K_1^2
588	294.0	962.6	926,542
518	259.0	848.0	719,068
420	210.0	687.6	472,726
336	168.0	550.0	302,544
290	145.0	474.7	225,376
241	120.5	394.5	155,648

Table F1.4 Calculated parameters used in the notch stress-intensity energy method - Livieri and Lazzarin data (with reference to steel joint) - 38×220 mm.

K'	K_t	K_f	
1076.7	5.75	4.4	
k_1	λ_1	ed_1	R_c
1.14	0.675	0.075	0.28
$\Delta\sigma_{loc}$ [MPa]	σ_{nt} [MPa]	K_1	K_1^2
638	319	1467.2	2,152,720
579	289.5	1331.5	1,772,978
480	240	1103.9	1,218, 509
429	214.5	986.6	973,331
351	175.5	807.2	651,569
314	157	722.1	521,441

Table F1.5 Calculated parameters used in the notch stress-intensity energy method -
Livieri and Lazzarin data (with reference to aluminium joint).

K'	K_t	K_f	
722.7	1	1	
k_1	λ_1	ed_1	R_c
0.5	0.675	0.075	0.12
$\Delta\sigma_{loc}$ [MPa]	σ_{nt} [MPa]	K_1	K_1^2
208	104.0	108.2	46,122
208	104.0	108.2	46,122
194	97.0	100.9	40,289
178	89.0	92.6	34,077
178	89.0	92.6	34,077
160	80.0	83.2	27,689
159	79.5	82.7	27,344
153	76.5	79.6	25,319
153	76.5	79.6	25,319
125	62.5	65.0	16,900
125	62.5	65.0	16,900
125	62.5	65.0	16,900
112	56.0	58.2	13,568
104	52.0	54.1	11,699
104	52.0	54.1	11,699
104	52.0	54.1	11,699

Table F1.6 Calculated parameters used in the notch stress-intensity energy method -
Reemsnyder data-h=1.5 mm.

K'	K_t	K_f	
810.0	2.94	2.10	
k_I	λ_I	ed_I	R_c
0.55	0.675	0.075	0. 28
$\Delta\sigma_{loc}$ [MPa]	σ_{nt} [MPa]	K_I	K_I^2
886	443.0	635.9	404,403
884	442.0	634.5	402,579
821	410.5	589.3	347,242
818	409.0	587.1	344,709
723	361.5	518.9	269,292
718	359.0	515.3	265,580
692	346.0	496.7	246,694
654	327.0	469.4	220,344
650	325.0	466.5	217,657
645	322.5	462.9	214,322
565	282.5	405.5	164,454
556	278.0	399.1	159,256
479	239.5	343.8	118,200
475	237.5	340.9	116,234
395	197.5	283.5	80,379

Table F1.7 Calculated parameters used in the notch stress-intensity energy method -
Reemsnyder data-h=2.3 mm.

K'	K_t	K_f	
810.0	3.30	2.30	
k_1	λ_1	ed_1	R_c
0.65	0.675	0.075	0. 28
$\Delta\sigma_{loc}$ [MPa]	σ_{nt} [MPa]	K_1	K_1^2
818	409.0	693.9	481,453
767	383.5	650.6	423,290
767	383.5	650.6	423,290
712	356.0	604.0	364,760
708	354.0	600.6	360,674
673	336.5	570.9	325,895
624	312.0	529.3	280,167
565	282.5	479.3	229,691
529	264.5	448.7	201,353
524	262.0	444.5	197,565
520	260.0	441.1	194,560
490	245.0	415.6	172,759
482	241.0	408.9	167,164
428	214.0	363.1	131,806
423	211.5	358.8	128,744
331	165.5	280.8	78,832

Table F1.8 Calculated parameters used in the notch stress-intensity energy method - Reemsnyder data-h=3.8 mm.

K'	K_t	K_f	
810.0	3.44	2.35	
k_l	λ_l	ed_l	R_c
0.7	0.675	0.075	0. 28
$\Delta\sigma_{loc}$ [MPa]	σ_{nt} [MPa]	K_l	K_l^2
872	436.0	796.6	634,527
786	393.0	718.0	515,540
782	391.0	714.4	510,306
656	328.0	599.3	359,108
652	326.0	595.6	354,742
491	245.5	448.5	201,178
491	245.5	448.5	201,178
399	199.5	364.5	132,850
297	148.5	271.3	73,609
297	148.5	271.3	73,609
288	144.0	263.1	69,215
253	126.5	231.1	53,414
240	120.0	219.2	48,066
198	99.0	180.9	32,715
190	95.0	173.6	30,125

Table F1.9 Calculated parameters used in the notch stress-intensity energy method -

Webber data.

K'	K_t	K_f	
810.0	2.70	1.95	
k_1	λ_1	ed_1	R_c
1.16	0.675	0.075	0. 12
$\Delta\sigma_{loc}$ [MPa]	σ_{nt} [MPa]	K_1	K_1^2
359	179.5	467.0	218,124
357	178.5	464.4	215,700
304	152.0	395.5	156,409
301	150.5	391.6	153,337
295	147.5	383.8	147,285
240	120.0	312.2	97,485
238	119.0	309.6	95,867
236	118.0	307.0	94,262
234	117.0	304.4	92,672
207	103.5	269.3	72,520
177	88.5	230.3	53,023
175	87.5	227.7	51,831
144	72.0	187.3	35,095
142	71.0	184.7	34,127
115	57.5	149.6	22,383
113	56.5	147.0	21,611
85	42.5	110.6	12,228
83	41.5	108.0	11,659
66	33.0	85.9	7,372

Table F1.10 Calculated parameters used in the critical plane/energy method -

Chapetti et al. data.

τ'_f [MPa]	γ'_f	K'	K_t	K_f				
554.83	0.97	1076.7	2.75	2				
$\Delta\sigma_{loc}$ [MPa]	$\sigma_{max}=\sigma_{1(90)}$ [MPa]	$\sigma_{min}=\sigma_{1(270)}$ [MPa]	$\varepsilon_{1(90)}$	$\varepsilon_{1(270)}$	$\Delta\varepsilon_n$	$\Delta\sigma_{nt}$ [MPa]	$\Delta(\gamma_{max/2})$	$\Delta\tau_{max}$ [MPa]
621	690.00	69.00	0.11147	0.00034	0.05557	310.50	0.05557	310.50
599	665.56	66.56	0.09351	0.00033	0.04659	299.50	0.04659	299.50
571	634.44	63.44	0.07415	0.00031	0.03692	285.50	0.03692	285.50
519	576.67	57.67	0.04690	0.00028	0.02331	259.50	0.02331	259.50
461	512.22	51.22	0.02688	0.00025	0.01331	230.50	0.01331	230.50
389	432.22	43.22	0.01254	0.00021	0.00617	194.50	0.00617	194.50
370	411.11	41.11	0.01013	0.00020	0.00497	185.00	0.00497	185.00
351	390.00	39.00	0.00815	0.00019	0.00398	175.50	0.00398	175.50
317	352.22	35.22	0.00547	0.00017	0.00265	158.50	0.00265	158.50
295	327.78	32.78	0.00422	0.00016	0.00203	147.50	0.00203	147.50

Table F1.11 Calculated parameters used in the critical plane/energy method -

Livieri and Lazzarin data (with reference to steel joint) - 13×10 mm.

τ'_f [MPa]	γ'_f	K'	K_t	K_f				
554.83	0.97	1076.7	3. 8	2.55				
$\Delta\sigma_{loc}$ [MPa]	$\sigma_{max}=\sigma_{1(90)}$ [MPa]	$\sigma_{min}=\sigma_{1(270)}$ [MPa]	$\varepsilon_{1(90)}$	$\varepsilon_{1(270)}$	$\Delta\varepsilon_n$	$\Delta\sigma_{nt}$ [MPa]	$\Delta(\gamma_{max/2})$	$\Delta\tau_{max}$ [MPa]
495	495.00	0.00	0.02143	0.00	0.01071	247.5	0.01071	247.5
443	443.00	0.00	0.01296	0.00	0.00648	221.5	0.00648	221.5
372	372.00	0.00	0.00625	0.00	0.00313	186.0	0.00313	186.0
335	335.00	0.00	0.00424	0.00	0.00212	167.5	0.00212	167.5
292	292.00	0.00	0.00272	0.00	0.00136	146.0	0.00136	146.0
246	246.00	0.00	0.00174	0.00	0.00087	123.0	0.00087	123.0
208	208.00	0.00	0.00125	0.00	0.00062	104.0	0.00062	104.0

Table F1.12 Calculated parameters used in the critical plane/energy method -

Livieri and Lazzarin data (with reference to steel joint) - 25×32 mm.

τ'_f [MPa]	γ'_f	K'	K_t	K_f				
554.83	0.97	1076.7	5	3.585				
$\Delta\sigma_{loc}$ [MPa]	$\sigma_{max}=\sigma_{1(90)}$ [MPa]	$\sigma_{min}=\sigma_{1(270)}$ [MPa]	$\varepsilon_{1(90)}$	$\varepsilon_{1(270)}$	$\Delta\varepsilon_n$	$\Delta\sigma_{nt}$ [MPa]	$\Delta(\gamma_{max/2})$	$\Delta\tau_{max}$ [MPa]
588	588.00	0.00	0.04861	0.00	0.02430	294.0	0.02430	294.0
518	518.00	0.00	0.02649	0.00	0.01325	259.0	0.01325	259.0
420	420.00	0.00	0.01028	0.00	0.00514	210.0	0.00514	210.0
336	336.00	0.00	0.00428	0.00	0.00214	168.0	0.00214	168.0
290	290.00	0.00	0.00267	0.00	0.00133	145.0	0.00133	145.0
241	241.00	0.00	0.00167	0.00	0.00083	120.5	0.00083	120.5

Table F1.13 Calculated parameters used in the critical plane/energy method -

Livieri and Lazzarin data (with reference to steel joint) - 38×220 mm.

τ'_f [MPa]	γ'_f	K'	K_t	K_f				
554.83	0.97	1076.7	5.75	4.4				
$\Delta\sigma_{loc}$ [MPa]	$\sigma_{max}=\sigma_{1(90)}$ [MPa]	$\sigma_{min}=\sigma_{1(270)}$ [MPa]	$\varepsilon_{1(90)}$	$\varepsilon_{1(270)}$	$\Delta\varepsilon_n$	$\Delta\sigma_{nt}$ [MPa]	$\Delta(\gamma_{max/2})$	$\Delta\tau_{max}$ [MPa]
638	638.00	0.00	0.07245	0.00	0.03623	319.0	0.03623	319.0
579	579.00	0.00	0.04510	0.00	0.02255	289.5	0.02255	289.5
480	480.00	0.00	0.01860	0.00	0.00930	240.0	0.00930	240.0
429	429.00	0.00	0.01126	0.00	0.00563	214.5	0.00563	214.5
351	351.00	0.00	0.00501	0.00	0.00251	175.5	0.00251	175.5
314	314.00	0.00	0.00340	0.00	0.00170	157.0	0.00170	157.0

Table F1.14 Calculated parameters used in the critical plane/energy method - Livieri and Lazzarin data (with reference to aluminium joint).

τ'_f [MPa]	γ'_f	K'	K_t	K_f				
377.59	0.78	722.7	1	1				
$\Delta\sigma_{loc}$ [MPa]	$\sigma_{max}=\sigma_{1(90)}$ [MPa]	$\sigma_{min}=\sigma_{1(270)}$ [MPa]	$\varepsilon_{1(90)}$	$\varepsilon_{1(270)}$	$\Delta\varepsilon_n$	$\Delta\sigma_{nt}$ [MPa]	$\Delta(\gamma_{max/2})$	$\Delta\tau_{max}$ [MPa]
208	208.00	0.00	0.00296	0.00	0.00148	104.00	0.00148	104.00
208	208.00	0.00	0.00296	0.00	0.00148	104.00	0.00148	104.00
194	194.00	0.00	0.00274	0.00	0.00137	97.00	0.00137	97.00
178	178.00	0.00	0.00250	0.00	0.00125	89.00	0.00125	89.00
178	178.00	0.00	0.00250	0.00	0.00125	89.00	0.00125	89.00
160	160.00	0.00	0.00224	0.00	0.00112	80.00	0.00112	80.00
159	159.00	0.00	0.00223	0.00	0.00111	79.50	0.00111	79.50
153	153.00	0.00	0.00214	0.00	0.00107	76.50	0.00107	76.50
153	153.00	0.00	0.00214	0.00	0.00107	76.50	0.00107	76.50
125	125.00	0.00	0.00175	0.00	0.00088	62.50	0.00088	62.50
125	125.00	0.00	0.00175	0.00	0.00088	62.50	0.00088	62.50
125	125.00	0.00	0.00175	0.00	0.00088	62.50	0.00088	62.50
112	112.00	0.00	0.00157	0.00	0.00078	56.00	0.00078	56.00
104	104.00	0.00	0.00146	0.00	0.00073	52.00	0.00073	52.00
104	104.00	0.00	0.00146	0.00	0.00073	52.00	0.00073	52.00
104	104.00	0.00	0.00146	0.00	0.00073	52.00	0.00073	52.00

τ'_f [MPa]	γ'_f	K'	K_t	K_f				
480.93	2.46	810	2.94	2.10				
$\Delta\sigma_{loc}$ [MPa]	$\sigma_{max}=\sigma_{1(90)}$ [MPa]	$\sigma_{min}=\sigma_{1(270)}$ [MPa]	$\varepsilon_{1(90)}$	$\varepsilon_{1(270)}$	$\Delta\varepsilon_n$	$\Delta\sigma_{nt}$ [MPa]	$\Delta(\gamma_{max/2})$	$\Delta\tau_{max}$ [MPa]
926	886.00	0.00	3.07245	0.00	1.53623	443.00	1.53623	443.00
924	884.00	0.00	2.98699	0.00	1.49350	442.00	1.49350	442.00
851	821.00	0.00	1.18776	0.00	0.59388	410.50	0.59388	410.50
836	818.00	0.00	1.13481	0.00	0.56740	409.00	0.56740	409.00
745	723.00	0.00	0.24525	0.00	0.12263	361.50	0.12263	361.50
736	718.00	0.00	0.22515	0.00	0.11258	359.00	0.11258	359.00
700	692.00	0.00	0.14318	0.00	0.07159	346.00	0.07159	346.00
657	654.00	0.00	0.07224	0.00	0.03612	327.00	0.03612	327.00
652	650.00	0.00	0.06713	0.00	0.03356	325.00	0.03356	325.00
648	645.00	0.00	0.06123	0.00	0.03061	322.50	0.03061	322.50
565	565.00	0.00	0.01391	0.00	0.00695	282.50	0.00695	282.50
559	556.00	0.00	0.01185	0.00	0.00592	278.00	0.00592	278.00
481	479.00	0.00	0.00380	0.00	0.00190	239.50	0.00190	239.50
477	475.00	0.00	0.00364	0.00	0.00182	237.50	0.00182	237.50
396	395.00	0.00	0.00210	0.00	0.00105	197.50	0.00105	197.50

Table F1.16 Calculated parameters used in the critical plane/energy method -

Reemsnyder data-h=2.3 mm.

τ'_f [MPa]	γ'_f	K'	K_t	K_f				
480.93	2.46	810	3.30	2.30				
$\Delta\sigma_{loc}$ [MPa]	$\sigma_{max}=\sigma_{1(90)}$ [MPa]	$\sigma_{min}=\sigma_{1(270)}$ [MPa]	$\varepsilon_{1(90)}$	$\varepsilon_{1(270)}$	$\Delta\varepsilon_n$	$\Delta\sigma_{nt}$ [MPa]	$\Delta(\gamma_{max/2})$	$\Delta\tau_{max}$ [MPa]
818	818.00	0.00	1.13481	0.00	0.56740	409.00	0.56740	409.00
767	767.00	0.00	0.50952	0.00	0.25476	383.50	0.25476	383.50
767	767.00	0.00	0.50952	0.00	0.25476	383.50	0.25476	383.50
712	712.00	0.00	0.20306	0.00	0.10153	356.00	0.10153	356.00
708	708.00	0.00	0.18947	0.00	0.09474	354.00	0.09474	354.00
673	673.00	0.00	0.10202	0.00	0.05101	336.50	0.05101	336.50
624	624.00	0.00	0.04147	0.00	0.02073	312.00	0.02073	312.00
565	565.00	0.00	0.01391	0.00	0.00695	282.50	0.00695	282.50
529	529.00	0.00	0.00751	0.00	0.00376	264.50	0.00376	264.50
524	524.00	0.00	0.00694	0.00	0.00347	262.00	0.00347	262.00
520	520.00	0.00	0.00653	0.00	0.00326	260.00	0.00326	260.00
490	490.00	0.00	0.00432	0.00	0.00216	245.00	0.00216	245.00
482	482.00	0.00	0.00393	0.00	0.00197	241.00	0.00197	241.00
428	428.00	0.00	0.00248	0.00	0.00124	214.00	0.00124	214.00
423	423.00	0.00	0.00241	0.00	0.00121	211.50	0.00121	211.50
331	331.00	0.00	0.00167	0.00	0.00083	165.50	0.00083	165.50

τ'_f [MPa]	γ'_f	K'	K_t	K_f				
480.93	2.46	810	3.44	2.35				
$\Delta\sigma_{loc}$ [MPa]	$\sigma_{max}=\sigma_{1(90)}$ [MPa]	$\sigma_{min}=\sigma_{1(270)}$ [MPa]	$\varepsilon_{1(90)}$	$\varepsilon_{1(270)}$	$\Delta\varepsilon_n$	$\Delta\sigma_{nt}$ [MPa]	$\Delta(\gamma_{max/2})$	$\Delta\tau_{max}$ [MPa]
851	872.00	0.00	2.51852	0.00	1.25926	436.00	1.25926	436.00
739	786.00	0.00	0.69055	0.00	0.34528	393.00	0.34528	393.00
735	782.00	0.00	0.64811	0.00	0.32406	391.00	0.32406	391.00
602	656.00	0.00	0.07493	0.00	0.03747	328.00	0.03747	328.00
598	652.00	0.00	0.06964	0.00	0.03482	326.00	0.03482	326.00
448	491.00	0.00	0.00437	0.00	0.00219	245.50	0.00219	245.50
448	491.00	0.00	0.00437	0.00	0.00219	245.50	0.00219	245.50
365	399.00	0.00	0.00214	0.00	0.00107	199.50	0.00107	199.50
270	297.00	0.00	0.00149	0.00	0.00074	148.50	0.00074	148.50
270	297.00	0.00	0.00149	0.00	0.00074	148.50	0.00074	148.50
264	288.00	0.00	0.00144	0.00	0.00072	144.00	0.00072	144.00
225	253.00	0.00	0.00127	0.00	0.00063	126.50	0.00063	126.50
219	240.00	0.00	0.00120	0.00	0.00060	120.00	0.00060	120.00
180	198.00	0.00	0.00099	0.00	0.00050	99.00	0.00050	99.00
174	190.00	0.00	0.00095	0.00	0.00048	95.00	0.00048	95.00

Table F1.18 Calculated parameters used in the critical plane/energy method -

Webber data.

τ'_f [MPa]	γ'_f	K'	K_t	K_f				
557.1	0.922	1007.3	2.70	1.95				
$\Delta\sigma_{loc}$ [MPa]	$\sigma_{max}=\sigma_{1(90)}$ [MPa]	$\sigma_{min}=\sigma_{1(270)}$ [MPa]	$\varepsilon_{1(90)}$	$\varepsilon_{1(270)}$	$\Delta\varepsilon_n$	$\Delta\sigma_{nt}$ [MPa]	$\Delta(\gamma_{max/2})$	$\Delta\tau_{max}$ [MPa]
359	359.00	0.00	0.00513	0.00	0.00256	179.50	0.00256	179.50
357	357.00	0.00	0.00510	0.00	0.00255	178.50	0.00255	178.50
304	304.00	0.00	0.00434	0.00	0.00217	152.00	0.00217	152.00
301	301.00	0.00	0.00430	0.00	0.00215	150.50	0.00215	150.50
295	295.00	0.00	0.00421	0.00	0.00211	147.50	0.00211	147.50
240	240.00	0.00	0.00343	0.00	0.00171	120.00	0.00171	120.00
238	238.00	0.00	0.00340	0.00	0.00170	119.00	0.00170	119.00
236	236.00	0.00	0.00337	0.00	0.00169	118.00	0.00169	118.00
234	234.00	0.00	0.00334	0.00	0.00167	117.00	0.00167	117.00
207	207.00	0.00	0.00296	0.00	0.00148	103.50	0.00148	103.50
177	177.00	0.00	0.00253	0.00	0.00126	88.50	0.00126	88.50
175	175.00	0.00	0.00250	0.00	0.00125	87.50	0.00125	87.50
144	144.00	0.00	0.00206	0.00	0.00103	72.00	0.00103	72.00
142	142.00	0.00	0.00203	0.00	0.00101	71.00	0.00101	71.00
115	115.00	0.00	0.00164	0.00	0.00082	57.50	0.00082	57.50
113	113.00	0.00	0.00161	0.00	0.00081	56.50	0.00081	56.50
85	85.00	0.00	0.00121	0.00	0.00061	42.50	0.00061	42.50
83	83.00	0.00	0.00119	0.00	0.00059	41.50	0.00059	41.50
66	66.00	0.00	0.00094	0.00	0.00047	33.00	0.00047	33.00

Table F2.1 Calculated hysteresis loop energy values - Chapetti et al. data.

W_{HL} [MPa]	$N_{exp.}$ [cycles]
2.44041	17,338
1.38653	43,804
0.95675	80,475
0.86052	95,748
0.40255	332,669
0.24116	770,535
0.23279	816,488
0.19167	1,122,831
0.13946	1,891,166
0.07254	5,522,534

Table F2.2 Calculated hysteresis loop energy values -
Livieri and Lazzarin data (with reference to steel joint-13×10 mm).

W_{HL} [MPa]	$N_{exp.}$ [cycles]
0.72309	127,355
0.58374	180,896
0.34673	424,910
0.25694	694,501
0.18905	1,148,496
0.14415	1,791,364
0.07804	4,898,879

Table F2.3 Calculated hysteresis loop energy values -
Livieri and Lazzarin data (with reference to steel joint-25×32 mm).

W_{HL} [MPa]	$N_{exp.}$ [cycles]
0.78213	111,978
0.54354	203,345
0.29636	549,624
0.19177	1,121,938
0.12498	2,263,558
0.07707	5,000,000

Table F2.4 Calculated hysteresis loop energy values -
Livieri and Lazzarin data (with reference to steel joint-38×220 mm).

W_{HL} [MPa]	$N_{exp.}$ [cycles]
0.70777	131,904
0.65434	150,018
0.34921	419,968
0.25330	710,941
0.20303	1,021,705
0.15816	1,538, 647

Table F2.5 Calculated hysteresis loop energy values -
Livieri and Lazzarin data (with reference to aluminium joint).

W_{HL} [MPa]	$N_{exp.}$ [cycles]
0.05724	47,863
0.04327	66,681
0.02472	129,420
0.02844	109,648
0.01812	187,068
0.01019	369,828
0.01267	285,759
0.01191	307,610
0.00846	461,318
0.00620	666,807
0.00440	1,000,000
0.00294	1,614,359
0.00179	2,910,717
0.00219	2,290,868
0.00133	4,130,475
0.00097	5,970,353

Table F2.6 Calculated hysteresis loop energy values - Reemsnyder data-h=1.5 mm.

W_{HL} [MPa]	$N_{exp.}$ [cycles]
0.43549	52,445
0.28959	87,902
0.29356	86,402
0.22671	119,832
0.12806	246,934
0.17039	172,019
0.15076	200,846
0.04681	882,738
0.16137	184,281
0.01758	3,048,810
0.01882	2,797,361
0.01395	4,085,348
0.02470	1,982,536
0.07742	466,880
0.02150	2,123,863

Table F2.7 Calculated hysteresis loop energy values - Reemsnyder data-h=2.3 mm.

W_{HL} [MPa]	$N_{exp.}$ [cycles]
0.16809	175, 006
0.17991	160,572
0.16137	184,282
0.31851	77,923
0.24266	109,949
0.12981	242,719
0.14085	218, 900
0.21471	128,374
0.06758	554,587
0.14872	204,334
0.01218	4,852,800
0.02127	2,395,859
0.01252	4,688,562
0.09240	373,361
0.02014	2,566,650
0.02070	2,479,784

Table F2.8 Calculated hysteresis loop energy values - Reemsnyder data-h=3.8 mm.

W_{HL} [MPa]	$N_{exp.}$ [cycles]
0.65490	31,290
0.61184	34,103
0.43549	52,445
0.32730	75,285
0.30578	82,052
0.10878	303,596
0.09366	366,890
0.07136	517,683
0.03424	1,311,560
0.02608	1,850,613
0.05663	693,685
0.04494	929,524
0.02437	2,016,961
0.02470	1,982,536
0.02150	2, 895,351

Table F2.9 Calculated hysteresis loop energy values - Webber data.

W_{HL} [MPa]	$N_{exp.}$ [cycles]
0.22532	9,060
0.13306	16,812
0.16637	12,934
0.13520	16,500
0.04868	54,726
0.15118	14,472
0.05357	48, 908
0.04567	58,984
0.04150	66,002
0.01494	218,907
0.10155	184,942
0.08917	349,670
0.08478	943,770
0.07663	1,425,141
0.07077	1,117,095
0.07298	1,565,085
0.06516	1,594, 681
0.06631	4,816,114
0.06838	6,030,155

Table F2.10 Calculated notch stress-intensity energy values - Chapetti et al. data.

W_{NS} [MPa]	$N_{exp.}$ [cycles]
0.17698	17,338
0.16466	43,804
0.14963	80,475
0.12362	95,748
0.09753	332,669
0.06945	770,535
0.06283	816,488
0.05654	1,122,831
0.04612	1,891,166
0.03994	5,522,534

Table F2.11 Calculated notch stress-intensity energy values -
Livieri and Lazzarin data (with reference to steel joint) - 13×10 mm.

W_{NS} [MPa]	$N_{exp.}$ [cycles]
0.35477	127,355
0.28415	180,896
0.20037	424,910
0.16249	694,501
0.12345	1,148,496
0.08762	1,791,364
0.06264	4,898,879

Table F2.12 Calculated notch stress-intensity energy values -

Livieri and Lazzarin data (with reference to steel joint) - 25×32 mm.

W_{NS} [MPa]	$N_{exp.}$ [cycles]
0.77919	111,978
0.60471	203,345
0.39755	549,624
0.25443	1,121,938
0.18953	2,263,558
0.13089	5,000,000

Table F2.13 Calculated notch stress-intensity energy values -

Livieri and Lazzarin data (with reference to steel joint) - 38×220 mm.

W_{NS} [MPa]	$N_{exp.}$ [cycles]
1.81036	131,904
1.49101	150,018
1.02472	419,968
0.81854	710,941
0.54795	1,021,705
0.43851	1,538, 647

Table F2.14 Calculated notch stress-intensity energy values -
Livieri and Lazzarin data (with reference to aluminium joint).

W_{NS} [MPa]	$N_{exp.}$ [cycles]
0.04645	47,863
0.04645	66,681
0.04038	129,420
0.03399	109,648
0.03399	187,068
0.02747	369,828
0.02712	285,759
0.02511	307,610
0.02511	461,318
0.01676	666,807
0.01676	1,000,000
0.01676	1,614,359
0.01346	2,910,717
0.01160	2,290,868
0.01160	4,130,475
0.01160	5,970,353

Table F2.15 Calculated notch stress-intensity energy values - Reemsnyder data-h=1.5 mm.

W_{NS} [MPa]	$N_{exp.}$ [cycles]
0.34689	52,445
0.34532	87,902
0.29786	86,402
0.29568	119,832
0.23099	246,934
0.22781	172,019
0.21161	200,846
0.18901	882,738
0.18670	184,281
0.18384	3,048,810
0.14106	2,797,361
0.13661	4,085,348
0.10139	1,982,536
0.09970	466,880
0.06895	2,123,863

Table F2.16 Calculated notch stress-intensity energy values - Reemsnyder data-h=2.3 mm.

W_{NS} [MPa]	$N_{exp.}$ [cycles]
0.41298	175, 006
0.36309	160,572
0.36309	184,282
0.31288	77,923
0.30938	109,949
0.27955	242,719
0.24032	218, 900
0.19702	128,374
0.17272	554,587
0.16947	204,334
0.16689	4,852,800
0.14819	2,395,859
0.14339	4,688,562
0.11306	373,361
0.11043	2,566,650
0.06762	2,479,784

Table F2.17 Calculated notch stress-intensity energy values - Reemsnyder data-h=3.8 mm.

W_{NS} [MPa]	$N_{exp.}$ [cycles]
0.54428	31,290
0.44222	34,103
0.43773	52,445
0.30803	75,285
0.30429	82,052
0.17257	303,596
0.17257	366,890
0.11396	517,683
0.06314	1,311,560
0.06314	1,850,613
0.05937	693,685
0.04582	929,524
0.04123	2,016,961
0.02806	1,982,536
0.02584	2,895,351

Table F2.18 Calculated notch stress-intensity energy values - Webber data.

W_{NS} [MPa]	$N_{exp.}$ [cycles]
0.92722	9,060
0.91692	16,812
0.66488	12,934
0.65182	16,500
0.62609	54,726
0.41440	14,472
0.40752	48, 908
0.40070	58,984
0.39394	66,002
0.30827	218,907
0.22539	184,942
0.22033	349,670
0.14918	943,770
0.14507	1,425,141
0.09515	1,117,095
0.09187	1,565,085
0.05198	1,594, 681
0.04956	4,816,114
0.03134	6,030,155

Table F2.19 Calculated critical plane energy values - Chapetti et al. data.

W_{CP}	$N_{exp.}$ [cycles]
0.06412	17,338
0.05186	43,804
0.03917	80,475
0.02248	95,748
0.01141	332,669
0.00446	770,535
0.00341	816,488
0.00259	1,122,831
0.00156	1,891,166
0.00111	5,522,534

Table F2.20 Calculated critical plane energy values -

Livieri and Lazzarin data (with reference to steel joint) - 13×10 mm.

W_{CP}	$N_{exp.}$ [cycles]
0.01000	127,355
0.00533	180,896
0.00220	424,910
0.00132	694,501
0.00074	1,148,496
0.00040	1,791,364
0.00024	4,898,879

Table F2.21 Calculated critical plane energy values -

Livieri and Lazzarin data (with reference to steel joint) - 25×32 mm.

W_{CP}	$N_{exp.}$ [cycles]
0.02655	111,978
0.01275	203,345
0.00401	549,624
0.00134	1,121,938
0.00072	2,263,558
0.00037	5,000,000

Table F2.22 Calculated critical plane energy values -

Livieri and Lazzarin data (with reference to steel joint) - 38×220 mm.

W_{CP}	$N_{exp.}$ [cycles]
0.04295	131,904
0.02426	150,018
0.00829	419,968
0.00449	710,941
0.00163	1,021,705
0.00099	1,538, 647

Table F2.23 Calculated critical plane energy values -
Livieri and Lazzarin data (with reference to aluminium joint).

W_{CP}	$N_{exp.}$ [cycles]
0.00104	47,863
0.00104	66,681
0.00090	129,420
0.00076	109,648
0.00076	187,068
0.00061	369,828
0.00060	285,759
0.00056	307,610
0.00056	461,318
0.00037	666,807
0.00037	1,000,000
0.00037	1,614,359
0.00030	2,910,717
0.00026	2,290,868
0.00026	4,130,475
0.00026	5,970,353

Table F2.24 Calculated critical plane energy values - Reemsnyder data-h=1.5 mm.

W_{CP}	$N_{exp.}$ [cycles]
1.15057	52,445
1.11604	87,902
0.41216	86,402
0.39235	119,832
0.07495	246,934
0.06833	172,019
0.04188	200,846
0.01997	882,738
0.01844	184,281
0.01669	3,048,810
0.00332	2,797,361
0.00278	4,085,348
0.00077	1,982,536
0.00073	466,880
0.00035	2,123,863

Table F2.25 Calculated critical plane energy values - Reemsnyder data-h=2.3 mm.

W_{CP}	$N_{exp.}$ [cycles]
0.39235	175, 006
0.16518	160,572
0.16518	184,282
0.06111	77,923
0.05670	109,949
0.02902	242,719
0.01094	218, 900
0.00332	128,374
0.00168	554,587
0.00154	204,334
0.00143	4,852,800
0.00089	2,395,859
0.00080	4,688,562
0.00045	373,361
0.00043	2,566,650
0.00023	2,479,784

Table F2.26 Calculated critical plane energy values - Reemsnyder data-h=3.8 mm.

W_{CP}	$N_{exp.}$ [cycles]
0.92823	31,290
0.22941	34,103
0.21422	52,445
0.02078	75,285
0.01919	82,052
0.00091	303,596
0.00091	366,890
0.00036	517,683
0.00019	1,311,560
0.00019	1,850,613
0.00018	693,685
0.00014	929,524
0.00012	2,016,961
0.000083	1,982,536
0.000076	2, 895,351

Table F2.27 Calculated critical plane energy values - Webber data.

W_{CP}	$N_{exp.}$ [cycles]
0.00179	9,060
0.00177	16,812
0.00129	12,934
0.00126	16,500
0.00121	54,726
0.00080	14,472
0.00079	48, 908
0.00078	58,984
0.00076	66,002
0.00060	218,907
0.00044	184,942
0.00043	349,670
0.00029	943,770
0.00028	1,425,141
0.00018	1,117,095
0.00018	1,565,085
0.00010	1,594, 681
0.000096	4,816,114
0.000061	6,030,155

Appendix G – Mean energy values for energy models

Appendix G tabulates mean energy values for the hysteresis loop model, the notch stress-intensity model, and the critical plane/energy model for all the data sets.

Table G.1 Calculated mean energy values[1].

Energy models / Experimental data	Hysteresis loop	Notch stress-intensity	Critical plane/energy
Chapetti et al. [32]	0.69244	0.09873	0.02022
Lazzarin [30] (steel joint-13×10 mm)	0.33168	0.18221	0.00286
Lazzarin [30] (steel joint-25×32 mm)	0.33597	0.39272	0.00654
Lazzarin [30] (steel joint-38×220 mm)	0.38764	1.02185	0.01180
Lazzarin [30] (aluminium joint)	0.01468	0.02529	0.00056
Reemsnyder-h=1.5 mm [33]	0.13857	0.20423	0.22129
Reemsnyder-h=2.3 mm [33]	0.12196	0.19759	0.05570
Reemsnyder-h=3.8 mm [33]	0.18944	0.18820	0.09433
Webber [34]	0.09006	0.35640	0.00069

---

[1] The units for the energy values of the hysteresis-loop model and the notch stress-intensity model are MPa. The critical plane/energy model has been normalized and therefore does not have any units.

References

[1] S. J. Maddox, 'An introduction to the fatigue of welded joints', Improving the Fatigue Performance of Welded Joints (TWI), 1983, Abington Cambridge.

[2] W. Fricke, 'Fatigue analysis of welded joints: state of development', Marine Structures, 2003, pp 185-200.

[3] D. Radaj, C. M. Sonsino, W. Fricke, Fatigue assessment of welded joints by local approaches, 2nd Ed., Woodhead Publishing Limited and CRC Press LLC, 2006, Abington Cambridge.

[4] T. R. Gurney, Fatigue of Welded Structures, 2nd Ed., Cambrideg University Press, 1979, Cambridge.

[5] K. G. Richards, Fatigue Strength of Welded Structures, The Welding Institute (TWI), 1969, Abington Hall, Cambridge.

[6] A. Hobbacher, Fatigue Design of Welded Joints and Components, The International Institute of Welding (IIW), Recommendations of IIW Joint Working Group XIII- XV, XIII-1539-96/XV-845-96, 1996, Abington Publishing.

[7] J. M. Ferreira, C. M. Branco, 'Influence of weld and plate geometry on the fatigue strength of cruciform joints', Theoretical and Applied Fracture Mechanics 9 (North-Holland), 1988, pp 23-32.

[8] F. V. Lawrence, S. D. Dimitrakis, W. H. Munse, 'Factors influencing weldment fatigue', ASM Handbook, Volume 19, 1996, pp 274-286.

[9] D. Radaj, 'Review of fatigue strength assessment of non welded and welded structures based on local parameters', International Journal of Fatigue, 18 (3), 1996, pp 153-170.

[10] H. Neuber, Theory of Notch Stresses, Ann Arbor Michigan, 1946, Edwards.

[11] R. E. Peterson, 'Relation between stress analysis and fatigue of metals', Proc SESA 11 (2), 1950, pp 199-206.

[12] R. Kuguel, 'A relation between theoretical stress concentration factor and fatigue notch factor deduced from the concept of highly stressed volume', ASTM Proc 61, 1961, pp 732-744.

[13] T. H. Topper, R. M. Wetzel, J. D. Morrow, 'Neuber's rule applied to fatigue of notched specimens', J. Matter., Vol. 4, No. 1, 1969, pp 200-209.

[14] C. C. Woodley, 'Practical applications of weld toe grinding', Improving the Fatigue Performance of Welded Joints (TWI), 1983, Abington Cambridge.

[15] Y. H. Zhang, S. J. Maddox, 'Fatigue life prediction for toe ground welded joints', International Journal of Fatigue 31, 2009, pp 1124-1136.

[16] N. E. Dowling, Mechanical Behavior of Materials; Engineering methods for deformation, fracture and fatigue, 2nd edition, 1999, Prentice Hall Inc.

[17] G. Dieter, Mechanical Metallurgy, 3rd edition, 1989, Mc Graw Hill Publications.

[18] D. Radaj, Design and analysis of fatigue resistant welded structures, 1st Ed., Woodhead Publishing in association with The Welding Institute, 1990, Abington Cambridge.

[19] P. Lazzarin, R. Tovo, 'A unified approach to the evaluation of linear elastic stress fields in the neighborhood of cracks and notches', International Journal of Fracture 78, 1996, pp 3-19.

[20] B. Atzori, P. Lazzarin, R. Tovo, 'From a local stress approach to fracture mechanics: a comprehensive evaluation of the fatigue strength of welded joints', Fatigue Fracture Engineering Mater Struct 22, 1999, pp 369-381.

[21] W. Cui, 'A state-of-the-art review on fatigue life prediction methods for metal structures', Journal of Marine Science and Technology (7), 2002, pp 43-56.

[22] T. Lagoda, Lifetime estimation of welded joints, Springer Publications, 2008, Springer-Verlag Berlin Heidelberg.

[23] P. Lazzarin, R. Tovo, 'A notch stress intensity factor approach to the stress analysis of welds', Fatigue & Fracture of Engineering Materials& Structures 21, 1998, pp 1089-1103.

[24] J. Dziubinskyi 'Fatigue failure criterion based on plastic strain energy density applied to welds', Int J Fatigue, 1991, 13 (3), pp 223-226.

[25] P. Lazzarin, T. Lassen, P. Livieri, 'A notch stress intensity approach applied to fatigue life prediction of welded joints with different local toe geometry', Blackwell Publishing Ltd. Fatigue Fracture Engineering Material Struct. 26, 2003, pp 49-58.

[26] G. Cheng, Z. B. Kuang, Z. W. Lou, H. Li, 'Experimental investigation of fatigue behaviour for welded joint with mechanical heterogeneity', Int J Pres. Ves. & Piping (67), 1996, pp 229-242.

[27] A. Varvani-Farahani, 'Advanced Fatigue Fracture Analysis-ME8136' class notes, fall 2008, Ryerson University.

[28] D. Lefebvre, F. Ellyin, 'Cyclic response and inelastic strain energy in low cycle fatigue', International Journal of Fatigue 6, 1984, pp 5-15.

[29] P. Lazzarin, P. Livieri, F. Berto, M. Zappalorto, 'Local strain energy density and fatigue strength of welded joints under uniaxial and multiaxial loading', Engineering Fracture Mechanics 75, 2008, pp 1875-1889.

[30] P. Livieri, P. Lazzarin, 'Fatigue strength of steel and aluminium welded joints based on generalized stress intensity factors and local strain energy values', International Journal of Fracture 133, 2005, pp 247-276.

[31] A. Varvani-Farahani, 'A new energy-critical plane parameter for fatigue life assessment of various metallic materials subjected to in-phase and out-of-phase multiaxial fatigue loading conditions', International Journal of Fatigue 22, 2000, pp 295-305.

[32] M. D. Chapetti, J. Belmonte, T. Tagawa, T. Miyata, 'Integrated fracture mechanics approach to analyze fatigue behaviour of welded joints', Science and Technology of Welding and Joining, 2004, Vol. 9, No. 5, pp 430-438.

[33] H. S. Reemsnyder, 'Development and application of fatigue data for structural steel weldments', Fatigue Testing of Weldments, ASTM STP 648, D. W. Hoeppner, Ed., American Society for Testing and Materials, 1978, pp 3-21.

[34] D. Webber, 'An evaluation of possible improvement methods for aluminium alloy fillet welded joints', Improving the Fatigue Performance of Welded Joints (TWI), 1983, Abington Cambridge.

[35] S. J. Maddox, D. Webber, 'Fatigue crack propagation in aluminum-zinc-magnesium alloy fillet-welded joints', Fatigue Testing of Weldments, ASTM STP 648, D. W. Hoeppner, Ed., American Society for Testing and Materials, 1978, pp 159-184.

[36] ANSYS, ANSYS product documentation set, ANSYS Manual for Release 5.4, 1997.

[37] J. A. Bannantine, J. J. Comer, J. L. Handrok, Fundamentals of Metal Fatigue Analysis, Prentice Hall, 1989.

[38] S. Berge, 'On the effect of plate thickness in fatigue of welds', Engineering Fracture Mechanics Vol. 21, No. 2, 1985, pp 423-435.

[39] S. Kainuma, I. T. Kim, 'Fatigue strength evaluation of load-carrying cruciform fillet-welded joints made with mild steel plates of different thickness', International Journal of Fatigue 27, 2005, pp 810-816.

[40] D. Taylor, N. Barrett, G. Lucano, 'Some new methods for predicting fatigue in welded joints', International Journal of Fatigue 24, 2002, pp 509-518.

[41] ASM International Handbook Committee, Fatigue and Fracture, ASM Handbook, Volume 19, third printing, September 2002, pp 968-979.